

287
10-94-83 85 (1)

1-11-83

Dr #1853-8

SANDIA REPORT SAND82-2365 • TTC-0398 • Unlimited Release • UC-71
Printed June 1983

SAND--82-2365

DE84 001629

An Assessment of the Safety of Spent Fuel Transportation in Urban Environs

R. P. Sandoval, J. P. Weber, H. S. Levine, A. D. Romig,
J. D. Johnson, R. E. Luna, G. J. Newton, B. A. Wong,
R. W. Marshall, Jr., J. L. Alvarez, F. Gelbard

Prepared by
Sandia National Laboratories
Albuquerque, New Mexico 87185 and Livermore, California 94550
for the United States Department of Energy
under Contract DE-AC04-76DP00789

MASTER

An Assessment of the Safety of Spent Fuel
Transportation in Urban Environs

SAND82-2365
TTC-0398

R. P. Sandoval, J. P. Weber, H. S. Levine, A. D. Romig, J. D. Johnson, R.
E. Luna, Sandia National Laboratories,¹ Albuquerque, New Mexico 87185

G. J. Newton, B. A. Wong, Lovelace Inhalation Toxicology Research
Institute,² P. O. Box 5890, Albuquerque, New Mexico 87185

R. W. Marshall, Jr., J. L. Alvarez, Idaho National Engineering
Laboratories,³ EG&G, Idaho, Inc., P. O. Box 1625, Idaho Falls, ID 83415

Fred Gelbard, Consultant, 861 South Glendcliff #31, La Habra, California,
90631

DISCLAIMER

This report was prepared as an account of work sponsored by an agency of the United States Government. Neither the United States Government nor any agency thereof, nor any of their employees, makes any warranty, express or implied, or assumes any legal liability or responsibility for the accuracy, completeness, or usefulness of any information, apparatus, product, or process disclosed, or represents that its use would not infringe privately owned rights. Reference herein to any specific commercial product, process, or service by trade name, trademark, manufacturer, or otherwise does not necessarily constitute or imply its endorsement, recommendation, or favoring by the United States Government or any agency thereof. The views and opinions of authors expressed herein do not necessarily state or reflect those of the United States Government or any agency thereof.

1. Under US Department of Energy Contract DE-AC04-76D00789
2. Under US Department of Energy Contract DE-AC04-76EV01013
3. Under US Department of Energy Contract DE-AC07-76ID01570

MASTER

ABSTRACT

The results of a program to provide an experimental data base for estimating the radiological consequences from a hypothetical sabotage attack on a light water reactor spent fuel shipping cask in a densely populated area are presented. The results of subscale and full scale experiments in conjunction with an analytical modeling study are described. The experimental data were used as input to a reactor safety consequence model to predict radiological health consequences resulting from a hypothetical sabotage attack on a spent fuel shipping cask in the Manhattan borough of New York City. The results of these calculations are presented in this report.

ACKNOWLEDGEMENTS

The authors would like to express their appreciation and thanks to the following people for their technical support and assistance in this study:

D. J. Alpert, Org 9415, SNL
R. E. Bohannon, Org 7533, SNL
D. M. Ericson, Jr., Org 9414, SNL
B. J. Joseph, Org 9783, SNL
W. B. Leisher, Org 9782, SNL
F. H. Mathews, Org 7533, SNL
M. G. Perdue, Org 7533, SNL
R. T. Reese, Org 9782, SNL
D. R. Stenberg, Org 9783, SNL
M. M. Sturm, Org 1822, SNL
M. G. Vigil, Org 9782, SNL
L. Isaacson, EG&G Geo-Centers, Inc.
R. C. Green, EG&G Idaho, Inc.
B. B. Kaiser, EG&G Idaho, Inc.
V. J. Novick, EG&G Idaho, Inc.
Y. S. Cheng, Lovelace Inhalation Toxicology Research Institute
B. B. Boecker, Lovelace Inhalation Toxicology Research Institute
G. M. Kanapilly*, Lovelace Inhalation Toxicology Research Institute
R. O. McCellan, Lovelace Inhalation Toxicology Research Institute
H. C. Yeh, Lovelace Inhalation Toxicology Research Institute

* deceased

AN ASSESSMENT OF THE SAFETY OF SPENT FUEL
TRANSPORTATION IN URBAN ENVIRONS

TABLE OF CONTENTS

	<u>Page</u>
1. Executive Summary	1
2. Introduction	5
3. Program Scope	7
4. Summary of Results	10
4.1 High Energy Device Evaluation Tests	10
4.2 Development of Measurement Techniques and Assessment of Experimental Precision: Subscale Tests	10
4.3 Quantification and Characterization of Material Released From a Full-Size Reference Sabotage Incident: Full-Size Test	36
4.4 Development of a Correlation Between Depleted UO ₂ and Spent Fuel	52
4.5 Analyses of Fuel and Cask Breakup and Aerosol Production	56
4.6 Analysis of Radiological Health Effects	80
5. Conclusions	89
5.1 Measured Source Term Release for a Full-Size One-PWR Fuel Assembly Reference Event	89
5.2 Calculated Source Term Release for a Three-PWR Fuel Assembly Truck Cask Sabotage Event	89
5.3 Calculated Health Effects	89
5.3.1 One-PWR Fuel Assembly Truck Cask Reference Event	89
5.3.2 Three-PWR Fuel Assembly Truck Cask Sabotage Event	89
5.4 Degree of Precision and Accuracy in Measured Parameters and Calculated Results	94

	<u>Page</u>
5.5 Comparison of This Study's Results With Other Study's Results	95
6. References	98

Volume II, (Classified, CNSI)

7. Appendices

7.1 APPENDIX A--HED Evaluation Tests: Test Data	100
7.2 APPENDIX B--Scaling Analyses: Extrapolation to Higher Energy Attack Devices	115
7.3 APPENDIX C--Subscale Tests/Full Scale Test: Test Data	120

Volume III, (Unclassified)

7.4 APPENDIX D--Correlation Experiments: Test Data	130
7.5 APPENDIX E--Analytical Methods	227
7.6 APPENDIX F--Radiological Health Consequence Modeling: CRAC	237

List of Figures

<u>Figure</u>		<u>Page</u>
4.2.1	Schematic of Confinement Chamber and 1/4-Scale Cask Used in Tests 3 Through 7	15
4.2.2	Schematic of the Experimental Setup for "Dry" Test 6 Prior to Detonation of HED.	17
4.2.3	Schematic of Test 6 (Dry) Immediately After Detonation.	18
4.2.4	Time History of UO ₂ Aerosol Mass Concentration Based on Sequential Filter Samples.	20
4.2.5	Time History of Mass Median Aerodynamic Diameter and Geometric Standard Deviation for Test 6 (Dry)	21
4.2.6	Schematic of Fuel Pin Damage and Damage Path Caused by HED Action for 1/4-Scale Test 6 (Dry)	22
4.2.7	Photograph Showing Cask Damage for 1/4 Scale-Cask Test 6 (Dry).	23
4.2.8	Schematic of Test 7 (Wet) Immediately After Detonation.	25
4.2.9	Time History of Aerosol Mass Concentration Within Chamber Based Upon Sequential Filter Samples and Front Surface Reentrant Filter Samples for Test 7	26
4.2.10	Time History of U and Zr Mass Concentration Based Upon Extractive Filter Samples	27
4.2.11	Time History of Aerosol Size and Geometric Standard Deviation for Test 7 (Wet).	28
4.2.12	TEM Photomicrograph of Aerosols Collected With Electrostatic Precipitator (ESP) Sampler for Test 7 (Wet)	29
4.2.13	TEM Photomicrograph of Aerosols Collected With Electrostatic Precipitator (ESP) Sampler for Test 6 (Dry).	30
4.2.14	UO ₂ and Total Mass Distribution Based Upon Sieved Debris Released From Cask Into Chamber for Tests 6 and 7	32
4.2.15	Total Aerosol Mass Concentration Based Upon Continuous Flow Condensation Nuclei Counters of Tests 6 (Dry) and 7 (Wet)	33

List of Figures (continued)

<u>Figure</u>		<u>Page</u>
4.2.16	Schematic of Fuel Pin Damage and Damage Path Caused by Action of HED for 1/4-Scale Test 7 (Wet).	34
4.2.17	Photograph Showing Cask Damage for 1/4-Scale Cask Test 7 (Wet).	35
4.3.1	Schematic of the Full-Scale Reference Test Configuration Showing Finned Cask Inside Pressure Chamber	37
4.3.2	Schematic of the Full-Scale Test Configuration Immediately After Detonation Showing Damage and Net Mass Loss	41
4.3.3	Photograph of 15 x 15 Depleted UO ₂ Fuel Assembly Showing Damage Caused by HED in Full-Scale Reference Test	44
4.3.4	Time History of UO ₂ Aerosol Mass Within Pressure Chamber Based Upon Sequential Filter Samples for Full-Scale Reference Test.	45
4.3.5	Total Mass and UO ₂ Mass Size Distribution for Sieved Debris of Full-Scale Test	46
4.3.6	Aerosol Size (MMAD) and Geometric Standard Deviation as a Function of Time for Full-Scale Test.	47
4.3.7	Scanning Electron Micrograph of a Typical Rotating Plate Sample Taken 400 msec After Detonation of the Full-Scale Event. Magnification is 200,000.	48
4.3.8	Scanning Electron Micrograph of Time Integrated (10 minutes) Aluminum Planchet Sample Showing a 70 μm (real diameter) UO ₂ Particle.	50
4.3.9	Comparison of Total Mass Concentration (mg/) as a Function of Time for Subscale Tests No. 6 and 7 in the Full-Scale Test.	51
4.5.1	UO ₂ and ZrO ₂ Aerosol Concentrations as a Function of Time for Test No. 7 (Wet)	57
4.5.2	FeO and PbO Aerosol Concentrations as a Function of Time After Detonation for Test No. 7 (Wet). Analyses Are by XRF	58
4.5.3	UO ₂ and ZrO ₂ Aerosol Concentrations as a Function of Time for Full-Scale Test (Dry).	59
4.5.4	PbO and FeO Aerosol Concentrations as a Function of Time After Detonation for Full-Scale Test (Dry).	60

List of Figures (continued)

<u>Figure</u>		<u>Page</u>
4.5.5	Aerosol Fraction for ZrO_2 and UO_2 as a Function of Time After Detonation for the Full-Scale Test	61
4.5.6	Aerosol Fraction of ZrO_2 , PbO , and FeO Components as a Function of Time for Full-Scale Test.	62
4.5.7	SEM Micrograph of Material Deposited on the Valve Door During the Full-Scale Cask Test	64
4.5.8	X-ray Spectra Showing the Elements Present in Figure 4.5.7.	65
4.5.9	Macrophotograph (1.5x) of the Stainless Steel Slug Taken From Cask After the Full-Scale Test Event	66
4.5.10	Micrograph of the Stainless Steel Slug in Cross Section (500x).	67
4.5.11	Macrophotograph of a Piece of Zircaloy Cladding After the Full-Scale Test Event (1.5x).	68
4.5.12	Micrograph of Zircaloy Cladding in Cross Section (100x).	69
4.5.13	Microscopic Cross Section of UO_2 Fuel Pellet (100x)	70
4.5.14	Plot of Measured Aerosol Mass Concentrations Obtained From Sequenced Cascade Impactors for Full-Scale Reference Test	73
4.5.15	Plot of Total Suspended Aerosol Mass Concentration as a Function of Time.	78
4.5.16	Plot Showing Comparison of Calculated Mass Concentration From Model With Measured Values After 52.5 Seconds Postdetonation.	79

List of Tables

<u>Table</u>		<u>Page</u>
4.1.1	Construction Material Data for Truck Spent Fuel Shipping Casks	11
4.1.2	High Energy Devices Surveyed.	12
4.2.1	Summary of Scaled Cask-High Energy Device Tests	13
4.2.2	Sampling Instrument Used in 1/4-Scale Chamber Tests	16
4.3.1	Sampling Instruments Used in Full-Scale Cask Test	38
4.3.2	Summary of Results of Full-Scale Test	42
4.4.1	Filter Data From Battelle Columbus Laboratory's Studies on Spent Fuel Release Fraction.	54
4.5.3	Surface Area for Aerosol Deposition	74
4.6.1	Measured Release Fractions for a 1 PWR Fuel Assembly and Calculated Release Fractions for a 3 PWR Fuel Assembly Track Cask.	82
4.6.2	Spent Fuel Cask Radionuclide Inventory Used in This Study . .	84
4.6.3	Population Distribution Used for This Analysis.	86
4.6.4	CRAC Computed Health Consequences for This Experimental Study	87
4.6.5	Peak Thyroid and Bone Marrow Doses as a Function of Distance From Release Point	88
5.1	Summary of Release Parameters for a 1 PWR Assembly Cask Event	90
5.2	Summary of Release Parameters for a 3 PWR Assembly Cask Event	91
5.3.1	Health Consequences for a One PWR Assembly Truck Cask Sabotage Event	92
5.3.2	Health Consequences for a Three PWR Assembly Truck Cask Sabotage Event	93
5.5.1	Comparison of Extrapolated Test Results With Urban Study Results	96
5.5.2	Comparison of CRAC Computed Health Effects With Urban Study Results	97

1. EXECUTIVE SUMMARY

In 1978 a study of radiological impacts from transport of radioactive material through urban areas, the 1978 Urban Study¹, indicated very severe consequences from a successful malevolent act on spent fuel shipments. On the basis of that analysis the NRC instituted stringent physical security requirements² for spent fuel transport which were designed to prevent sabotage events in urban areas. A subsequent version of Reference 1, the 1980 Urban Study,³ reduced the postulated release quantity by a factor of 14 and thus showed reduced numbers of early fatalities, morbidities and latent cancer fatalities. As a result of the second report, the NRC reduced the stringency of the physical security measures, but they remain a serious restriction on the shipment of spent fuel and have resulted in increased shipping costs.

Since no relevant experimental data base was available for use in the Urban Studies, source term estimates were based upon assumed physical and chemical characteristics and estimated quantities of the released fuel. Consequently, there was a high degree of uncertainty in the estimated source terms and radiological consequences. A need existed to provide experimental data characterizing the quantity, physical, and chemical form of fuel released from hypothetical attacks on spent fuel shipping casks.

This report describes the results of a program conducted at Sandia National Laboratories (SNL) to provide the experimental data base for estimating the radiological consequences from a hypothetical sabotage attack on a spent fuel shipping cask. The primary objectives of the program were limited to (1) evaluating the effectiveness of selected high energy devices in breaching full-size spent fuel casks, (2) quantifying and characterizing relevant aerosol properties of the released fuel, and (3) using the resulting experimental data to evaluate the radiological health consequences resulting from a hypothetical sabotage attack on a spent fuel shipping cask in a densely populated area.

Subscale and full-scale experiments in conjunction with an analytical modeling study were performed to meet the programmatic objectives. The program was divided into the following tasks:

- Perform subscale and full-scale tests to evaluate the capability of available high energy devices (HEDs) to breach generic spent fuel truck casks and disperse cask contents. According to the results of this evaluation, a reference case HED was selected for further evaluation and full-scale testing.

- Perform subscale tests on casks filled with surrogate fuel subjected to scaled versions of the reference HED to establish measurement techniques and to determine a preliminary release fraction for surrogate material subjected to HED environments.

- Perform subscale tests on surrogate and actual irradiated fuel pellets subjected to scaled HED attacks in order to quantify and characterize radioactive particle production for various high energy environments. A correlation between aerosol and fine particle parameters for spent fuel and depleted UO_2 for a range of shock impact loadings was developed.
- Conduct a full-scale source-term characterization test using the reference HED and a generic truck cask containing unirradiated UO_2 fuel to characterize the released fuel (quantity, particle size, composition, etc).
- Develop an understanding of the cask and fuel material response to high energy/explosive environments and to develop a basis for predicting the response of similar casks to larger HEDs.
- Use the experimental data obtained to evaluate the health consequences resulting from a hypothetical sabotage attack on a spent nuclear fuel shipping cask in a densely populated area.

HED Evaluation An extensive survey of available high energy devices (HEDs) was performed to select those that might be capable of breaching a full-size spent fuel truck cask. From the many different types of attack devices considered in the survey, four general types of HEDs were selected for testing and further evaluation. These devices were those discussed in the 1978¹ and 1980³ Urban Studies:

1. Conical-shaped charges.
2. Contact-breaching charges.
3. Platter charges.
4. Pyrotechnic torches.

Tests subjecting both simulated and actual spent fuel truck casks to the four types of HEDs were performed to provide data for final selection of a reference HED which showed the greatest potential for penetrating a full-size cask and dispersing its contents.

An HED was selected from the four types tested and was used as the reference attack device for the full-scale source term characterization test from which the needed source term data base was obtained. Volume II of this report elaborates on the selection of the HED; more detail cannot be provided here because of national security limitations.

Subscale Tests Five subscale tests of 1/4-scale casks containing full-size fuel pins made up of unirradiated UO_2 pellets as targets for scaled versions of the selected reference HED were conducted. These tests provided initial experimental data characterizing the fuel material released from a cask subjected to a sabotage incident. The results of these experiments indicated that approximately 48.6 ± 5 g of UO_2 fuel mass was released from the 1/4-scale cask as a result of the attack. Approximately 1.6 percent (0.78 g) of the total released UO_2 mass was in the respirable size range (ie, less than 10 micrometers aerodynamic diameter). A calculation of the

fraction of released airborne respirable aerosol for a full-size event assuming a three assembly pressurized water reactor (PWR) cask (1.4 t of heavy metal (tHM) inventory) of the type used in the Urban Study^{1,3} was made based on the measured 1/4-scale release parameters. This calculation assumed the longest path of interaction through the cask together with rupture of, and subsequent release through, the cask's walls. The results of these extrapolations of the scaled tests indicated that approximately 0.0023 percent (32 g) of the total solid fuel inventory could be released from a full-scale sabotage event as respirable radioactive materials.

Full-Scale Test A full-scale test subjected a 25.45 t generic truck cask containing a single PWR-like unirradiated depleted UO₂ fuel assembly to the reference full-scale HED. A total UO₂ fuel mass of 2.548 kg was released from the cask as a result of the explosive attack. Approximately 0.0006 percent (3 g) of the total unirradiated fuel inventory (0.5 t) was released as a respirable radioactive aerosol. These full-scale test data were used to calculate the quantity of radioactive material that could be released as a result of an explosive attack on a three-PWR fuel assembly generic truck cask. These calculations indicated that approximately 0.0005 percent (6 g) of the total unirradiated fuel inventory (1.4 t) could be released as a respirable radioactive aerosol as a result of an explosive attack on a 3 PWR fuel assembly truck cask.

Correlation Tests: Effects of the high energy environments created by a variety of HEDs on breakup and particulation of spent commercial nuclear reactor fuel and its surrogate, depleted uranium dioxide (d-UO₂), were evaluated in a series of single pellet tests. Tests conducted on single irradiated fuel pellets and single depleted UO₂ pellets enabled measurement of the radioactive aerosols typical of the high energy environments.

Correlation functions were obtained from both filter and sieve data relating particle size distributions for fracture, breakup, and aerosolization of depleted UO₂ fuel to that of irradiated fuel. Using filter data, a spent fuel to depleted UO₂ particle mass production ratio of 0.53 was obtained. This would result in a smaller respirable aerosolized release than obtained in the scaled and full-scale cask tests with depleted uranium surrogate fuel rods. An extrapolation of wet sieve data into the respirable range (a doubtful procedure) resulted in a correlation ratio of 5.6. This value would increase the released quantity of aerosolized fuel from the scaled and full-scale tests. Similar data are available from an NRC-sponsored test program at Battelle Laboratories in Columbus, Ohio.⁴ In their experiments a ratio of spent fuel to depleted uranium respirable release of 0.7 was obtained.

In considering which correlation ratio is the most appropriate, it appears that a value less than one is the most probable. This implies that the aerosolized respirable release from the reference base incident (one PWR fuel assembly cask) would be less than 3 g of irradiated fuel, and the aerosolized respirable release from a 3 PWR fuel assembly cask of the type used in the Urban Study¹ would be less than 6 g. However, for conservatism in the health risk assessment the correlation value of 5.6 was used; this leads to an

upper limit release value of 17 g (3.4×10^{-3} percent) of aerosolized respirable irradiated fuel for a one-PWR assembly cask and 34 g (2.4×10^{-3} percent) for the maximum respirable aerosol release from a three-PWR assembly shipping cask.

Health Effects Evaluation The reactor safety study consequence model, CRAC,⁵ was used in the Urban Study to estimate human health consequences from an attack using the reference HED on a 3 PWR fuel assembly truck cask. The basic scenario as defined in the Urban Study was (1) the attack occurred in the borough of Manhattan in New York City, (2) the attack occurred on a weekday, midafternoon, (3) the spent fuel inventory was typical of PWR assemblies after 150 days cooling at the reactor, (4) all consequence estimates were made without any evacuation to avoid early exposure. For this scenario the Urban Study¹ estimated the health consequences to be 4/60 (mean/peak) early fatalities, 160/1600 (mean/peak) early morbidities and 350/1300 (mean/peak) early latent cancer fatalities. Using the same CRAC model and assumptions and this study's experimentally determined release fraction (3.4×10^{-3} percent) for the same attack mode on a single PWR fuel assembly truck cask (0.5 tHM, 150 days cooled), values of health consequences were found to be 0/0 (mean/peak) early fatalities, 0/0 (mean/peak) early morbidities, 0.3/1.3 (mean/peak) early latent cancer fatalities, and 2/7 total latent cancer fatalities. Extrapolating the experimentally determined release fractions for a single PWR fuel assembly cask to the Urban Study¹ 3 PWR fuel assembly cask scenario, an estimate of the health consequences of 0/0 (mean/peak) early fatalities, 0/0 (mean/peak) early morbidities, 1/3 (mean/peak) early latent cancer fatalities, and 4/14 total latent cancer fatalities were obtained. These newly calculated latent cancer fatalities are smaller by a factor of 350/433 (mean/peak early latent cancer fatalities) than the original Urban Study predictions upon which the NRC interim regulations for US transport of spent fuel were based.

Overall Program Result The data from this program, together with that from the NRC sponsored BCL program⁴, indicate that the Urban Studies^{1,3} greatly overestimated the impact of malevolent acts directed at spent fuel casks in urban environs. From that standpoint this work could be the basis of additional regulatory revisions of the NRC physical protection requirements. In a larger sense this work can also be the basis of more credible "worst case" analyses since it defines the actual result of an event which is well beyond any expectation of cask failures in accident environments. Thus this experimental program has provided significant new information on the behavior of spent fuel and surrogate materials under severe shock and thermal environments which can be the basis of a better understanding of spent fuel transport risks and safety analyses.

2. INTRODUCTION

Public attention has been focused on the environmental impact that could result from the sabotage of spent nuclear fuel shipments in densely populated urban areas. Previous studies have been sponsored to assess the potential of several generic HEDs to breach large spent fuel shipping casks and to evaluate the radiological hazards which could result from the transportation of radioactive material (RAM) in urban areas for various types of environments, including those caused by sabotage.^{1,3} The most recent version³ of the 1978 study¹ predicted approximately 100 total latent cancer fatalities could occur from the successful sabotage of spent fuel shipping systems. Since no experimental data were available for these studies, certain bounding conditions and specific chemical and physical characteristics of the released material were assumed. Since the analysis became the basis of a potentially costly Nuclear Regulatory Commission (NRC) regulation, the need to verify the assumptions in the analysis received high priority in the Department of Energy (DOE).

This report describes the results of a program conducted at Sandia National Laboratories (SNL) to establish this needed data base. Subscale and full-scale experiments¹ were performed in conjunction with an analytical modeling effort to develop a data base characterizing the release of radioactive material from a spent fuel shipping cask subjected to a hypothetical sabotage event. The experimental data base was used to develop improved estimates of the radiological health consequences resulting from the sabotage of spent fuel transports in urban regions.

The origin of the program can be traced back to 1975 when the US Department of Energy (DOE) sponsored a study at SNL to determine the ability of several generic HEDs to disrupt a large truck spent fuel shipping container. The results of this study indicated that it was indeed possible for certain HEDs to breach a large spent fuel cask.

In 1977, the NRC published a final environmental impact statement on the transportation of radioactive materials by air and other modes (NUREG-0170)⁸ which concluded that spent fuel shipments do not constitute a threat to the public health and safety. This same study stated that the risk of sabotage of radioactive materials transports is sufficiently small to constitute no adverse major impact to the environment or to public health.

However, in 1978, the NRC published a draft environmental assessment of the transport of radionuclides in urban environments.¹ The so-called "Urban Study" evaluated the radiological hazards resulting from the transportation of radioactive material in urban areas for various types of environments including those caused intentionally. The first draft version of this study, SAND77-1927¹ predicted that several hundred latent fatalities could occur from the successful sabotage of spent fuel shipments subjected to certain modes of attack. A second version of the urban study, NUREG/CR-0743³ reduced the latent fatalities to fewer than 100 based upon a reevaluation of released quantities of radioactive material.

In 1979, the NRC reacted to the initial urban study by requiring physical protection measures² for spent fuel shipments in the United States pending the availability of credible experimental data supporting or disproving these predictions. These safeguards include (1) the routing of truck and rail shipments of spent fuel to avoid densely populated areas, where possible, (2) requiring armed escort(s) for shipments traversing heavily populated areas, (3) requiring that the transport vehicle be equipped with NRC approved immobilization devices, (4) requiring that the shipments be accompanied by at least two drivers (escorts) and (5) requiring that the shipment be under constant surveillance at all stops.

In 1979, the Comptroller General of the United States published a study⁹ of federal actions needed to improve safety and security of nuclear material transportation. This study recommended that the NRC and DOE develop experimental data bases characterizing the quantity of material that could be released from the sabotage of spent fuel casks.

In response to these data requirements and requirements to support DOE fuel programs, the DOE initiated a study at SNL to evaluate the effects of intentional acts on spent fuel shipping systems and to determine experimentally the quantity, size, and chemical form of any released material. This source term data base was to be used in existing health consequence models to assess the safety and security of spent fuel transportation for these types of environments. This report describes the details and results of the DOE sponsored program.

3. PROGRAM SCOPE

The program scope was to conduct subscale and full-scale tests in conjunction with an analytical modeling study to fulfill the following objectives:

1. To evaluate the effectiveness of selected high explosives and high energy devices (HEDs) to breach a generic spent fuel cask and disperse cask contents.
2. To quantify the fraction of cask contents released as a result of the high explosive or high energy attacks on a generic cask. Mass fraction and, in cases where applicable, activity fraction were to be measured.
3. To characterize the physical and chemical properties relevant to human health risk estimates of the released radioactive material. Particle size, morphology, mass, mass concentration and elemental composition were some properties of the released material that were to be measured.
4. To develop an understanding of the material response (of both cask and fuel) to the high explosive/high energy attacks in order to develop a basis for predicting the response of similar generic casks to larger quantities of high explosives or HEDs of similar design.
5. To use this experimental and analytical data base to evaluate the health consequences resulting from a successful sabotage attack on a spent nuclear fuel shipping cask in a densely populated area.
6. To provide data to regulatory agencies for setting standards governing the shipment of civilian reactor spent fuel in the US.

Early in the program, it was realized that it would not be feasible from cost and safety standpoints to perform full-scale tests involving spent fuel in the atmosphere. It was also realized that in order to achieve the programmatic objectives in a cost efficient manner, a series of scaled tests using irradiated and unirradiated fuel should be performed. It also became clear that to maximize the precision of mass accountability and to minimize the mass loss from the event, the subscale and full-scale tests should be performed in a pressure vessel (aerosol chamber). The chamber offered the advantages of confining the released material and permitting all of the dispersed material to be recovered for mass balance and particle size measurements.

Another area of concern was the need to select a worst case attack device (ie, a device capable of causing the greatest amount of damage to the cask and maximum release of fuel while being relatively available and requiring minimal technical expertise) for the full-scale reference event.

In order to achieve the programmatic objectives and to address these areas of concern, the program was divided into the following tasks:

- Task 1:** To evaluate and characterize the effectiveness of several types of HEDs to breach generic truck casks and aerosolize and disperse spent fuel elements. Also important in this evaluation was the scaling of cask and spent fuel response parameters. This task consisted of full-scale tests using simulated cask walls and/or full-scale generic truck casks as targets for four types of HEDs described in the Urban Study¹: (1) conical-shaped charges (CSC), (2) contact-breaching charges (CBC), (3) platter charges, and (4) pyrotechnic torches. Surrogate fuel elements (depleted UO₂ fuel pins) were placed between the simulated cask walls in some of these tests. The results of this experimental evaluation were used to select a worst case attack device (HED) for the full-scale test (Task 4).
- Task 2:** To develop measurement techniques and establish maximum achievable measurement sensitivities and precisions, subscale tests were performed on spent fuel casks filled with depleted UO₂ fuel pellets (zircaloy cladding) subjected to a scaled version of the reference base HED selected in Task 1. These tests were conducted in a pressure chamber to confine the released material and permit recovery of all of the dispersed material for mass balance and particle size measurements.
- Task 3:** To develop a correlation between selected radionuclide particulate size distributions for spent fuel subjected to scaled explosive attacks and that for depleted UO₂ fuel, single pellet tests were performed. This task was completed by EG&G/Idaho National Engineering Laboratories (INEL) and involved subjecting single H. B. Robinson 2 spent fuel pellets and depleted UO₂ pellets to a scaled version of the reference base HED selected in Task 1. The correlation function developed was used to quantify released radionuclides and their fractionation for comparison with the full-scale reference test results (Task 4).
- Task 4:** To quantify and characterize the release of unirradiated fuel in a full-scale event, a generic truck cask was subjected to the reference base HED selected in Task 1. The full-scale test provided a source term data base for the reference base sabotage event which in conjunction with the results of the subscale experiments performed in Task 2 were used as primary input and data base to the Consequence Reactor Safety Model (CRAC)⁵ for estimating the radiological consequences.
- Task 5:** To develop an understanding of the cask and spent fuel material response to selected HEDs and to model the fuel breakup for various types of energy loadings, an analysis was performed to determine thermal and mechanical response of the unirradiated fuel and cask material to the reference HED. A method was developed for scaling

subscale source term parameters (released mass fractions, size fractions, etc) to the full-scale event through detailed consideration of HED characteristics, material properties and geometry.

Task 6: To complete the study, the evaluation of the radiological health effects using the experimental data derived in Tasks 1 through 5 was completed using the Consequence Reactor Safety Model (CRAC) used in the Urban Study. The expected health and economic consequences were calculated assuming a release in the Manhattan borough of New York City.

This multidisciplinary research effort was divided among the following laboratories or contractors:

- (a) Tasks 1, 2, 4 and 6 were performed at Sandia National Laboratories, Albuquerque, New Mexico. Lovelace Inhalation Toxicology Research Institute, Albuquerque, New Mexico supported the aerosol measurement activities of Tasks 1, 2, 3 and 4.
- (b) The experimental work of Task 3 was performed at EG&G Idaho National Engineering Laboratory, Idaho Falls, Idaho.
- (c) Task 5 was performed by SNL personnel and by Professor F. M. Gelbard while at the Massachusetts Institute of Technology.

The analytical and experimental results of the work performed in Tasks 1-6 are summarized in Section 4, Summary of Results.

4. SUMMARY OF RESULTS

4.1 HED Evaluation Tests

An extensive survey of attack devices which could be available to a saboteur and which showed a potential for breaching a nuclear spent fuel shipping container was performed. The types of shipping containers with which this study was concerned limited the modes of attack to high energy and/or high explosive devices. Because of the heavy radiation shields and container damage-resistance requirements, spent fuel shipping casks are very large and massive and may weigh from 22 to 88 t or more depending on the type of cask. Wall construction of these casks include combinations of stainless steel, lead, depleted uranium, water, wet cement, and resin. Table 4.1.1 provides wall material data for five spent fuel truck casks considered in this study. A previous study at SNL of several high explosive devices has shown that the variety of attack devices capable of penetrating and/or breaching a full-size truck cask is limited. A survey of the attack devices shown in Table 4.1.2 was performed in this study for the purpose of selecting several candidates for more detailed evaluation and subsequent testing. From Table 4.1.2, the devices were selected based on their availability to the perpetrator and their potential to breach truck casks of the type listed in Table 4.1.1. The details of the tests performed and the HED device selected is contained in Appendix A of Volume II of this report.

4.2 Development of Measurement Techniques and Assessment of Experimental Precision: Subscale Tests

Seven tests using 1/4-scale casks and/or depleted UO_2 fuel pins were conducted in support of the second task to develop source aerosol measurement techniques and to provide a data base for assessing measurement precisions and experimental feasibilities in anticipation of the full-scale cask/fuel test.

The results of two preliminary tests* (Tests 1 and 2) subjecting simulated cask walls and depleted UO_2 fuel pins to explosive charges in an open environment indicated that it was not feasible to make accurate mass balances of uranium fuel released in an unconfined area. For this reason, and also in order to obtain time histories of source aerosol parameters, subsequent scaled and full-scale tests were conducted in containment. The containment pressure vessel offered the advantages of confining the aerosol and permitting all of the disrupted and/or dispersed fuel to be recovered for mass, elemental and particle size analyses. Table 4.2.1 lists the five confined scaled cask/ UO_2 fuel tests (3 through 7) conducted together with the purpose and results of each test.

* Appendix C: Subscale/Full-scale Tests: Test Data

TABLE 4.1.1
Construction Material Data for Truck Spent Fuel Shipping Casks

CASK	NFS-4 (mm)	NLI 1/2 (mm)	TNS (mm)	TN-9 (mm)				
Material Layers - Side ¹ (Thickness)	7.9	321 SS	1.27	SS	6	304 SS	6	304 SS
	168.4	Lead	69.9	Dep. Uran.	5	Copper Plates	5	Copper Plates
					150-185	Lead	150	Lead
	31.8	321 SS	54	Lead	10	Wet cement	10	Cement
	114.3	Borated water	22.2	SS	20	Carbon steel	20	Carbon Steel
	4.2	321 SS	127	Water	150	Borated resin	150	Borated Resin
		6.4	SS	200	Copper fins	200	Copper Fins	
Material Layers - Bottom (Thickness)	203.2	SS	31.8	SS (Inner cavity)	7.6	304 SS	7.6	304 SS
			88.9	SS	226.1	Lead	226	Lead
			200.7	Dep. Uran.	16	304 SS	16	304 SS
			80.8	SS				
Material Layers - Top (Thickness)	190.5	SS	48.3	SS	38	304 SS	38	304 SS
			193	Dep. Uran.	208	Lead	208	Lead
			80.2	SS	25.4	304 SS	25.4	SS
			72.4	SS (outer closure)				

¹Dimensions given in millimeters. Material layers are listed in order from inside of cask.

Reference: Directory of Certificates of Compliance for Radioactive Materials Packages, US Nuclear Regulatory Commission, NUREG-0383, December 1981

TABLE 4.1.2

High Energy Devices Surveyed

THERMAL	MECHANICAL (LOW VELOCITY)	MECHANICAL (HIGH VELOCITY)	ELECTRICAL	CHEMICAL
Pyrotechnic Torch	Demolition Saw	Explosive Air Blast	Arc	Acid
Gas Torch	Grinder	Explosive Shaped Charge	Electron Beam	Exothermic
Thermite	High Speed Drills	Explosive Flyer Plate	Laser	Reagents
Burn Bar		High-Velocity Projectiles		
		Rod Penetrators		
		Explosive Contact Charge		
		High-Velocity Particles		

TABLE 4.2.1

Summary of Scaled Cask-Explosive Device Tests

<u>No.</u>	<u>Date</u>	<u>Target</u>	<u>Test Type</u>	<u>Purpose and Results</u>
3	1/80	Thick steel target	Chamber (1/4-scale HED)	Feasibility of chamber test. Evaluation of aerosol sampling instruments and isolation valve. Multicomponent aerosol observed requiring several aerosol instruments for measurement of mass and size.
4	2/80	Thick steel target	Chamber (1/4 scale HED)	(Same as Test No.3)
5	3/80	Zircaloy clad depleted UO ₂ fuel pins	Chamber (1/4-scale HED)	(Same as Test No.3) Verification of uranium fluorometric analyses.
6	6/80	1/4-scale cask containing short sections of a 5 x 5 array of surrogate fuel pins. No water coolant was used in this test.	Chamber (1/4-scale HED)	Determined respirable UO ₂ release fraction based upon removed fuel mass (0.0036) from dry 1/4-scale cask using 1/4-scale EID.
7	3/81	1/4-scale cask containing short sections of a 5 x 5 array of surrogate fuel pins. Water was used in fuel cavity and outer water jacket.	Chamber (1/4-scale HED)	Determined respirable UO ₂ release fraction based upon removed fuel mass (0.00014) from a wet 1/4-scale cask using a 1/4-scale EID.

Tests 3, 4, and 5 were conducted to evaluate aerosol measurement and analytical techniques for explosive environments and to evaluate the overall experimental system. Five 3 in. thick steel blocks were used as targets for a scaled version of the reference HED in Tests 3 and 4, and three 30 cm long sections of depleted UO_2 fuel pins were the targets for Test 5. Test 6 used a 1/4-scale dry cask containing a 5 x 5 array of 0.9 m long full-scale UO_2 fuel pins and Test 7 used a 1/4-scale cask containing $3.96 \times 10^{-3} \text{ m}^3$ of water coolant and a 5 x 5 array of 0.9 m long full-scale UO_2 fuel pins in the fuel cavity. The results of Tests 6 and 7 were used to predict release parameters for a full-scale event and to provide an understanding of the achievable precision measures and experimental resolution of measured release parameters.

Figure 4.2.1 is a schematic of the steel confinement chamber which was used in Test 3 through 7. The steel cylindrical chamber was a 28.9 m^3 (net volume) pressure vessel sealed at one end and having an air-tight door at the other end. The HED was mounted externally to the chamber and fired into the chamber through a 6.4-mm-diameter port in a flanged assembly mounted externally to the chamber. An explosively actuated isolation slide valve was used between the HED and the chamber to prevent release of gases and dispersed fines from the chamber.

Five sampling ports penetrated the chamber in various locations. The ports were closed by remotely operated pneumatic 2.5-cm-diameter valves. The valves were kept closed until after detonation to prevent damage to the aerosol sampling equipment by the shock wave. Since no single aerosol instrument can size particles over the size range of interest (from $0.01 \mu\text{m}$ to about 2 mm diameter), a battery of instruments listed in Table 4.2.2 was selected to measure the size and mass of particles collected. Aerosol size parameters as a function of time were determined from cascade impactor samples obtained at various time intervals after HED detonation. Similarly, filter samples provided a time history of the change in mass concentration. Changes in morphology were shown by sequential electrostatic precipitator (ESP) samples and changes in number concentration were shown by continuous recording condensation nuclei counters. After each test, all debris were collected from surfaces inside the test chamber and separated into material not containing uranium and materials suspected of containing uranium. All uranium containing material was sieved, the mass determined, and uranium fluorometric and wavelength dispersive x-ray fluorescence analyses performed. Transmission (TEM) and scanning (SEM) electron microscopy and energy dispersive x-ray analysis (EDXA) were used to determine the elemental composition and morphology of particles collected by ESPs.

The aerosol-sampling procedure was designed to provide a time history of selected aerosol parameters (such as concentration, particle size distribution, and morphology) in the chamber. From the aerosol time history, calculations could be performed to determine initial release parameters. Figure 4.2.2 is a schematic of the experimental setup for Test 6 prior to detonation of the HED. A total UO_2 fuel mass of 15.3474 kg was measured before the event. Figure 4.2.3 is a reconstruction of the test configuration

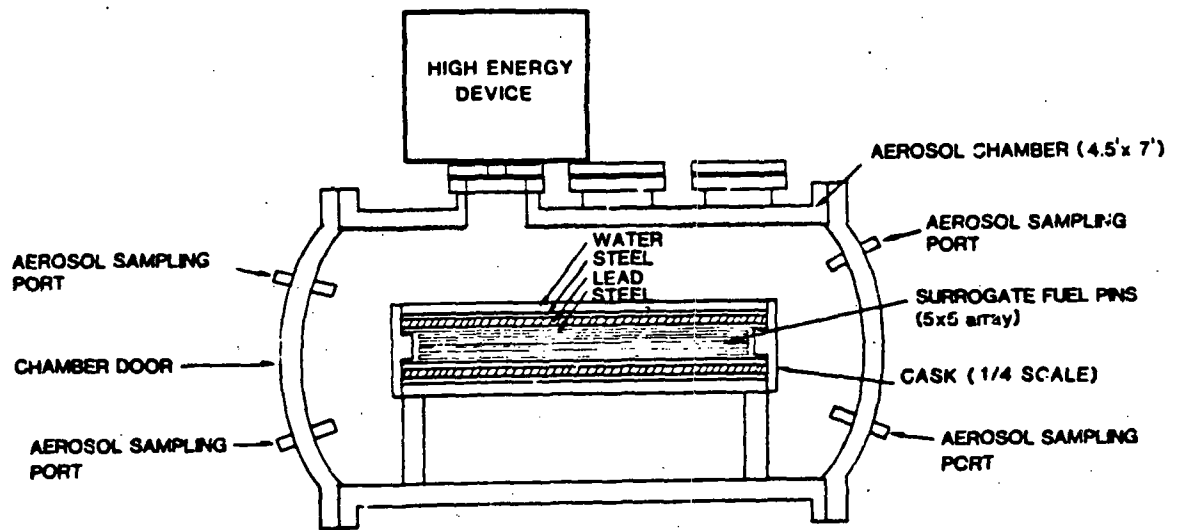


Figure 4.2.1 Schematic of Confinement Chamber and 1/4-Scale Cask Used in Tests 3 Through 7.

TABLE 4.2.2

Sampling Instruments Used in 1/4-Scale Chamber Tests

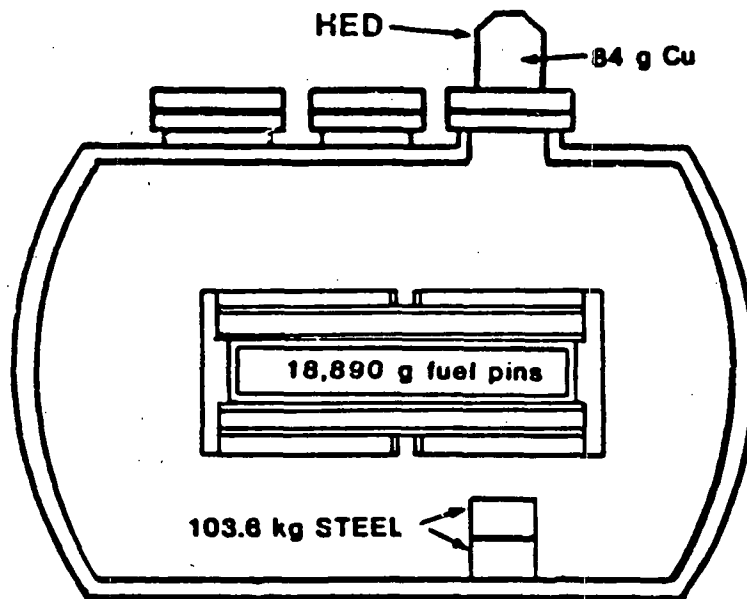
Instrument and Applicable Size Range	Purpose of Samples	Analytical Model
LMJ Cascade impactors 0.5 - 12 μm	Aerodynamic size, geometric standard deviation of total aerosol mass and UO_2 mass.	Gravimetric (Cahn microbalance) and fluorometry for determination of uranium.
Point-to-plane electrostatic precipitator TEM & SEM 0.01 - 12 μm	Particle morphology, count distribution and elemental distribution	Transmission and scanning electron microscopy and energy dispersive x-ray analysis
Filter 37 mm, sequential, 0.01 - 12 μm	Provide a time history of total aerosol and uranium mass after EID detonation. Samples for surface area measurements.	Gravimetric for total mass and uranium by fluorometry, BET nitrogen absorption for surface area measurements.
Filter 37 mm, front surface reentrant filter (FSRP) 0.01 - 12 μm	Sequential filter samples from filters inside chamber to compare with filters obtained by extractive techniques to address aerosol line losses.	Gravimetric for total mass of aerosol and uranium by fluorometric techniques.
^b Condensation nuclei counter (CNC) 0.001 - 12 μm	Total count of aerosol particles vs. time after detonation.	Optical light scattering instrument.
^a Electrical aerosol analyzer (EAA) Dia 1.0 μm	Size distribution parameters for particles between 0.01 and 1.0 μm .	Electrical mobility.
Sieves (38 - 2000 μm)	Provide size distribution data on larger particles of surrogate spent fuel.	Mechanical sieving followed by weighing for total mass and fluorometry for uranium determination.

^aLovelace Multijet.

^bData from these instruments are not included in this report.

QUARTER SCALE TEST (DRY)

SURROGATE FUEL/CASK



BEFORE EVENT

CASK wt. = 316.04 kg

18,890 g fuel pins \rightarrow 15,347.4 g UO_2 + 3,548.8 g Zr-4

Figure 4.2.2. Schematic of the Experimental Setup for "Dry" Test 6 Prior to Detonation of HED

QUARTER SCALE TEST (DRY)

AFTER EVENT

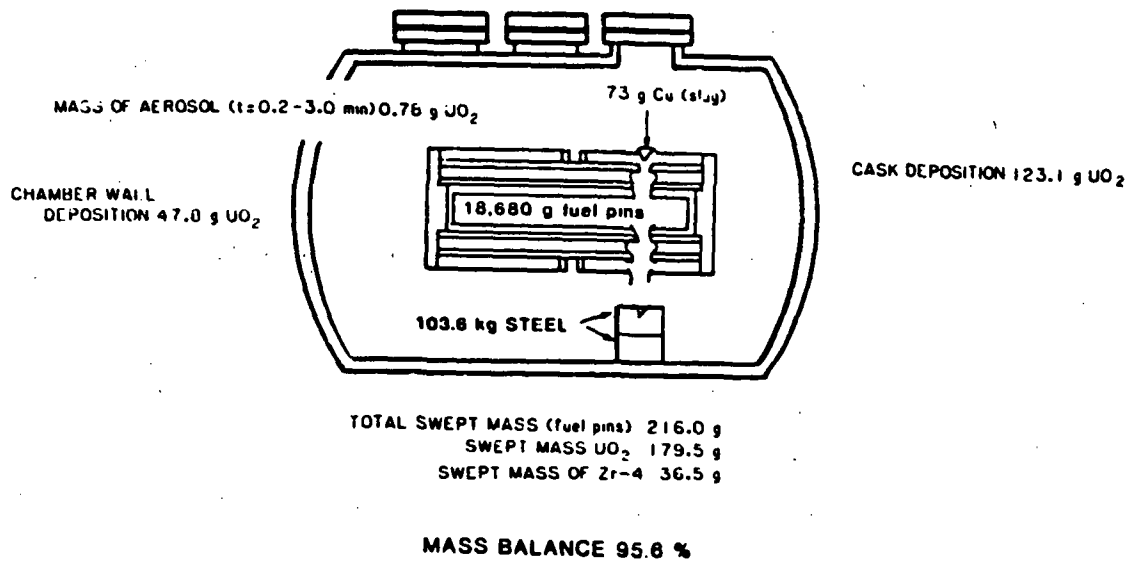


Figure 4.2.3. Schematic of Test 6 (Dry) Immediately After Detonation.

immediately after detonation. A total UO_2 fuel mass of 15.1679 kg remained in the cask after the event which indicated that approximately 179.5 g of UO_2 fuel was removed from the fuel assembly as a result of the HED action. One hundred and twenty three grams of UO_2 were deposited in the cask, 47.8 g of UO_2 were deposited and recovered from the chamber walls and floor and 0.78 g of UO_2 was released as an airborne aerosol. Not accounted for in this test was 7.8 g of UO_2 , approximately 4.3 percent of the total UO_2 fuel mass. The unaccounted-for UO_2 mass was believed to be of particle sizes greater than $30 \mu\text{m}$ which were deposited, but not collected, on surfaces inside the test chamber.

Figure 4.2.4 shows a time history of the UO_2 aerosol mass within the chamber based on sequential filter samples. The exponential decay of UO_2 aerosol mass indicates that no unusual phenomena were occurring in the chamber and that the first filter sample taken from 0.2 min to 3 min after detonation is consistent with all subsequent filter samples. A maximum UO_2 aerosol mass concentration of 0.27 mg/l was detected at 12 seconds postdetonation. Using the containment chamber volume of 2886 l and assuming a uniform spatial concentration, a total released UO_2 aerosol mass of 0.78 g was calculated. Assuming that 100 percent of the measured UO_2 aerosol mass is in the respirable size range, a total UO_2 respirable mass of 0.78 ± 0.005 g was released from the cask as a result of the event.

Sequential cascade impactor samplers were also taken to give a time history of aerosol size distribution parameters. Figure 4.2.5 shows the mass median aerodynamic diameter (MMAD) and geometric standard deviation as a function of time for Test 6. Assuming a single-mode lognormal distribution, mass median aerodynamic diameter (MMAD) reached a maximum of $3.5 \mu\text{m}$ after approximately 12 min. The size then stabilized at $2.0 \mu\text{m}$ after 30 min. Fluorometric determination of uranium dioxide concentrations indicated concentrations ranging from 7 percent of the total aerosol mass at early times to about 2 percent 10 min after detonation. Similar UO_2 aerosol percentages were also observed in EDXA studies of ESP collected samples with spectra attributable to Pb, Cu, Al, Fe, and U.

Figure 4.2.6 summarizes the fuel pin damage caused by the action of the HED. Ten fuel pins sustained a net mass loss of 216 g (zircalloy and UO_2) and the remaining fifteen fuel pins sustained no detectable mass loss. Twelve fuel pins sustained some degree of cladding failure ranging from small cracks to complete shearing of the cladding and five of these fuel pins were completely sheared. The average fuel pin length completely removed by the action of the HED was 21 mm. The average diameter of the hole in the 5 x 5 fuel pin array was approximately 19.8 mm. The average diameter of the entrance hole in the cask steel wall was 12.7 mm. The average entrance hole diameter in the cask lead wall was 50 mm. The 27.9-cm-diameter cylindrical cask was completely penetrated by the action of the HED. Figure 4.2.7 is a photograph of the cask cross section showing relative hole sizes in the steel/lead cask wall. Further details of Test 6 are reported in Appendix C--Subscale/Full-scale Test Data.

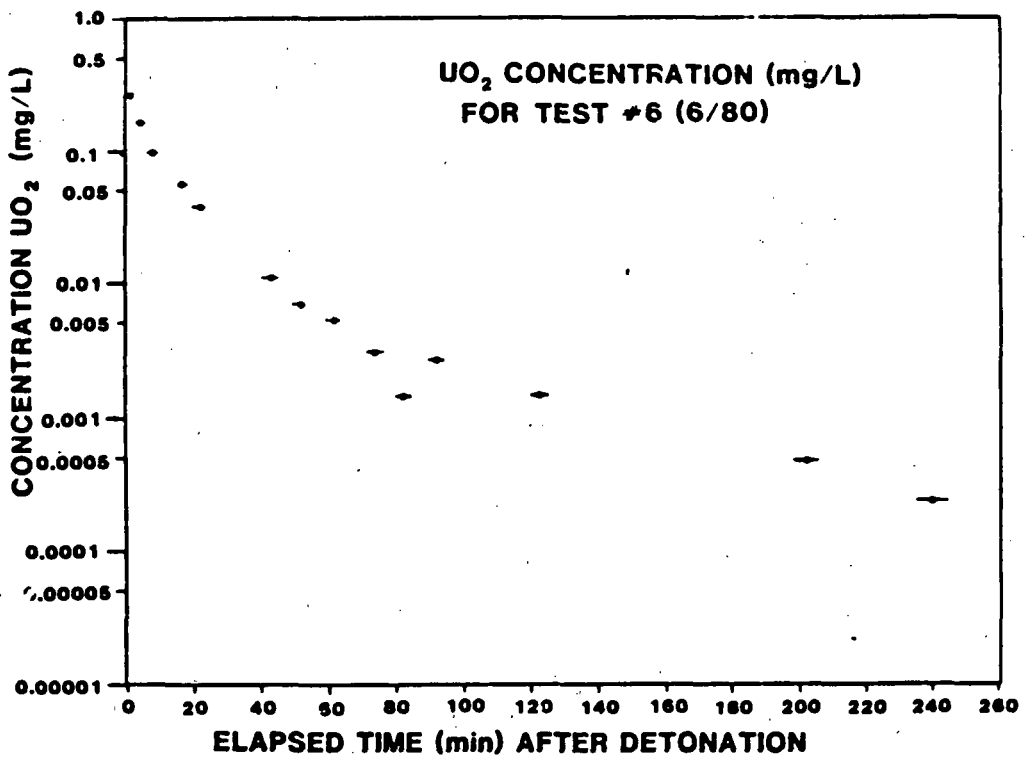


Figure 4.2.4 Time History of UO₂ Aerosol Mass Concentration Based on Sequential Filter Samples.

TIME HISTORY OF MASS MEDIAN AERODYNAMIC DIAMETER
AND GEOMETRIC STANDARD DEVIATION, TEST #6, 6/80

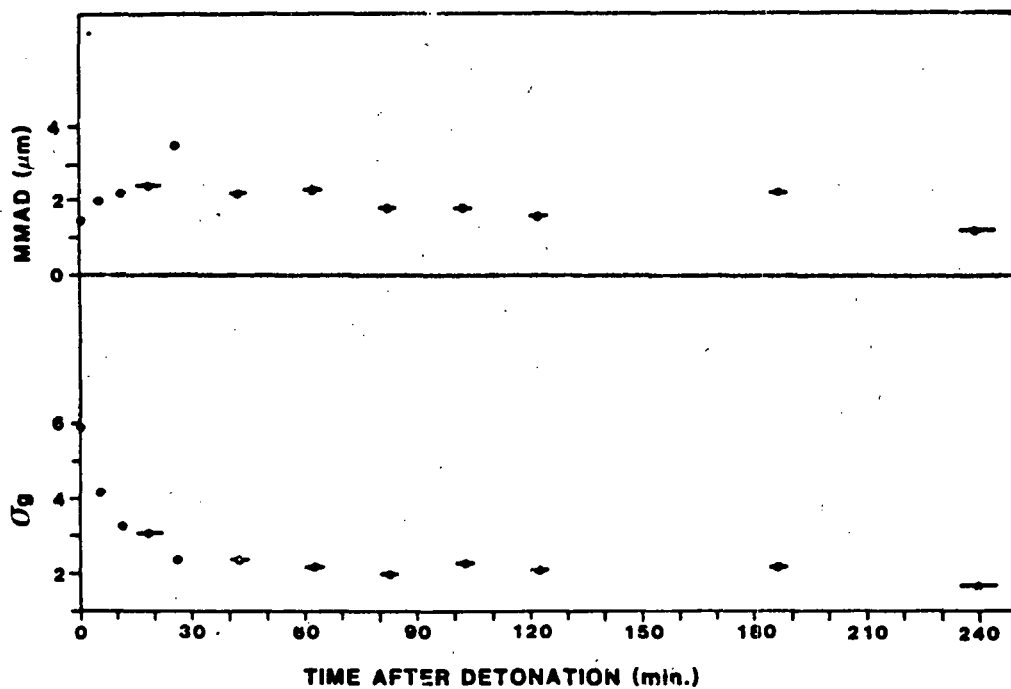


Figure 4.2.5 Time History of Mass Median Aerodynamic Diameter and Geometric Standard Deviation for Test 6.

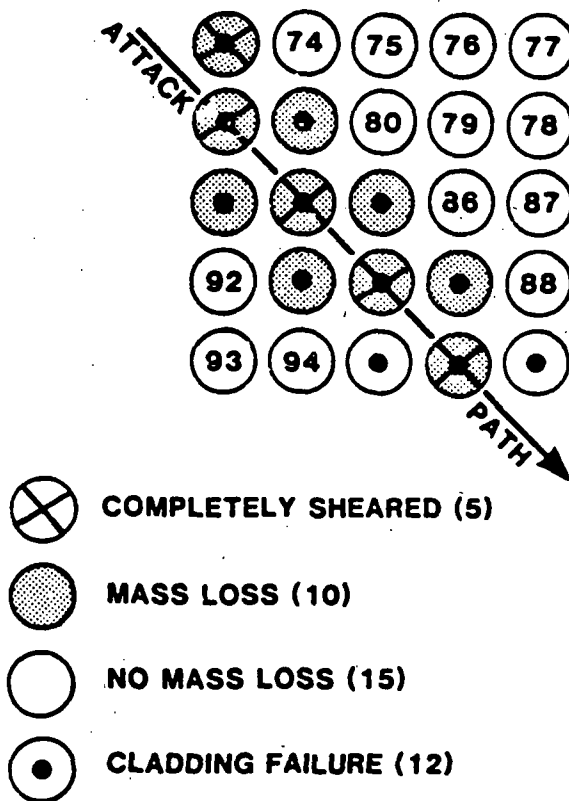


Figure 4.2.6 Schematic of Fuel Pin Damage and Damage Path Caused by Action of HED for 1/4-Scale Dry Test 6.

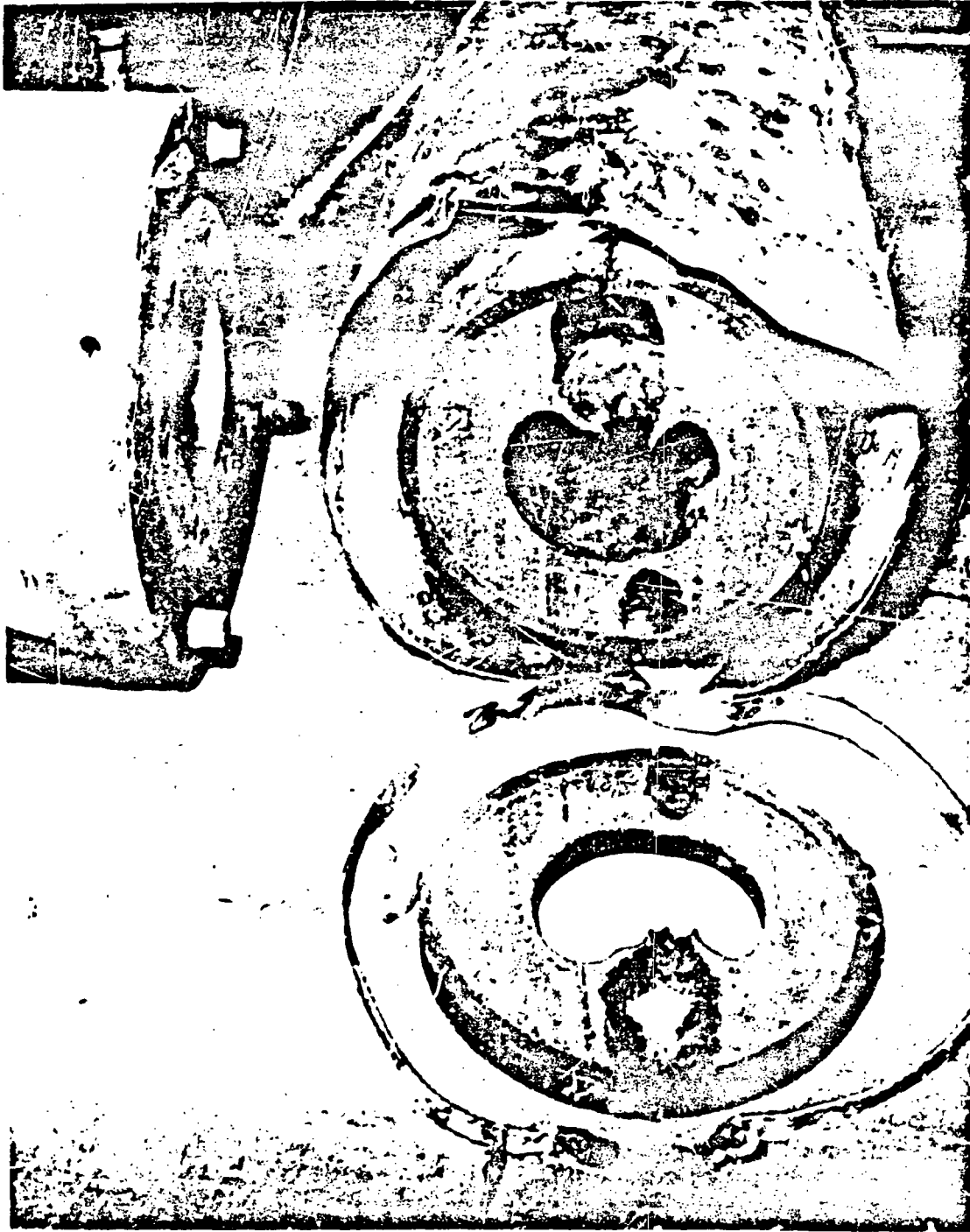


Figure 4.2.7 Photograph Showing Cask Damage for 1/4-Scale Cask Test 6 (Dry)

Some light water reactor shipping casks have been designed so that the outer shell and fuel cavities may be filled with water (see Table 4.1.1). This configuration was investigated to determine the impact on aerosol production from a "wet" shipping cask subjected to high explosive attacks. Figure 4.2.8 is a schematic for Test 7 showing the cask immediately after detonation. The cask fuel cavity and cask outer shell contained $3.96 \times 10^{-3} \text{ m}^3$ and $16.6 \times 10^{-4} \text{ m}^3$ of water respectively. A total respirable uranium dioxide mass of $19.6 \pm 2.0 \text{ mg}$ was measured at 12 seconds after detonation. This mass of released aerosol from the "wet" scaled Test 7 was approximately a factor of 40 less than that for the "dry" Test 6. A similar reduction was also reflected in the total removed fuel mass of 143 g from the "wet" fuel assembly versus 216 g in the case of the "dry" test. "Removed" in this context is defined to be that mass which is displaced from the fuel assembly but not necessarily from the cask cavity. Apparently, the presence of water in the cask water jacket and cavity resulted in scrubbing of the suspended particles and reduction in the total aerosol release. Further details of the scrubbing process is described in Appendix C: Subscale/Full-scale.

Figure 4.2.9 shows a time history of the aerosol mass concentration within the chamber based upon sequential filter samples extracted from the chamber and also shows front surface reentrant filter measurements. The exponential decay of the aerosol mass in Figure 4.2.9 indicates that the first filter samples (used for respirable release calculations) is consistent with all subsequent filter samples obtained. This figure also indicates that the front surface reentrant filter saw essentially the same concentration as did extractive techniques using externally mounted filters and that aerosol transport line losses in the extractive filter samples did not account for significant losses. Figure 4.2.10 shows the time history of the uranium and zirconium concentration versus time. These samples were based on uranium fluorometric analyses of extractive filters, uranium x-ray fluorescence analyses of alternate front surface reentrant filters and zirconium x-ray fluorescence analyses of front surface reentrant filters. These data indicate that no significant line losses occurred in the extractive sampling system and that the fraction of aerosolized zirconium was proportional to the fraction of zirconium present in the fuel pins before testing. Figure 4.2.11 shows the time history of the aerosol size for the subscale wet test. Whereas in the case of the dry test, the MMAD stabilized around $2 \mu\text{m}$, in the case of the wet test, the MMAD started out at about $1 \mu\text{m}$ at $t \approx 0$ and stabilized near $0.8 \mu\text{m}$ after 30 minutes post detonation. The geometric standard deviation (σ_g) also remained fairly constant at around 2.5.

The morphology of aerosol particles from the wet test is dramatically different than aerosols obtained in the dry test. Figure 4.2.12 is a TEM photomicrograph of aerosols obtained with the point-to-plane ESP for Test 7. Figure 4.2.13 is a TEM photomicrograph of aerosols obtained with the point-to-plane ESP for the "dry" Test 6. In contrast to the aerosols from the "dry" test wherein the aerosol size distribution was dominated by the ultrafine chain agglomerate aerosols, the aerosols from the "wet" test were larger particles consisting mainly of collapsed ultrafine chain agglomerate filaments. Apparently, the large amount of vaporized water results in supersaturation within the chamber and subsequent scavenging of the chain agglomerate aerosols. Subsequent evaporation of the droplet collapses the

QUARTER SCALE TEST (WET)

AFTER EVENT

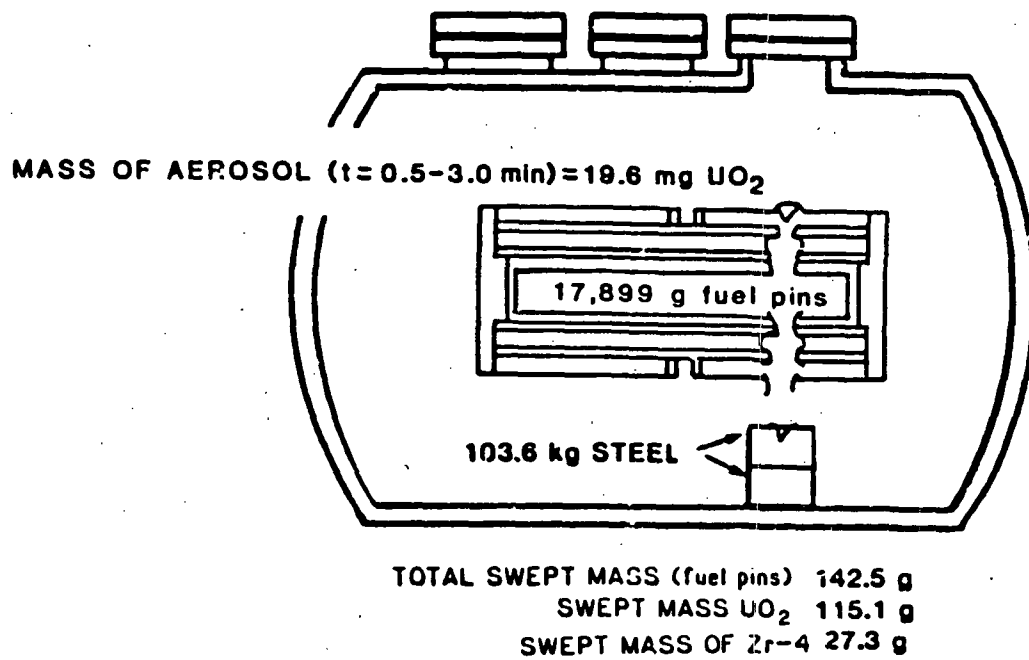


Figure 4.2.8. Schematic of Test 7 (Wet Test) Immediately After Detonation

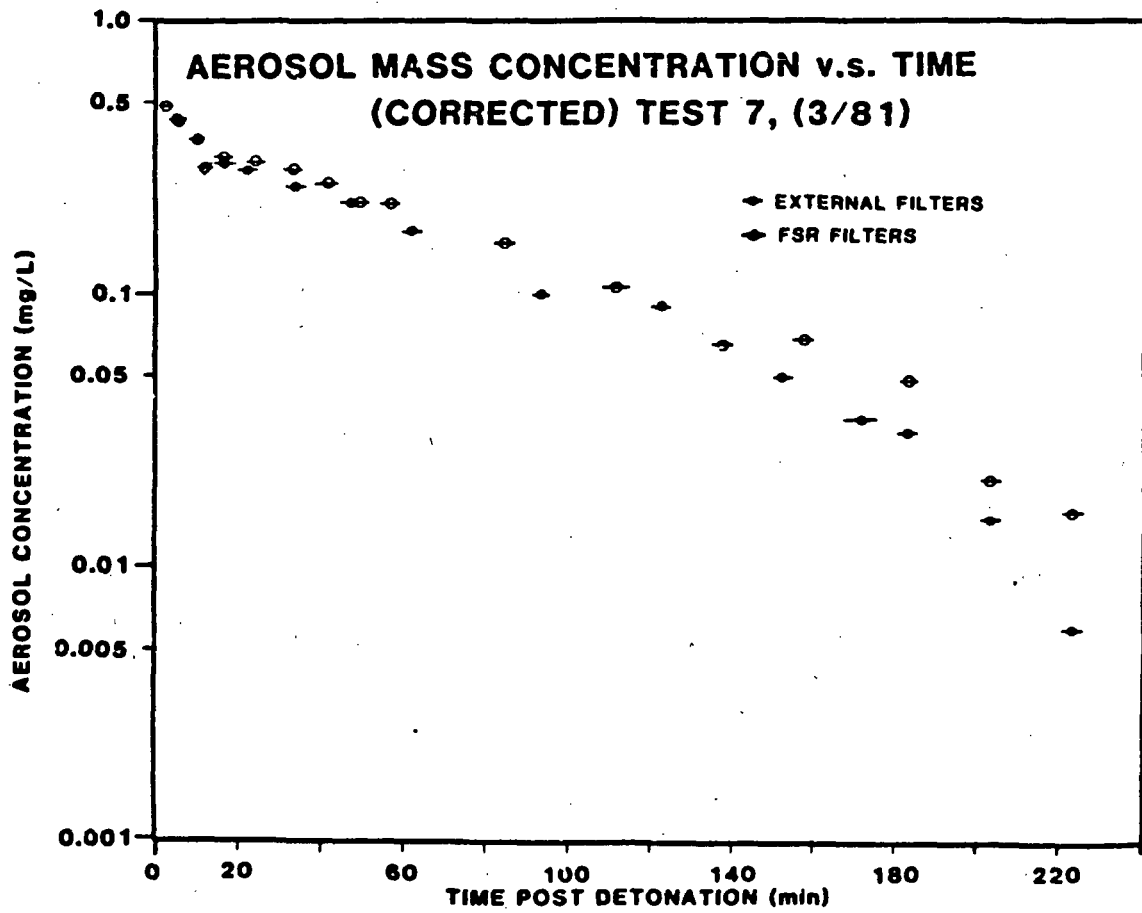


Figure 4.2.9. Time History of Aerosol Mass Concentration Within Chamber Based Upon Sequential Filter Samples and Front Surface Reentrant Filter Samples for Test 7.

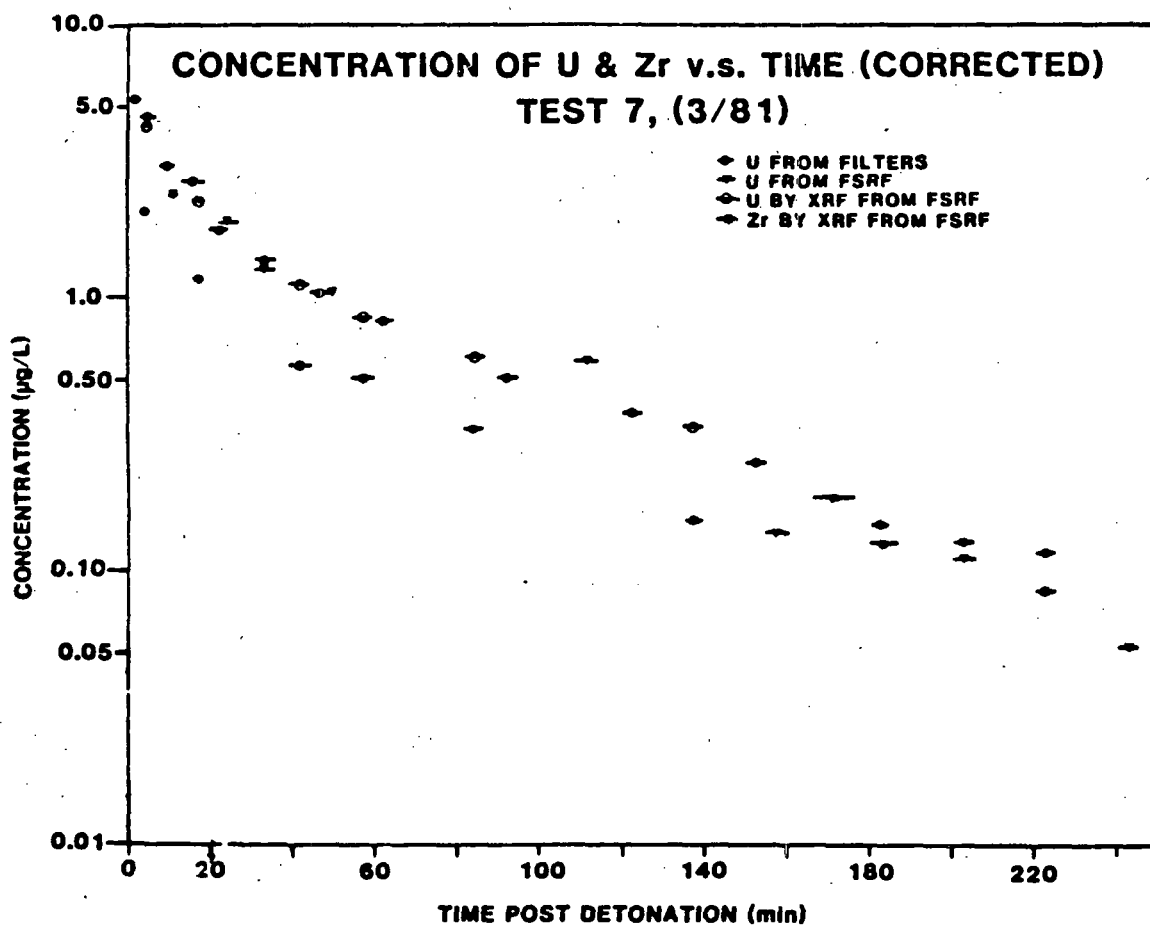


Figure 4.2.10. Time History of U and Zr Mass Concentration Based Upon Extractive Filter and front surface reentrant filter (FSRF) Samples. X-ray Fluorescence analyses were performed on FSRF samples.

SANDIA TTC SSEP TEST #7, 3/5/81
AEROSOL SIZE DISTRIBUTION

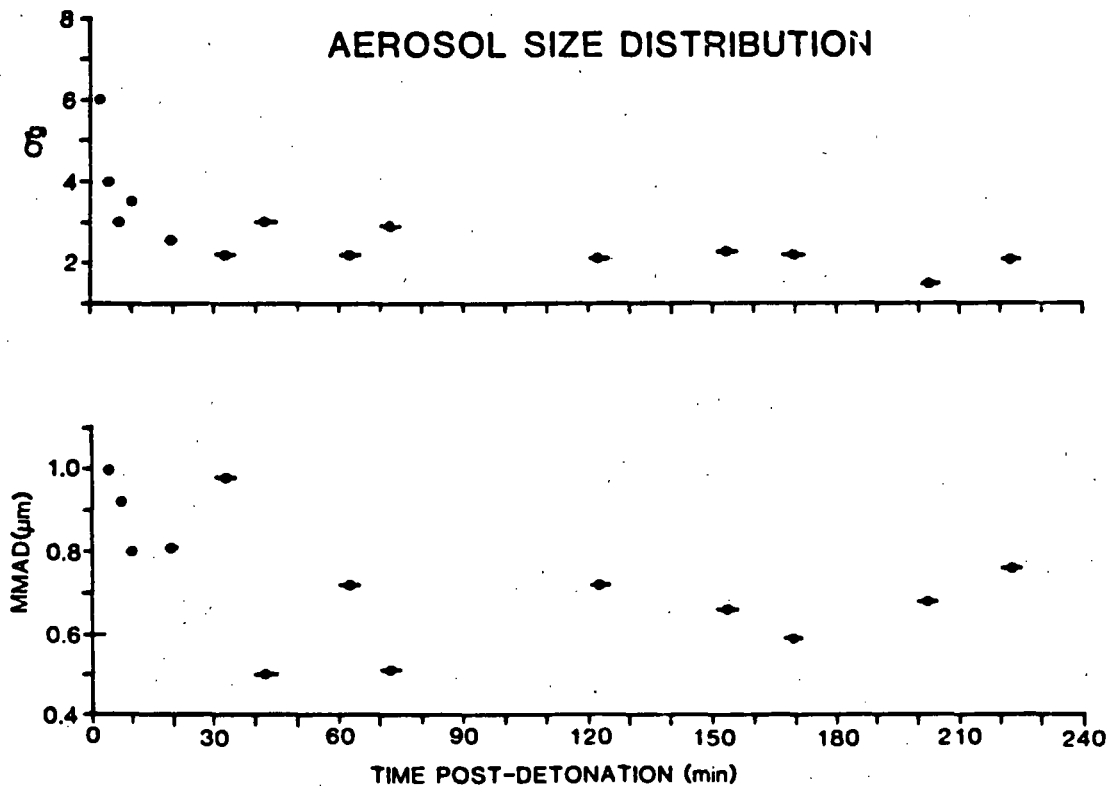
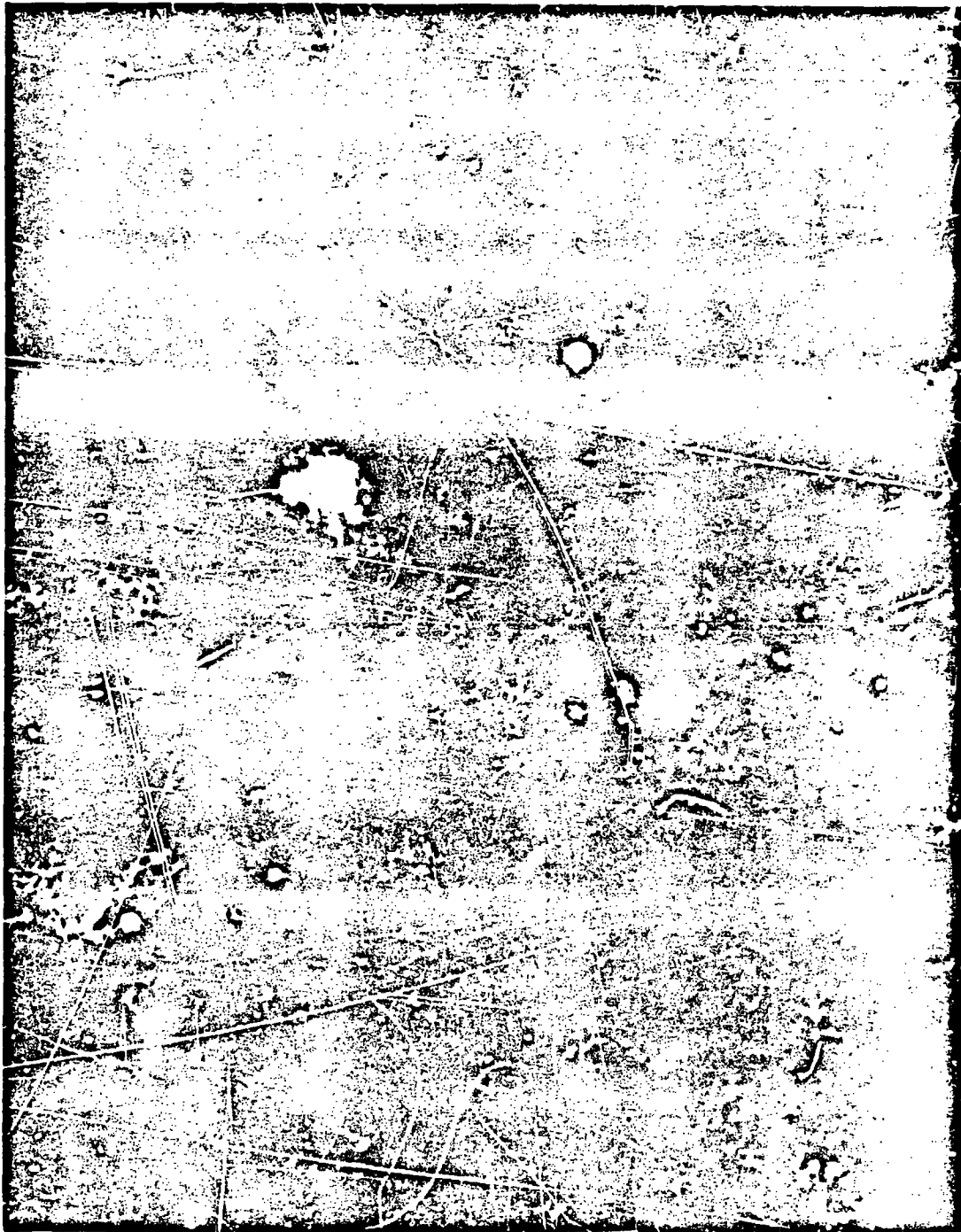


Figure 4.2.11 Time History of Aerosol Site (MMAD) and Geometric Standard Deviation (σ_g) for Wet Test 7.



5.0 μm

Figure 4.2.13. TEM Photomicrograph of Aerosols Collected With Electrostatic Precipitator (ESP) Sampler for Dry Test 6.

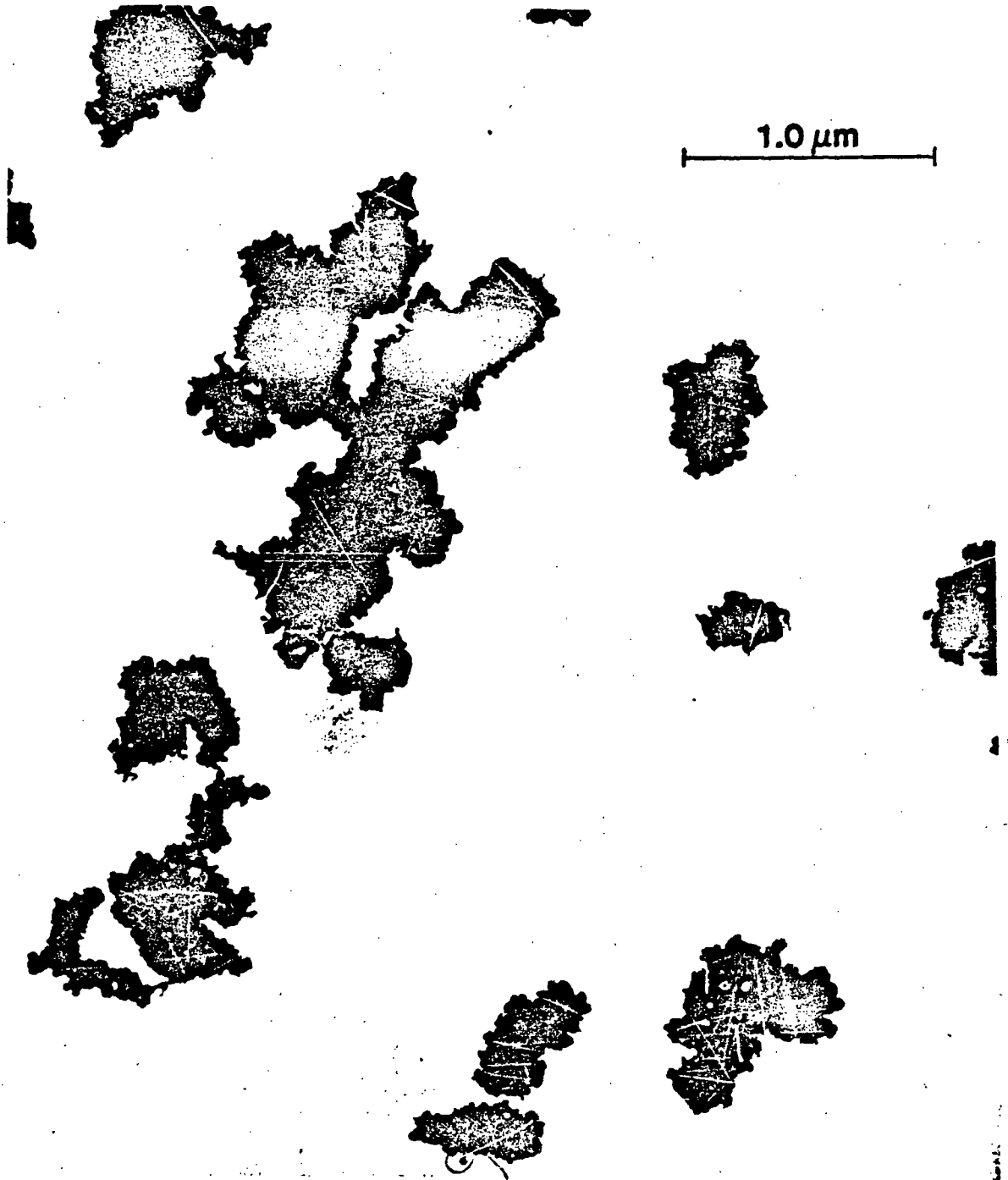


Figure 4.2.12 TEM Photomicrograph of Aerosols Collected With Electrostatic Precipitator (ESP) Sampler for Wet Test 7. Magnification is 40,000x.

filamentous structure of the chain agglomerate aerosol. The resultant size distribution is shifted from the $2 \mu\text{m}$ aerodynamic diameter typical of the chain agglomerate structure, as seen in the highly concentrated aerosol from the "dry" test to a smaller size distribution typical of particle clumps of mean diameter of about $0.8 \mu\text{m}$ in the case of the "wet" test. A large amount of debris varying in size from several micrometers to centimeter-size chunks of metal and fuel pins remained on the floor of the chamber following both types of tests. These samples were passed through a series of sieves ranging in size from $2,000 \mu\text{m}$ diameter to $38 \mu\text{m}$ diameter. The results of the sieve analysis are shown in Figure 4.2.14, where sieve diameter versus cumulative mass percent for both "dry" (Test 6) and "wet" (Test 7) are displayed. Both total mass and UO_2 mass distribution are shown for Tests 6 and 7. These data indicate that the total debris were bimodal in size distribution, probably as a result of two different mechanisms of formation: (1) a mechanical fracture of the UO_2 fuel target; and (2) vaporization/melting of some of the components (lead and steel) in the 1/4-scale cask.

Figure 4.2.15 shows the results of aerosol mass concentration calculated from the continuous flow condensation nuclei counters. These data reflect the fact that the "dry" Test 6 produced 40 times as much aerosolized mass as did the "wet" Test 7. Additionally, the wet test shows a "catastrophic decay" of aerosol mass concentration after a time period of ~ 200 min postdetonation. This phenomenon has also been reported by investigators in the Netherlands.¹⁰

Figure 4.2.16 summarizes the fuel pin damage for Test 7. Eight fuel pins sustained a net mass loss of 142.5 g (UO_2 and zircaloy). The remaining 16 fuel pins sustained no detectable mass loss. Nine fuel pins showed some degree of cladding failure and eight of these fuel pins (the same fuel pins which sustained a net mass loss) were completely sheared by the action of the HED. The average fuel pin length which was completely removed by the action of the HED was 20 mm. The average diameter of the entrance hole in the cask steel wall was 12.5 mm. The outer 0.76 mm thick steel shell was peeled back from the cask as shown in Figure 4.2.17 and was caused by hydrodynamic forces from the HED transmitted through the water in the outer jacket. The average entrance hole diameter of the cask lead shell was 48 mm. The 27.9 cm diameter cylindrical cask was completely penetrated by the HED.

Summary of Subscale Test. Measurements conducted in the subscale test program are summarized in the following statements:

1. A measured released respirable quantity (maximum) of $0.78 \text{ g} \pm 0.05 \text{ g}$ of UO_2 was determined for a 1/4-scale dry cask Test 6. A linear extrapolation from the 1/4-scale event to a full-scale event using the selected reference HED and a full-scale truck cask containing three PWR assemblies yields a respirable aerosolized release fraction of 0.0023 percent of the total heavy metal inventory.

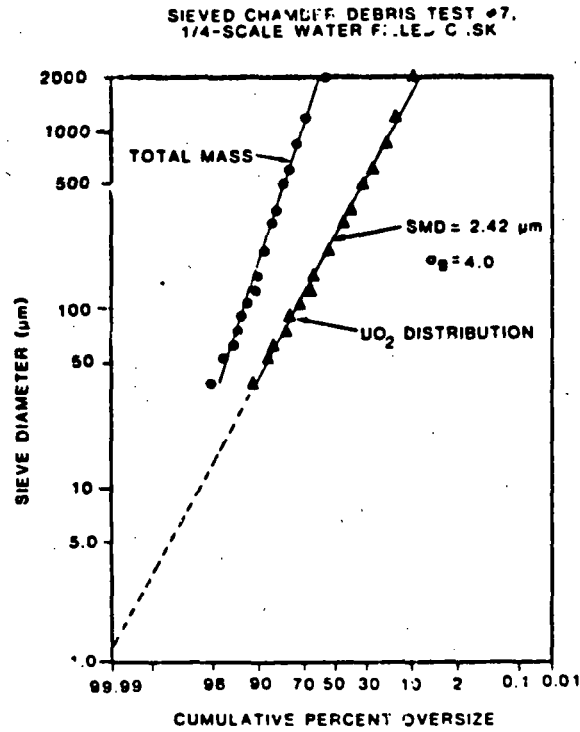
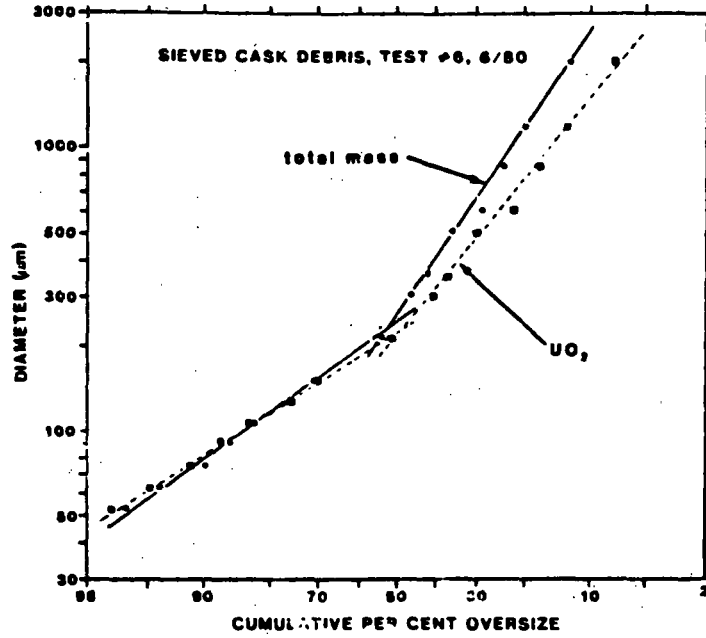


Figure 4.2.14. UO₂ and Total Mass Distribution Based Upon Sieved Debris Released From Cask Into Pressure Chamber for Tests 6 and 7.

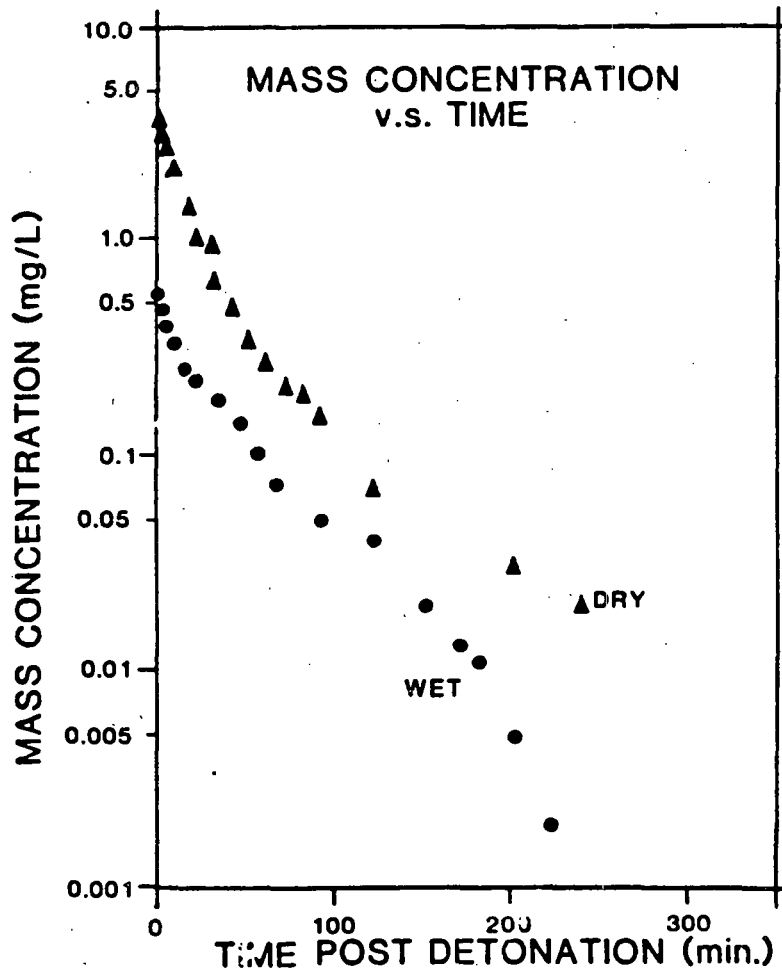
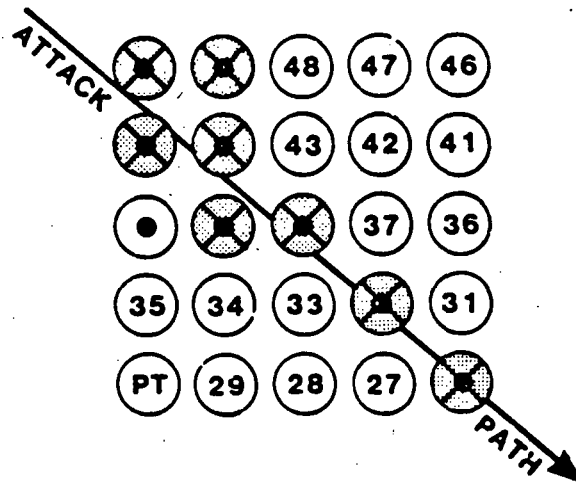


Figure 4.2.15. Total Aerosol Mass Concentration Based Upon Continuous Flow Condensation Nuclei Counters of Tests 6 (Dry) and 7 (Wet).







-  COMPLETELY SHEARED (8)
-  NO MASS LOSS (16)
-  MASS LOSS (8)
-  CLADDING FAILURE (9)

Figure 4.2.16. Schematic of Fuel Pin Damage and Damage Path Caused by Action of HED for 1/4-Scale Wet Test 7.

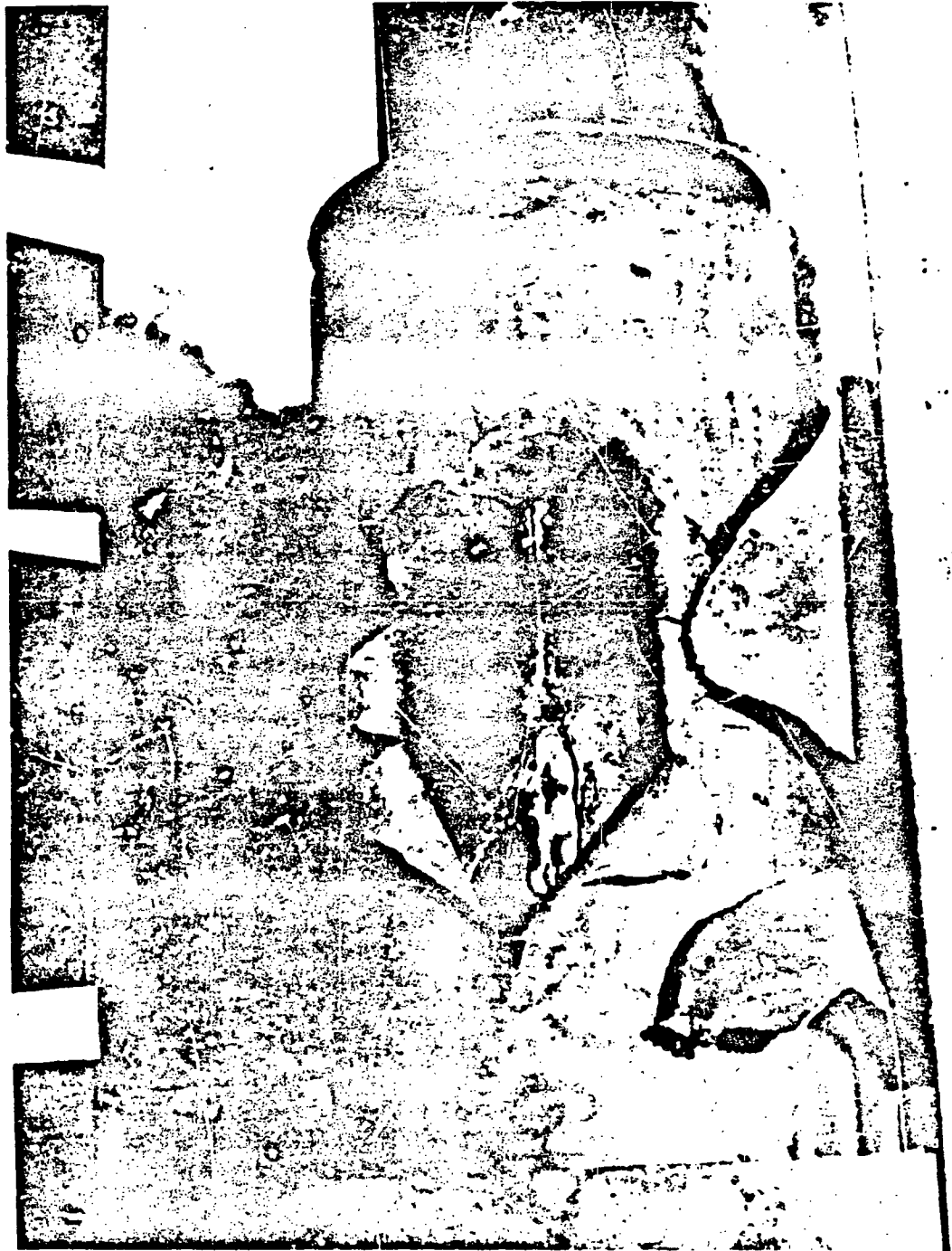


Figure 4.2.17. Photograph Showing Cask Damage for 1/4-Scale Cask Test 7 (Wet). View of exit hole produced by HED.

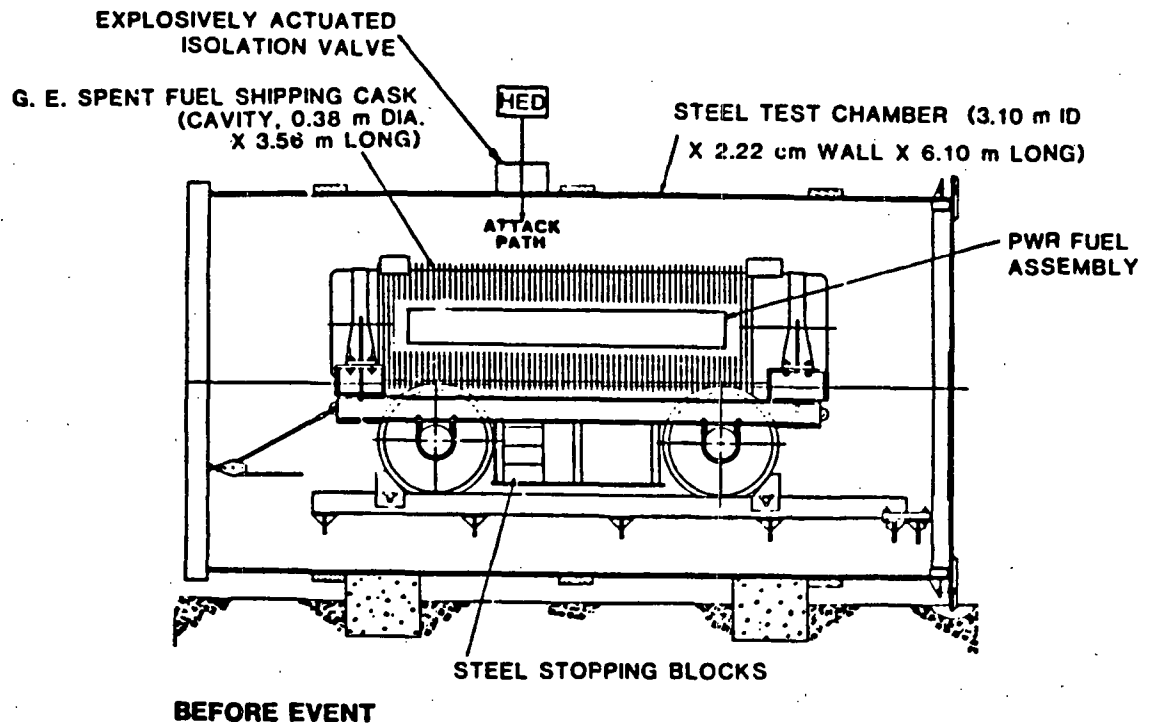
2. A measured maximum released quantity of 19.6 ± 2.0 mg of UO_2 was determined for the 1/4 scale wet cask Test 7. This aerosol mass was approximately 40 times less than that for the dry cask Test 6. Based on these results and the intent to select the more conservative test case, the dry cask configuration was chosen for the reference base full-scale test.
3. Testing and aerosol sampling techniques which provided aerosol samples as a function of time following an explosive attack on a target in a containment structure were evaluated and developed for the full-scale reference base test.

4.3 Quantification And Characterization of Material Released From A Full-Size Reference Sabotage Incident: Full Scale Test

A full-scale test subjecting a 25.45 MT generic truck cask containing a section of a single surrogate PWR spent fuel assembly to an attack by a reference full-scale high explosive device (HED) was performed to extend the results of the subscale experiments. The surrogate fuel assembly consisted of a 15 x 15 array, 1.2 m long zircaloy tubing filled with depleted UO_2 fuel pellets (9.33 mm diameter by 15.2 mm length). The dimensions and mass of the UO_2 pellets were similar to those of fresh reactor fuel pellets. The stainless steel/lead cask wall consisted of a 2.54 cm thick stainless steel outer shell, 21.3 cm thick lead middle shell and a 1.9 cm thick stainless steel inner shell. The cavity dimensions were 38 cm in diameter and 356 cm in length. The shipping cask was placed inside a 3.1 m I.D. x 0.02 m thick wall x 6.1 m long cylindrical chamber for aerosol containment. The HED was mounted and detonated externally to the chamber. An explosively actuated sliding isolation valve placed between the HED and chamber port was designed to close milliseconds after detonation in order to prevent the release of the source aerosol and fragments to the surrounding area. Eleven sampling ports penetrated the chamber at various locations. These 2.5 cm I.D. sampling ports were closed before and during detonation by remote controlled pneumatically actuated ball valves and were opened shortly after detonation in order to allow sampling of the aerosol. Figure 4.3.1 is a schematic diagram of the test setup for the full-scale test and shows the spent fuel shipping cask inside the aerosol containment chamber. Fuel pins weighing 258.048 kg were configured in a 15 x 15 array inside the cask cavity.

A 61-cm cubical high-pressure fiberglass filter was connected to the chamber via a 15-cm I.D. port to vent the high-pressure gases from the chamber to the atmosphere. This filter was designed to handle the high-pressure shock wave and a gas flow rate of $31 \text{ m}^3/\text{min}$. The filter had a filtration efficiency of 99.99 percent for $0.3 \mu\text{m}$ monodisperse aerosols. After the test, the filter was washed in an HNO_3 acid solution and analyzed for uranium using uranium fluorometry.

Based on experience with subscale tests, the battery of instruments listed in Table 4.3.1 were selected to sample and characterize the released particles



258.048 kg FUEL PINS: 201.053 kg UC_2 + 56.995 kg Zr-4

Figure 4.3.1. Schematic of the Full-Scale Reference Test Configuration Before Detonation Showing Finned Cask Inside Pressure Chamber.

TABLE 4.3.1

Sampling Instruments Used in Full-Size Cask Test

Instrument and Applicable Size Range	Purpose of Samples	Analytical Method
Cascade impactor 0.5-12 μm	Aerodynamic size and geometric standard deviation, total aerosol mass and UO_2 mass.	Gravimetry (Cahn micro- balance) and fluorometry for determination of uranium.
Point-to-plane electrostatic precipitator 0.01-12 μm	Particle morphology, count distri- bution and elemental distribution.	Transmission and scanning electron microscopy and energy dispersive x-ray analysis.
Filter, 47 mm, sequential, 0.01-12 μm	Provide a time history of total aerosol and uranium mass after HED detonation. Samples for surface area measurements.	Gravimetry for total mass and uranium by fluorometry. Nitrogen absorption for surface area measurements.
Filter, 37 mm, front surface reentrant filter (FSRP) 0.01-12 μm	Sequential filter samples from filters inserted inside chamber to compare with filters obtained by extractive techniques to address aerosol line losses.	Gravimetry for total mass of aerosol and uranium by fluorometric techniques.
Screen type dif- fusion battery with condensa- tion nuclei counter (CNC) 0.005-12 μm	Total count of aerosol particles vs. time after detonation.	Optical light-scattering instrument.

TABLE 4.3.1 (Continued)

Sampling Instruments Used in Full-Size Cask Test

<u>Instrument and Applicable Size Range</u>	<u>Purpose of Samples</u>	<u>Analytical Method</u>
Electrical aerosol analyzer (EAA) < 1.0 μm	Size distribution parameters for particles between 0.01 μm and 1.0 μm .	Electrical mobility.
Sieves (38 - 2000 μm)	Provide size distribution data on larger particles of surrogate spent fuel.	Mechanical sieving followed by weighing for total mass and fluorometry for uranium determination.
Integrated time deposition aluminum planchets (0.01 μm to 100 μm)	Provide size, morphology, and elemental composition data of particles diffusively and explosively deposited on chamber surfaces.	Scanning electron microscopy (SEM) and energy dispersive x-ray (EDS) analyses (Z > 11 of deposited particles).
Rotating Plate Samplers (RPS): discrete time (0.01 μm to 100 μm)	Provide size, morphology, and elemental composition data on explosively deposited particles.	Scanning electron microscopy (SEM) and energy dispersive x-ray (EDS) analyses (Z > 11 of deposited particles).

and debris. The sampling procedure was designed to provide measurement of high velocity particles as well as the lower velocity aerosols within the chamber. From these data, calculations could be performed to determine the initial release parameters, such as initial fuel mass aerosol concentration and released fuel mass. Aerosol size parameters as a function of time were determined from cascade impactor samples obtained at sequential time intervals after HFD detonation. Similarly, filter samples provided a time history of the change in elemental mass concentration and total mass. Changes in particle morphology and elemental composition as a function of time were determined using sequential point-to-plane electrostatic precipitator (ESP) samples. Scanning electron microscopic (SEM) and energy dispersive spectroscopic (EDS) analyses of the ESP samples provided information on particle size, morphology, and elemental composition. The electrical aerosol analyzer provided information on size distributions for size modes smaller than $1 \mu\text{m}$ aerodynamic diameter.

A Sandia Laboratory developed time-resolving rotating-plate aerosol sampler was used to collect the high velocity particles for examination by SEM and EDS. These samplers consisted of a collector plate which rotated beneath a cover plate containing two $3 \text{ mm} \times 4 \text{ mm}$ rectangular sampling ports. Three millimeter diameter copper grid discs were placed 6 mm apart on an inside circular path and 12 mm apart on an outside circular path of the rotating collector plate. This grid spacing allowed sampling at 200 ms intervals. The sampling grids were removed after the test for examination using SEM and EDS analyses. The problem of diffusively deposited particles covering and obscuring the early-time explosively-driven particle deposits was solved by pressurizing the sampler housing with air so that the gas flow exiting the sampling ports permitted entry only of early-time, high velocity particles and prevented entry of lower velocity aerosols. In addition to these surface deposition samplers, time-integrated deposition aluminum planchets were placed at various locations in the test chamber to sample particles deposited over long periods of time. These aluminum planchets provided information on the size, morphology, and elemental composition of diffusively and explosively deposited particles.

After the test, all debris were collected from surfaces inside the test chamber and separated into nonuranium material and material suspected of containing uranium. All suspected uranium debris was sieved, the total mass determined, and uranium fluorometric analyses performed. The intact UO_2 fuel and zircalloy-cladding mass were measured before and after the test and the quantity of UO_2 and zircalloy mass removed as a result of the HED attack was determined.

Figure 4.3.2 is a reconstruction of the test configuration immediately after detonation. A total UO_2 fuel mass of 195.593 kg remained in the fuel pin assembly in the cask after the event which indicated that 5.460 kg of UO_2 fuel was removed from the fuel assembly as a result of the event. Table 4.3.2 summarizes the measured values and results of the full-scale test. After detonation, 198.504 kg of the UO_2 fuel remained in the cask; 2.549 kg

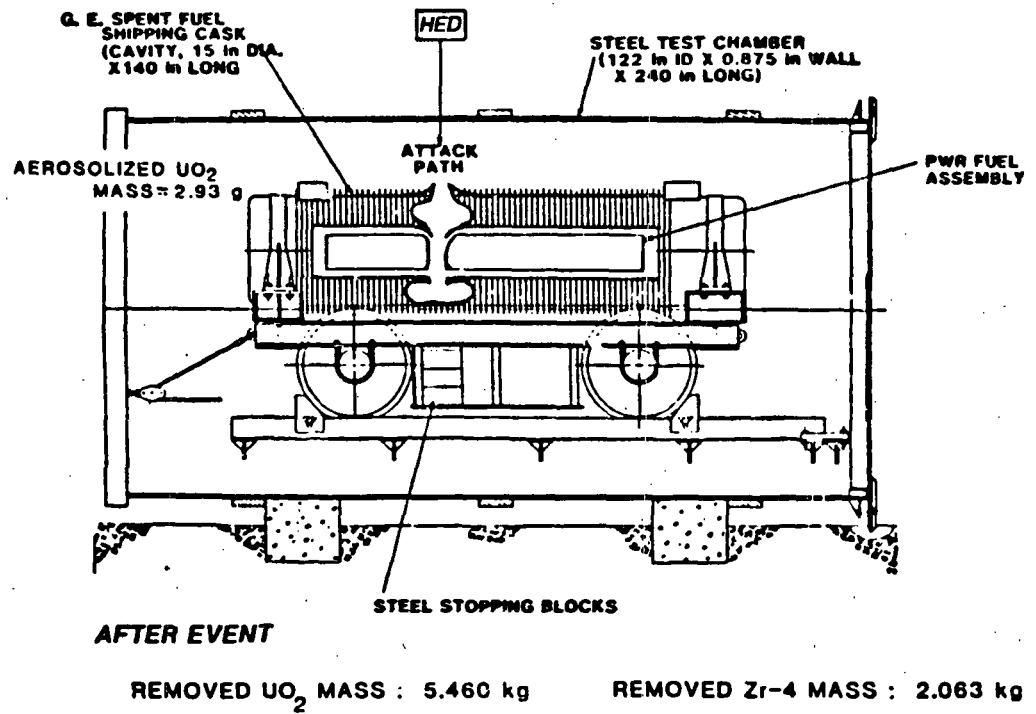


Figure 4.3.2. Schematic of the Full-Scale Test Configuration Immediately After Detonation Showing Damage and Net Mass Loss.

TABLE 4.3.2

Summary of Results of Full-Scale Test

NO.	PARAMETER	VALUE
1	UO ₂ fuel mass before event (kg)	201.053
2	Zr-4 mass before event (kg)	56.995
3	UO ₂ fuel mass remaining in cask after event (kg)	198.504
4	UO ₂ fuel mass removed from assembly (kg)	5.400
5	UO ₂ fuel mass released from cask ^a (kg)	2.549
6	Maximum UO ₂ fuel mass fractured ^b (kg)	20.820
7	No. of fuel rods before event	223
8	No. of fuel rods with mass loss	111
9	Maximum length of UO ₂ fuel fractured (mm)	275
10	Maximum length of fuel rod removed ^c (mm)	76
11	Average entrance hole diameter of cask (mm)	152.5
12	Average exit hole diameter of cask ^d (mm)	None
13	UO ₂ fuel mass released as aerosol (g)	2.94
14	UO ₂ fuel mass released as respirable aerosol (g)	2.94

^aAll sizes.

^bNot necessarily released or removed.

^cAs a result of the event.

^dHED did not completely penetrate cask.

of UO_2 was released from the cask as a result of the event. Approximately 0.115 percent (2.94 g) of the released UO_2 fuel was airborne aerosol and all of the airborne UO_2 aerosol was assumed to be respirable. Fifty percent (111) of the 223 fuel rods sustained some degree of mass loss (damage). Figure 4.3.3 shows the damage to the simulated fuel bundle. Approximately 10.3 percent (20.820 kg) of the pretest UO_2 fuel mass was fractured. The maximum missing (removed as a result of the energy loading) fuel pin length was 76 mm. The entrance hole in the 2.54 cm thick stainless steel skin was approximately 15.25 cm in diameter (average). The opposite cask wall was not completely penetrated but the 1.9 cm thick inner stainless-steel shell and 14.29 cm of the 21.27 cm thick lead shell was penetrated. The outer 2.54 cm thick stainless-steel skin was not breached. Figure 4.3.4 shows a time history of the UO_2 aerosol mass within the chamber based on sequential filter samples. A maximum UO_2 aerosol mass concentration of $23.8 \mu\text{g}/\ell$ was detected at 12 seconds postdetonation. Using the containment chamber volume of 42.29 m^3 and a measured uniform spatial concentration of $23.8 \mu\text{g}/\ell$, a total released UO_2 aerosol mass of 1.01 g was calculated. Another 1.93 g of UO_2 was collected by the pressure release fiberglass filter assembly. Assuming that 100 percent of the measured UO_2 aerosol mass is in the respirable size range, a total respirable UO_2 mass of 2.94 ± 0.30 g was released from the cask as a result of the event.

The debris swept and vacuumed from the chamber walls and cask surfaces were collected, sieved and analyzed using uranium fluorometry to determine the size distribution of the larger UO_2 particles. Figure 4.3.5 shows the cumulative UO_2 particle size distribution of the sieved debris. Extrapolation of the size distribution to the respirable regime suggests that less than 10^{-3} percent of the chamber and cask surface deposited UO_2 debris was smaller than $10 \mu\text{m}$ aerodynamic diameter. Since the collected surface debris contained ≈ 540 g of UO_2 , the inference is that less than 5 mg of UO_2 particles deposited on the chamber surfaces was smaller than $10 \mu\text{m}$ aerodynamic diameter.

Figure 4.3.6 shows the aerosol size parameters versus time for the full-scale test. Whereas in the subscale tests, aerosol size distribution MMAD was approximately $2 \mu\text{m}$ for the "dry" Test No. 6 and slightly less than $1 \mu\text{m}$ for the "wet" Test No. 7, in the case of the full-scale test, the MMAD was $3 \mu\text{m}$ immediately after detonation and stabilized near $2.5 \mu\text{m}$, 30 minutes after detonation. The geometric standard deviation (σ_g) also was larger for the full-scale test than that for the "dry" Test No. 6 (2.6 versus 2.2). The larger MMAD in the case of the full-scale test is attributed to the fact that the relative ratio of the chamber volume for the full-scale test to that for the subscale test was smaller in proportion to the explosive charge mass ratio and, therefore, a much higher concentration of aerosol from all sources resulted from the explosive attack in the full-scale test. A higher aerosol concentration would lead to more particle interactions, agglomeration and, hence, larger diameters.

Figure 4.3.7 shows an SEM photomicrograph of a typical rotating plate sampler (RPS) sample taken 400 millisecond after detonation. High velocity particles were collected on this sample. No uranium particles and no uranium

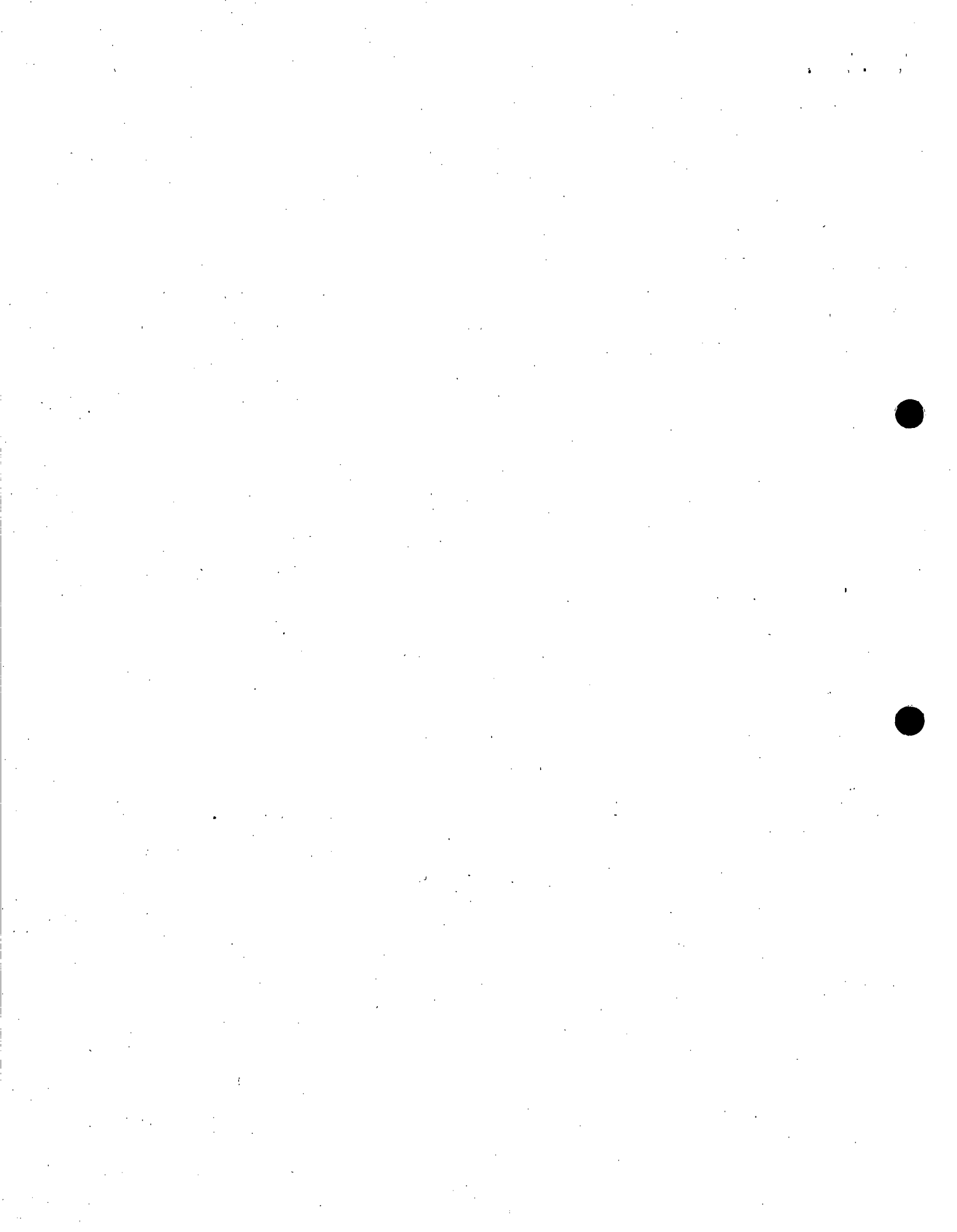




Figure 4.3.3 Photograph of 15 x 15 Depleted UO_2 Fuel Assembly Showing Damage Caused by HED in Full-Scale Reference Test.

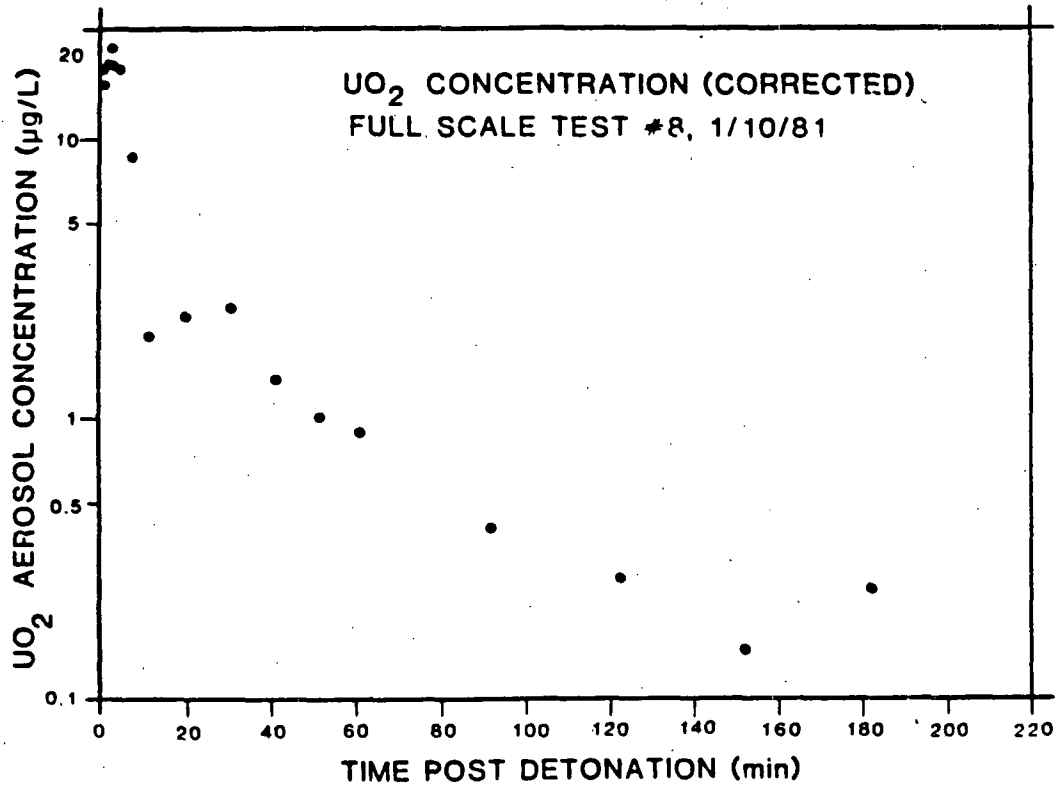


Figure 4.3.4. Time History of UO₂ Aerosol Mass Within Pressure Chamber Based Upon Sequential Filter Samples for Full-Scale Reference Test.

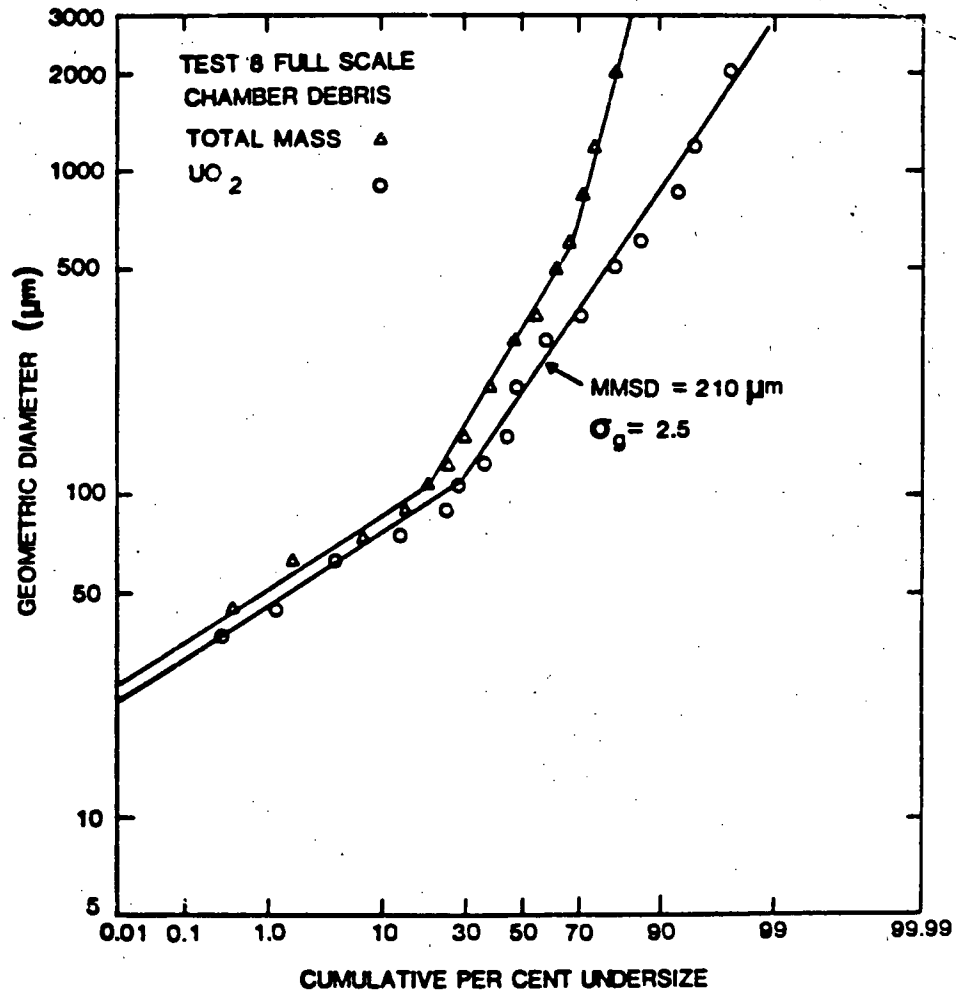


Figure 4.3.5. Total Mass and UO_2 Mass Size Distribution for Sieved Debris of Full-Scale Test.

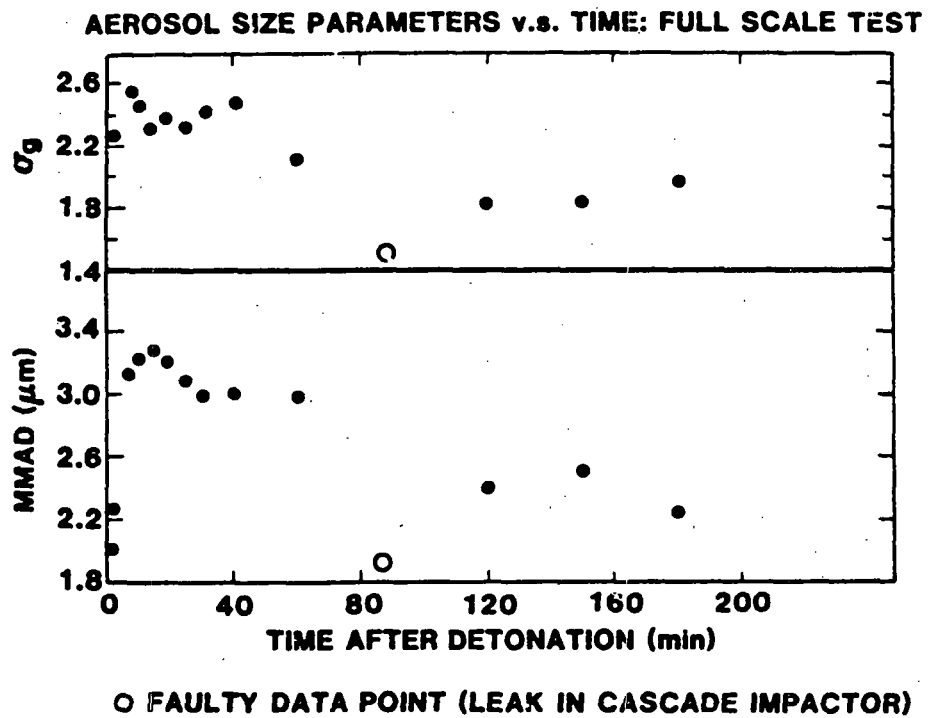


Figure 4.3.6. Aerosol Size (MMAD) and Geometric Standard Deviation (σ_g) as a Function of Time for Full-Scale Test.

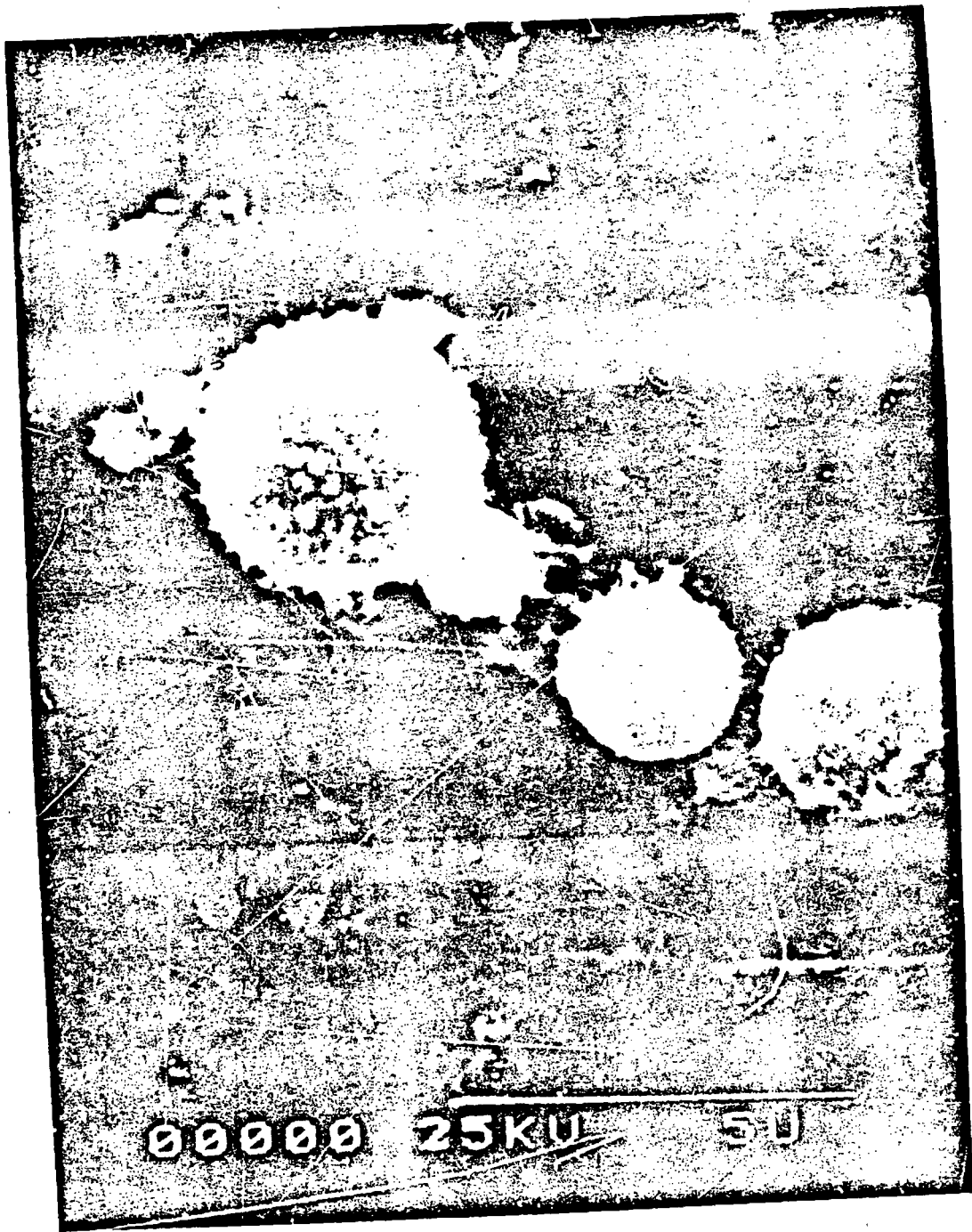


Figure 4.3.7. Scanning Electron Micrograph of a Typical Rotating Plate Sample Taken 400 msec After Detonation of the Full-Scale Event. Magnification is 200,000.

coating was detected on this sample or any of the other RPS samples analyzed. However, numerous spherical globules of stainless steel (Fe, Cr, Ni) ranging in size from submicrometer to tens of micrometers were found on the copper substrates. Additionally, networks of submicrometer lead fibers and wisps of lead were detected on the surfaces of the stainless steel globules and the copper substrate surfaces. Figure 4.3.8 shows an SEM photomicrograph of a time-integrated aluminum planchet sample of both high and low velocity material ejected during and in the time period following detonation. Fractured particles of uranium ranging in size from 70 to hundreds of micrometers real diameter were detected using EDS. The morphology of the uranium particles was irregular and was indicative of a mechanical fracturing mechanism. The aluminum substrate was covered with stainless steel globules and both the stainless steel globules and uranium particles were covered with a network of ultrafine submicrometer lead fibers. This lead coating had the appearance of having been formed from a vapor state. The stainless steel globules had the appearance of having been deposited in a molten state.

The analyses of the RPS and time-integrated aluminum planchet samplers suggested the following: (1) A lead vaporization/condensation aerosol formation mechanism, (2) a stainless steel melting/solidification aerosol formation mechanism, and (3) a UO_2 nonmelting mechanical fracture aerosol formation mechanism. The conclusion from these analysis was that the maximum temperature seen by the fuel mass was greater than $1744^\circ C$ but less than $1850^\circ C$.

Estimating the precision of measured parameters and using standard error propagation techniques, the uncertainty of the measured respirable UO_2 mass released from the cask was calculated. Uncertainties of the measured parameters, such as mass concentration, chamber volume, sampling flow rates and mass fraction of uranium determined by fluorometric spectroscopy were estimated and propagated to determine the uncertainty of the derived UO_2 respirable release mass. The estimated error of the released UO_2 aerosol mass based on this analysis was ± 10 percent.

Figure 4.3.9 compares condensation nuclei counter (CNC) data where mass has been calculated for both the two subscale Tests No. 6 and 7 and the full-scale tests. In all cases for the dry tests, mass concentration starts out at about 7 mg/l and decays in time through several orders of magnitude. As previously mentioned in the case of the subscale wet Test No. 7, the concentration of UO_2 aerosol was a factor of 40 less than that for the dry tests (subscale and full-scale) and a catastrophic decay of mass concentration was observed at about 200 minutes postdetonation. This indicates that the presence of water in the cask jacket and cavity would reduce the consequences of a malevolent act on spent fuel shipping casks.

The results of the full-scale HED attack on a full-scale generic shipping cask may be summarized as follows: A total respirable UO_2 mass of $2.94 \pm 0.30 \text{ g}$ was released as a result of a successful sabotage attack event on a single PWR fuel assembly truck cask containing 0.5 metric tonnes of heavy metal charged to a light water reactor. This released quantity corresponds to a release fraction of 6.0×10^{-6} of the total fuel inventory in the cask.



Figure 4.3.8. Scanning Electron Micrograph of Time-Integrated (10 minutes) Aluminum Planchet Sample Showing a $70\ \mu\text{m}$ (real diameter) UO_2 Particle. Magnification is 20,000 X.

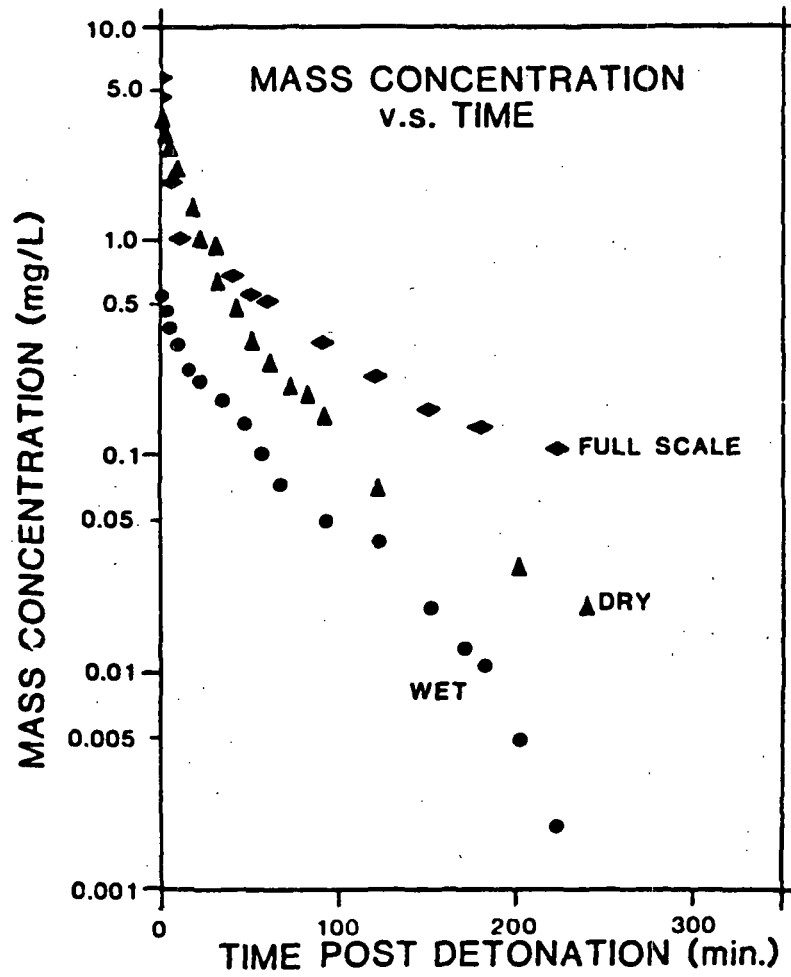


Figure 4.3.9. Comparison of Mass Concentration (mg/l) as a Function of Time for Subscale Tests No. 6 (Dry) and 7 (Wet) and the Full-Scale Test.

4.4 Development of a Correlation Between Depleted UO_2 and Spent Fuel

In order to obtain a correlation function for the aerosolization of spent fuel versus depleted uranium dioxide, it is useful to consider data produced during this program and that generated during similar experiments at BCL.⁴ Since no aerosol measurements were attempted for a full-scale reference base attack on spent fuel, data from subscale attacks on both spent and depleted uranium dioxide must be used.

Subscale Tests Performed by EG&G/INEL

Tests performed by personnel at EG&G/INEL in support of SNL's research effort involved single fuel pellets of both depleted uranium dioxide and H. B. Robinson Unit-2 spent fuel subjected to subscale attack by a scaled version of the reference base attack device (see Appendix D for details). Two types of measurements were made that can be used in calculating a spent fuel to depleted uranium dioxide aerosol production correlation. The first measurement type was obtained from filters which collected aerosols generated following exposure of both spent and depleted uranium dioxide fuel pins to HED attacks. Because of their refractory nature the radionuclides $^{154}\text{-Eu}$ and $^{144}\text{-Ce}$ were used as a tracer for uranium in the spent fuel pellets; amounts of these two fission products were determined by gamma spectroscopy. For the case of depleted uranium dioxide the total mass of aerosolized materials collected on the filter was 17 mg¹¹ (gravimetrically determined). Assuming that the total mass consists of combustion products, fuel pin cladding and pellet material, an estimate of the relative masses represented by the three main components was made. It was estimated that 25 percent of the total collected aerosol mass was combustion products. The pellets consisted of 89 percent by weight of UO_2 for experiments with either spent fuel or depleted uranium dioxide. Therefore a 17 mg aerosol sample implied that 11.35 mg was uranium dioxide. The measured mass of aerosolized spent fuel was found to be 5.95 ± 1.67 mg. This analysis suggests the correlation ratio is approximately equal to 0.53:1.

A second series of measurements used for the calculating the spent fuel versus depleted uranium dioxide correlation was based on sieving of debris resulting from identical experiments involving spent fuel and depleted uranium dioxide. Details are included in Appendix D in this report. Sieves used for classifying particles ranging in size from 5 μm diameter to 212 μm diameter were used to separate masses of spent fuel and depleted uranium dioxide. The mass remaining on each sieve were then used to calculate a ratio of spent fuel to depleted uranium dioxide for each sieve size fraction. A regression line was fitted to the data and a ratio extrapolated for the respirable size range ($<3 \mu\text{m}$ actual particle diameter). For particles 3 μm and smaller, the ratio of spent fuel to depleted uranium dioxide mass was 5.6:1.

Subscale Tests Performed at Battelle Columbus Laboratories

Under the aegis of the U.S. Nuclear Regulatory Commission (NRC), a series of subscale tests on spent fuel was performed by personnel at Battelle Columbus Laboratories (BCL).⁴

These tests used a short five-pin array of H. B. Robinson Unit-2 spent fuel which was subjected to attack by a subscale precision version of an HED device. Results of selected early time aerosol measurements by filters are summarized in Table 4.4.1. These data indicate that the uranium aerosol concentration from the spent fuel ranged from 50 to 500 μg per liter for the time period 0-3 minutes post-attack. The mean of these measurements was 118.2 μg per liter with a standard deviation of ± 130 μg per liter. If we eliminate the extremes of the measured aerosol concentration the resultant mean and standard deviation are 70.4 ± 31.4 μg per liter, respectively. Eliminating the two highest measurements is justified for the following reasons:

1. During "Hot Shot 8" one filter cassette measured a concentration of 447 and 411 μg per liter of uranium dioxide while another filter cassette operated simultaneously with the 447-411 measurements indicated a UO_2 concentration of 43 to 130 μg per liter.
2. A statistical test ("standard box plot"), which assumes a Gaussian distribution, was applied to the data to evaluate the validity of the outliers. This statistical test indicated that the values of 447 and 411 $\mu\text{g}/\ell$ have less than 2 chances out of 1,000,000 probability of belonging in the assumed Gaussian distribution.

Based on scaling theories developed at BCL for extrapolating to the 3 fuel assembly PWR truck cask incident, an aerosolized uranium mass of 4.24 ± 4.66 g was calculated for the case using all of the filter data from BCL. If the aerosolized mass is calculated based on filter data where the extremes of the measurements are not used, then 2.53 ± 1.12 g of aerosolized uranium would be released as a result of the reference base attack on the 3 PWR fuel assembly truck cask. The data from the subscale and full-scale experiments performed in this study suggest a release of 6 grams from a reference base attack on a 3 PWR fuel assembly truck cask. From these mean values a correlation ratio (spent fuel:D- UO_2) of 0.71:1 and 0.42:1 is calculated for all filter data and for the truncated versions, respectively.

BCL, in the analysis of their data, utilized the maximum measured release instead of a mean value. This led to a correlation ratio 5 times the largest value quoted above or about 3.0.

Analysis

There are potential errors implicit in all of these correlation ratios. While estimates for the BCL results are based on actual spent fuel aerosolized mass, there were no comparable results for depleted uranium dioxide in the same test set-up. Given this uncertainty the most definitive statement that can be made is that the value is likely to be on the order of unity.

Calculations based on EG&G/INEL data for filter measurements were suspect because the mass of depleted uranium dioxide was not determined analytically but was calculated from the total mass collected by sampling filters. Unknown amounts of test fixture support materials could lead to an overestimate of

Table 4.4.1

Filter Data From Battelle Columbus Laboratories
Studies⁴ on Spent Fuel Release Fraction

<u>Experiment</u>	<u>Filter No.</u>	<u>Time Interval (Min)</u>	<u>Concentration</u> <u>µg/l</u>
Hot shot* 1.11	3	1.0-2.0	93.8
1.12	2	0.5-1.0	60.2
1.12	3	1.0-2.0	79.8
Hot shot* 2.11	3	1.0-2.0	50.6
2.12	2	0.5-1.0	95.5
Hot shot* 7.11	1	0 -0.5	54.5
	2	0.5-1.0	25.4
	3	1.0-2.0	27.8
7.12	1	0 -0.5	67.7
	3	1.0-2.0	84.9
Hot shot* 8.11	1	0 -0.5	447
	2	0.5-1.0	411
8.12	1	0 -0.5	107.7
	2	0.5-1.0	129.9
	3	1.0-2.0	43.1

*Spent Fuel Experiment

aerosolized depleted uranium dioxide. Since it is unlikely that the estimates of mass allocation are an order of magnitude off, the available data suggests the correlation is of order unity.

The correlation based on wet sieving of debris from both spent fuel and depleted uranium dioxide was based on extrapolating sieve results down to the respirable regime. In order for this process to be valid, a single mode particle size distribution was assumed to extend into the respirable regime. Since the ultrafine aerosol size distributions in the scaled and full scale tests were determined to be multimodal as were larger diameter sieve size distributions, the assumptions of a single mode representing both wet sieve fractions and respirable size fractions may not be valid. The value of 5.6 obtained for the ratio was greatly impacted by the 10-20 μm sieve fraction which exhibited a ratio of 125:1, spent fuel to depleted uranium dioxide. This extremely high ratio has a significant effect on the calculated regression line that was fitted to the data. Since this size fraction is very similar to the original grain size of the uranium dioxide prior to pellet fabrication it may represent an anomolus peak resulting from a breakdown in the sintered matrix of the fuel produced by grain swelling in the reactor environment. If this hypothesis were true, then the ratio of spent fuel to depleted uranium respirable aerosol would be of order unity and not 5.6.

Summary of Correlation Data

The following statements summarize the calculation of a correlation function:

- The NRC/BCL studies yielded a maximum UO_2 release value of 500 μg per liter which resulted in a spent fuel to depleted uranium dioxide correlation ratio of 3.
- Using the original data from the BCL studies and using standard statistical tests an estimate of 0.42 was obtained.
- Using filter data from EG&G/INEL that was collected in support of this DOE program, a value of 0.53 was obtained.
- Based on wet sieve data from EG&G/INEL on material released as a result of subscale attack on both spent fuel and depleted uranium dioxide, a correlation ratio of 5.6 was obtained.

In considering which correlation ratio is appropriate for use in risk analysis and calculation of radiological impacts, it would seem that a value of unity is most appropriate. This implies that the aerosolized release from the reference HED used on a 3 PWR fuel assembly truck cask would yield approximately 6 g of spent fuel as a respirable aerosol. However, for conservatism in the health risk assessment, a maximum value of 5.6 will be used. This implies that the maximum aerosolized respirable release from a 3 PWR fuel assembly cask subjected to the reference HED attack would be 33.6 g of spent fuel and for a single PWR fuel assembly truck cask a release of 16.8 g.

4.5 Analyses of Fuel and Cask Breakup and Aerosol Production

In order to develop an understanding of mechanisms of aerosol production, and the mechanisms causing breakup of fuel and cask, elemental analyses of aerosol samples, using x-ray fluorescence, standard metallurgical analytical techniques, and aerosol dynamics modeling were performed.

4.5.1 Elemental Analyses and Quantification of Aerosol Samples by Wavelength of Dispersed X-Ray Fluorescence (XRF) Spectroscopy.

Aerosol samples collected on filters during a 1/4-scale wet and a full-scale dry test were analyzed for U, Zr, Pb, and Fe by the use of a new x-ray fluorescence (XRF) thin film technique. These analyses were made to characterize the composition and time-dependent behavior of the aerosol produced by a reference HED attack on a fully loaded spent fuel shipping cask.

Figures 4.5.1 and 4.5.2 display the time-dependent behavior of the four aerosol components in the 1/4-scale wet Test No. 7. The corresponding results for the full-scale dry test are presented in Figures 4.5.3 and 4.5.4. The UO_2 aerosol concentration decreased in both tests from roughly 5 to 0.1 $\mu\text{g}/\text{l}$ over a period of 150 min after detonation. The results for UO_2 concentration correlated well with those obtained by U fluorometry. The ZrO_2 aerosol concentration varied in roughly the same concentration range as that of UO_2 whereas those for PbO and FeO were roughly one to two orders of magnitude greater with the $PbO > FeO$ in the full-scale test and $FeO > PbO$ in Test 7 (wet test).

The essential behavior of the full-scale dry test aerosol is illustrated in Figures 4.5.5 and 4.5.6 where the aerosol fraction of the components are presented as a function of time.

The aerosol composition at any particular time was defined by the ratios of the various oxide component concentrations to the total aerosol concentration. The aerosol fractions of lead oxide, iron oxide, and zirconium oxide in the full-scale test were found to be 0.64, 0.20, and 0.003, respectively, independent of time. The aerosol fraction of uranium oxide, however, was found to decrease exponentially with time from about 0.005 initially to 0.0003 after 180 min. The aerosol fraction (AF) by (XRF) for UO_2 , was found by multiple regression to vary as

$$AF_{UO_2} = 0.0040 \exp [-.012t]$$

where t is in minutes so that initially (t = 0) it is 0.4 percent of the total aerosol.

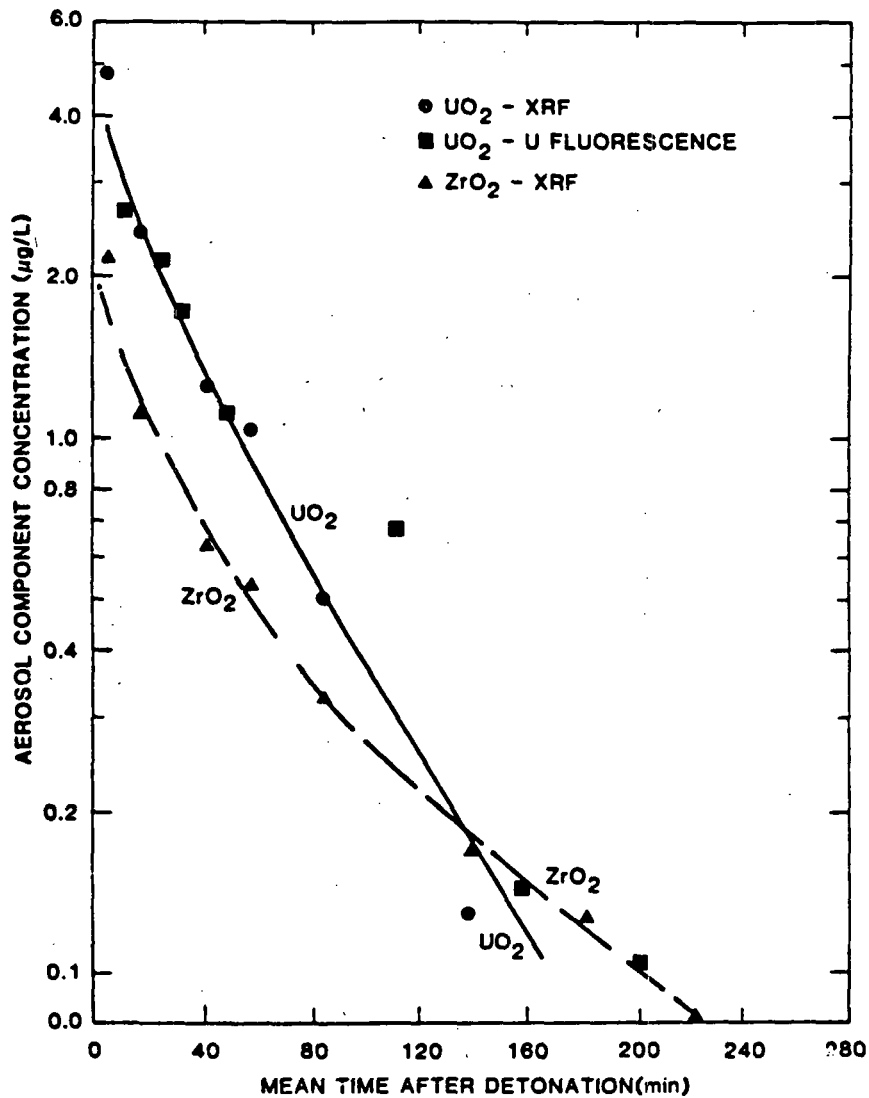


Figure 4.5.1. UO₂ and ZrO₂ Aerosol Concentrations as a Function of Time for Wet Test No. 7. Comparison of XRF and uranium fluorescence analyses.

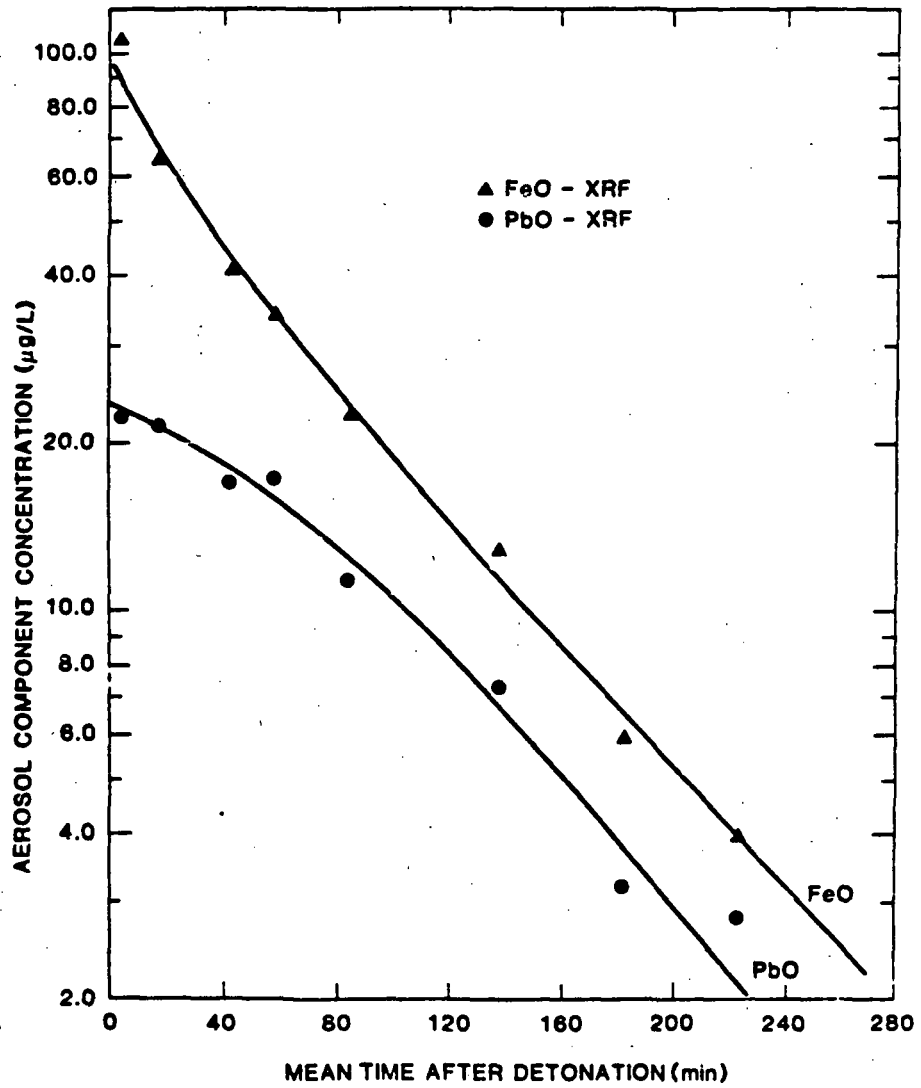


Figure 4.5.2. FeO and PbO Aerosol Concentrations as a Function of Time After Detonation for Wet Test No. 7. Analyses are by XRF.

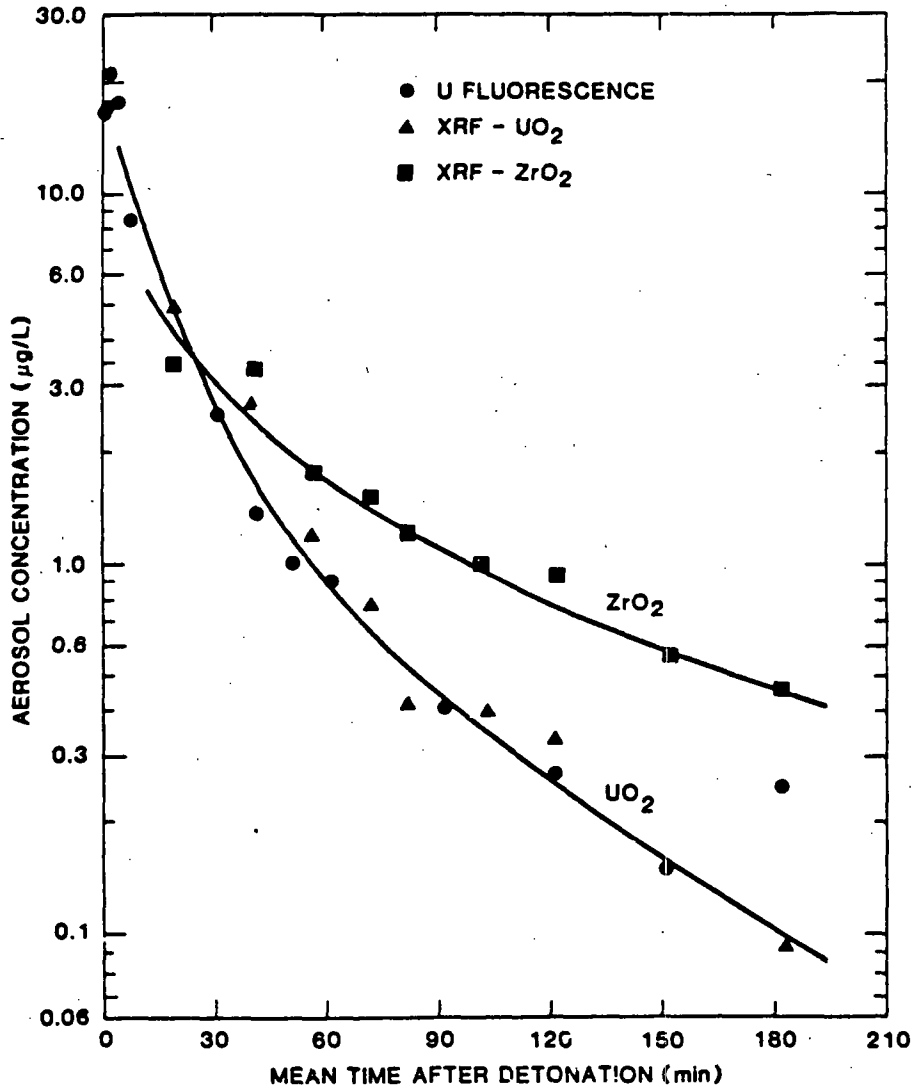


Figure 4.5.3. UO_2 and ZrO_2 Aerosol Concentration as a Function of Time for Full-Scale Dry Test. Comparison of XRF with uranium fluorescence analysis technique.

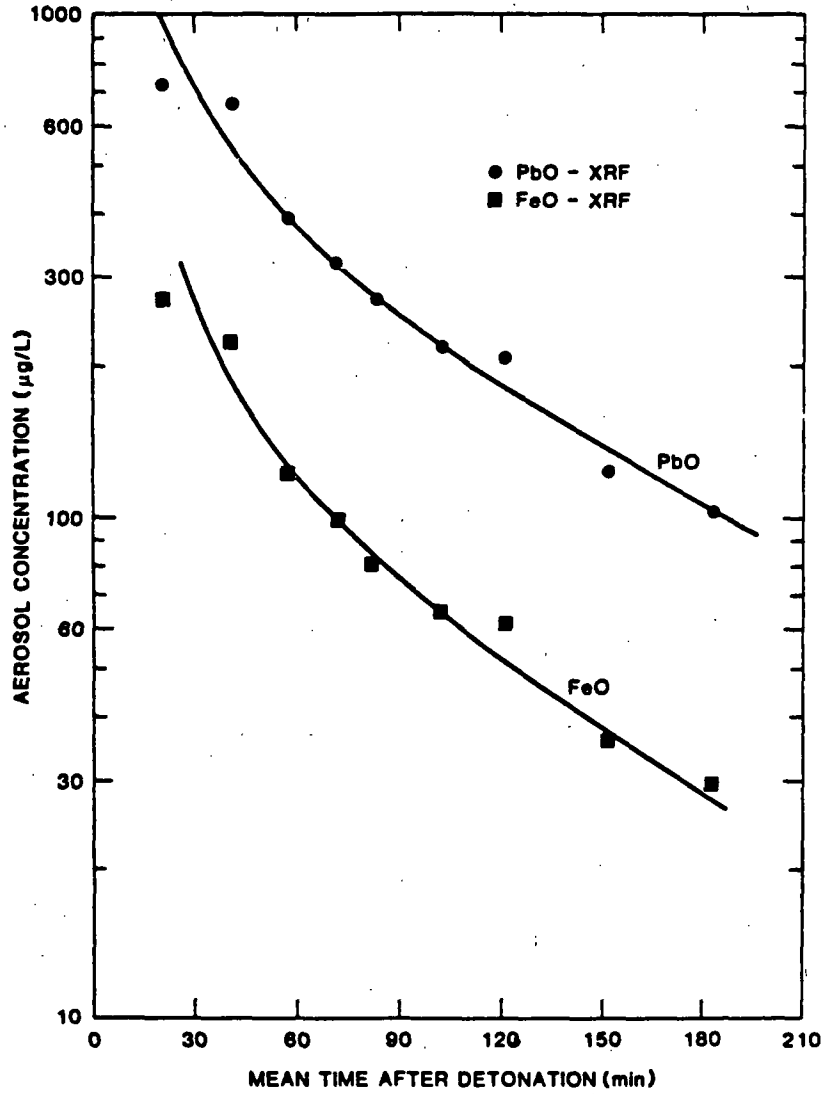


Figure 4.5.4. PbO and FeO Aerosol Concentrations as a Function of Time After Detonation for Full-Scale Dry Test

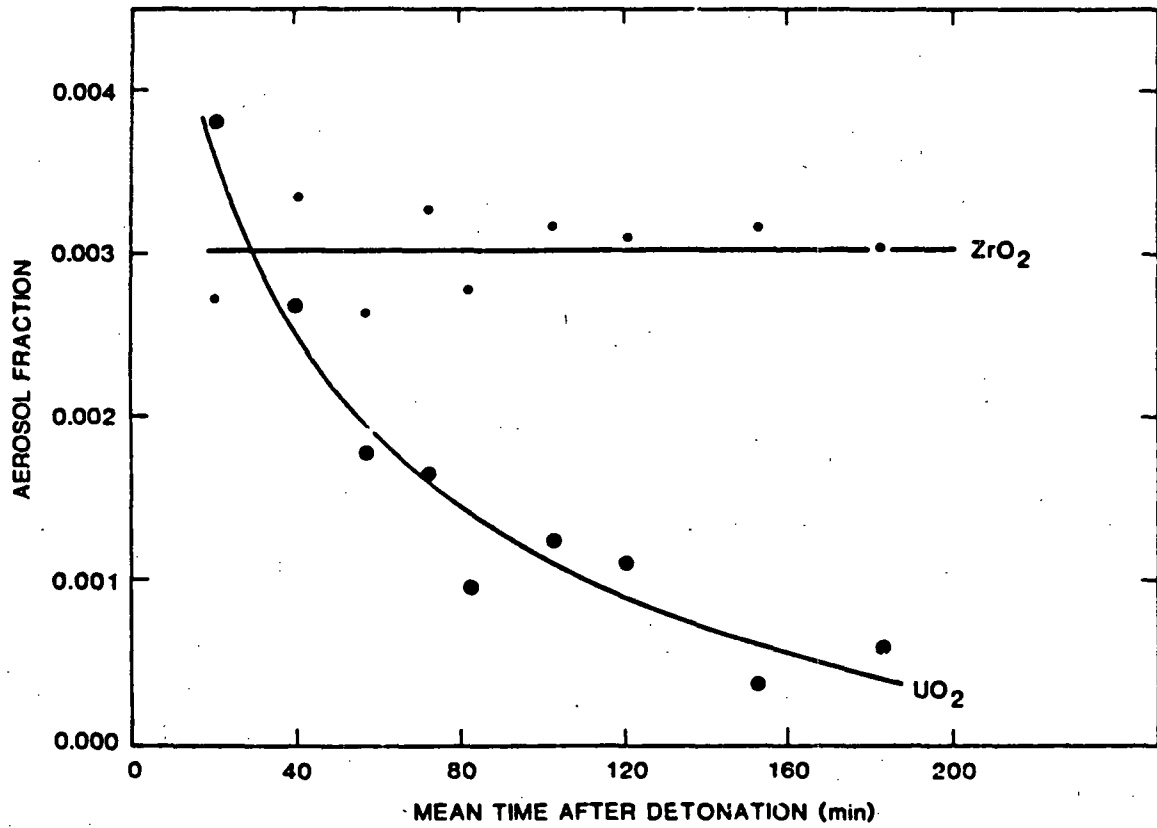


Figure 4.5.5. Aerosol Fraction for ZrO₂ and UO₂ as a Function of Time After Detonation for the Full-Scale Dry Test (No. 8)

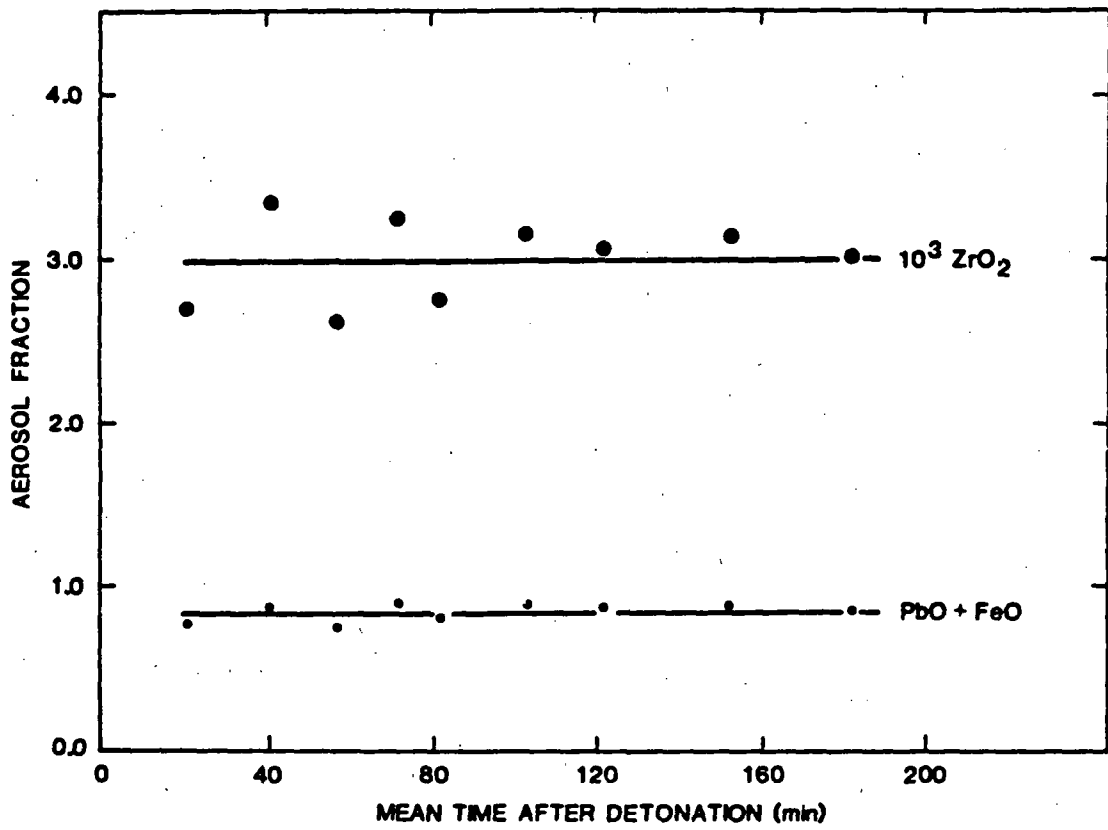


Figure 4.5.6. Aerosol Fraction of ZrO₂, and PbO plus FeO Components as a Function of Time for Full-Scale Test

These results for the dry full-scale test describe an aerosol with essentially two components in terms of time-dependent behavior. One component is formed of ZrO_2 , and the other is PbO plus FeO which all fall out at the same rate as the total aerosol. This unique result suggests condensation and/or coagulation of these components after formation by vaporization and/or melting of metal components (Pb and Fe) in the shipping cask. The UO_2 aerosol, however, falls out exponentially more rapidly than the total aerosol. It appears to be a completely different component of larger particles (than the lead and iron oxides) and could have been formed by fragmentation only of the UO_2 fuel.

Comparable results for the aerosol fraction in the 1/4-scale wet test (Test No. 7) could not be obtained because of moisture in the weighed filters.

4.5.2 Metallurgical Analyses

Metallurgical analyses of the materials recovered from the full-scale test were performed to determine the maximum temperature, T_{max} , attained in the region where the blast front, generated by the HED, impinges on the fuel rods. A knowledge of the temperature of this event is important, since it would be useful in estimating the amount and species of fission product radionuclide contaminated aerosols that would be released during an attack. Thermocouples were not a viable way to determine the temperature. Thermocouples have too large a thermal mass, and therefore would respond too slowly. Alternatively, it is possible to make some reasonable estimate of temperature by examination of the phase transformations (microstructures) induced during the explosive event.

Several components from the full-scale cask test have been examined with a variety of metallurgical techniques, including optical metallography, scanning electron microscopy (SEM), and x-ray diffraction. Other electron optical techniques, including transmission electron microscopy (TEM) and electron microprobe analysis were also used. However, in this case, these more complex techniques yielded no additional information relative to the SEM.

Since the objective of this analysis was to determine the maximum temperature attained at the fuel rods during the test, several samples were used. Samples analyzed included (1) the explosive-actuated valve door, (2) millipore filters, (3) aluminum SEM stubs, (4) Cu discs which collected (a) explosively driven particles only and (b) explosively driven plus diffusion particles, and (5) a disc sampler similar to (4) but containing 3-mm TEM grids. These samples also included (6) a stainless steel slug from the cask, (7) zircaloy cladding, and (8) a UO_2 fuel pellet, all from the site of blast impingement. Figures 4.5.7 through 4.5.14 show the results of this analysis. Each figure is fully described by its caption. Briefly, the SEM analysis of the samples showed evidence, as shown in Figures 4.5.7, and 4.5.8, of vaporized lead and molten stainless steel.

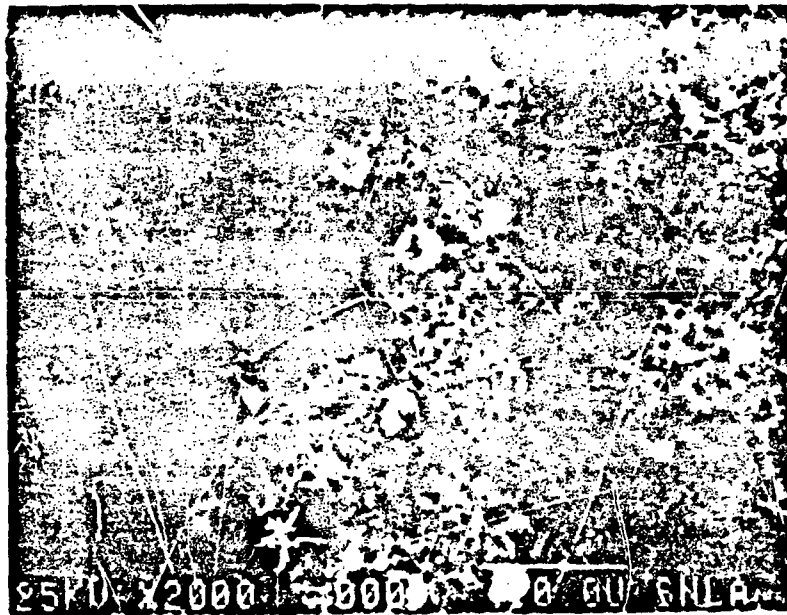


Figure 4.5.7. SEM Micrograph of Material Deposited on the Valve Door During the Full-Scale Cask Test. Spherical particles of droplets of stainless steel, indicating the stainless steel from the cask was melted. The wispy material is lead, probably condensed from a vapor.

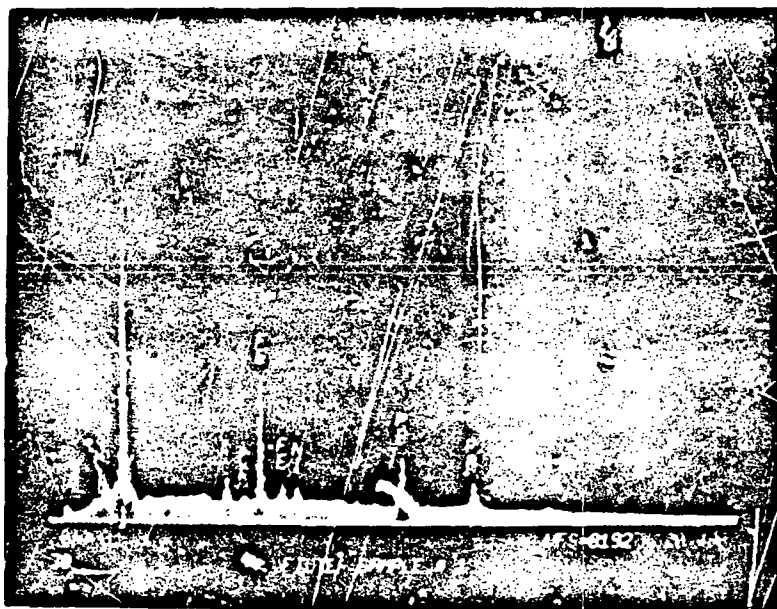


Figure 4.5.8. X-Ray Spectra Showing the Elements Present in Figure 4.5.7. Fe, Cr, and Ni are from the stainless steel, Pb is simply Pb, and the Si is probably due to the presence of a small amount of sand. The Pb and stainless steel are probably from the cask.

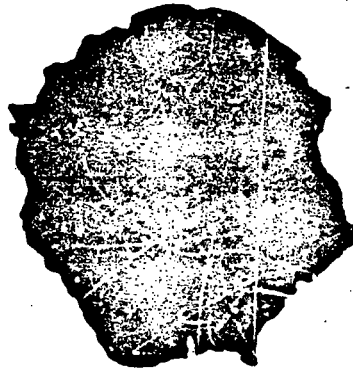


Figure 4.5.9. Macrophotograph (1.5x) of the Stainless Steel Slug
Taken From the Cask After the Full-Scale Test Event.



Figure 4.5.10. Micrograph of the Stainless Steel Slug in Cross Section (500x). Signs of surface melting are present. Exterior of slug is coated with Pb.



Figure 4.5.11. Macrophotograph of a Piece of Zircaloy Cladding Taken
After Full-Scale Test Event (1.5x)

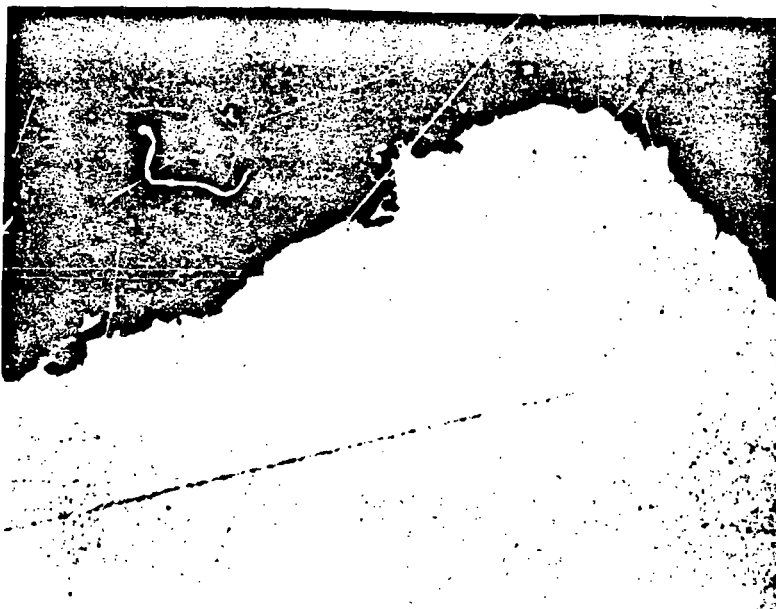


Figure 4.5.12. Micrograph of Zircaloy Cladding in Cross Section (100x).
No signs of melting or ablation.

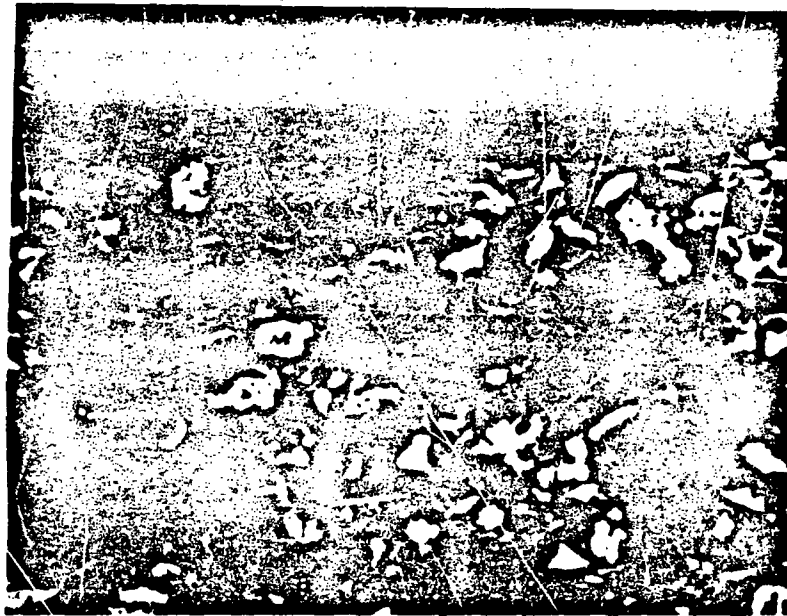


Figure 4.5.13. Microscopic Cross Section of UO_2 Fuel Pellet (100x).
Basic microstructure has been unaltered by the explosive event.

The Plug of stainless steel, probably from the cask itself, is shown macroscopically in Figure 4.5.9. Metallographic examination of the slug in cross section shows signs of melting and ablation, as shown in Figure 4.5.10. The sample is also coated with lead, which was probably deposited after condensation from a vapor state. This evidence points to a temperature in excess of the melting point of stainless steel, 1400°C, and the vaporization point of lead, 1744°C.

The sample of zircaloy cladding is shown macroscopically in Figure 4.5.11 and in microscopic cross section in Figure 4.5.12. Although the cladding material is coated with vapor-deposited lead, there are no signs of melting or ablation of the zircaloy cladding itself. Hence it may be assumed that the melting temperature of zircaloy, 1850°C, was not attained. It has been suggested that since it is highly pyrophoric, it may have oxidized during the event and all signs of melting removed. X-ray diffraction studies of fines recovered from the test showed the presence of ZrO_2 . However, it is contended that physical signs of melting would have been retained in the material despite oxidation. Such evidence could include subsurface hot plastic flow or pockets of trapped oxide (ZrO_2).

The UO_2 fuel pellet was examined by x-ray diffraction and optical metallography. The x-ray diffractometer data showed only UO_2 ; no other forms of uranium oxide were present. There was no evidence of the formation of a glassy phase. No signs of melting or ablation were apparent in the metallographic samples, as shown in Figure 4.5.13. Depending on the reference, the melting point of UO_2 is listed to be between 2500°C and 3000°C.

It has been suggested that it may be possible to infer the thermal history of the fuel pellet accurately by detecting the presence of uranium oxides other than UO_2 . Such inferences would be tentative and of dubious value. Oxidation reactions are dependent on many parameters other than temperature including (1) total pressure, (2) identity of all gaseous species present (CO_2 , CO, $HxCy$, etc), and (3) the partial pressures of each species listed in (2). It is not possible to accurately define these parameters. In addition, all simple thermodynamic calculations intended to predict phase stability apply only to the state of equilibrium. The assumptions of equilibrium between the cask solid materials and its components and atmospheric and blast gases are probably not valid.

In summary, the evidence derived from examination of these components from the full-scale test indicate the maximum temperature attained was most likely between the vaporization point of lead, 1744°C, and the melting point of zircaloy, 1850°C. No particles of UO_2 indicating melting or vaporization were found. All UO_2 particles examined indicated particles produced by mechanical fracturing mechanisms. From these results, it is predicted that a full-scale attack on spent fuel would result in similar conditions of temperature and aerosol formation. Consequently, from these temperature ranges inferred, certain volatile fission product radionuclides such as

^{137}Cs , ^{106}Ru , and ^{125}Sb could be vaporized and could be expected to have an enhanced release as compared to the fuel matrix. Furthermore, it is expected that these vaporized fission product radionuclides would then condense onto available surfaces and would be associated with smaller (respirable) particle sizes. None of the more biologically significant radionuclides such as the actinides (^{239}Pu , ^{238}Pu , $^{242-244}\text{Cm}$ and ^{241}Am) or beta-gamma emitters such as ^{90}Sr , or ^{144}Ce would be vaporized and thereby result in an enhanced release compared to the fuel mass. Although certain volatile fission-product radionuclides (^{137}Cs and ^{106}Ru) would exhibit an enhanced release, all of these radionuclides are less biologically significant than the actinides and the resultant calculated dose increase does not affect the overall risk estimate.

4.5.3 Modeling the Dynamics of Aerosol Production

A mathematical model of aerosol dynamics is essential for understanding the processes which govern the particle size distribution produced from an explosive environment. The model serves not only to elucidate the dynamics of measured particle size distributions but also to predict the effects of conditions not encountered in the course of the experimental program. Since it would be impractical and cost prohibitive to arrange an exhaustive set of experiments to encompass all possible scenarios, a model has great utility in supplementing existing data in regions not explored experimentally. Thus the major objective of the model presented is to elucidate and quantify the mechanisms contributing to the dynamics of the particle size distribution of a confined aerosol generated by an explosion.

Since quantifying the confinement effects are crucial to extrapolating the data to unconfined conditions, it is important to determine the mechanisms for aerosol removal in the chamber. If surface diffusive deposition is important, then it should be noted that this mechanism will not exist in an open atmosphere. However, gravitational settling would be present in confined and unconfined conditions. Thus, it is important for the model to determine which process resulted in aerosol removal in the confined experiments.

Figure 4.5.14 shows the aerosol mass concentration from each cascade impactor stage for sample times taken at 5-30 sec., 1-1.5 min. and 13-13.5 min. postdetonation for the full-scale reference test (No. 8). Note that the mass concentration over an aerodynamic particle diameter range is drawn as a horizontal line. Thus for particles in the diameter range $0.75-1.73\ \mu\text{m}$, approximately 2.0, 0.5, and $0.085\ \text{g/m}^3$ were measured at the three sampling times, respectively. From Figure 4.5.14 we note that more than half of the aerosol mass was removed within about the first minute of sampling.

In this work, three models are considered to elucidate the observed initial rapid aerosol mass loss. It is shown that diffusive wall deposition and gravitational settling alone, do not explain the data. Finally a coupled coagulation-settling model is shown to provide some insight to the data. From these calculations, a lower limit estimate of the median aerodynamic diameter is made for confined aerosol within the first minute after the explosion.

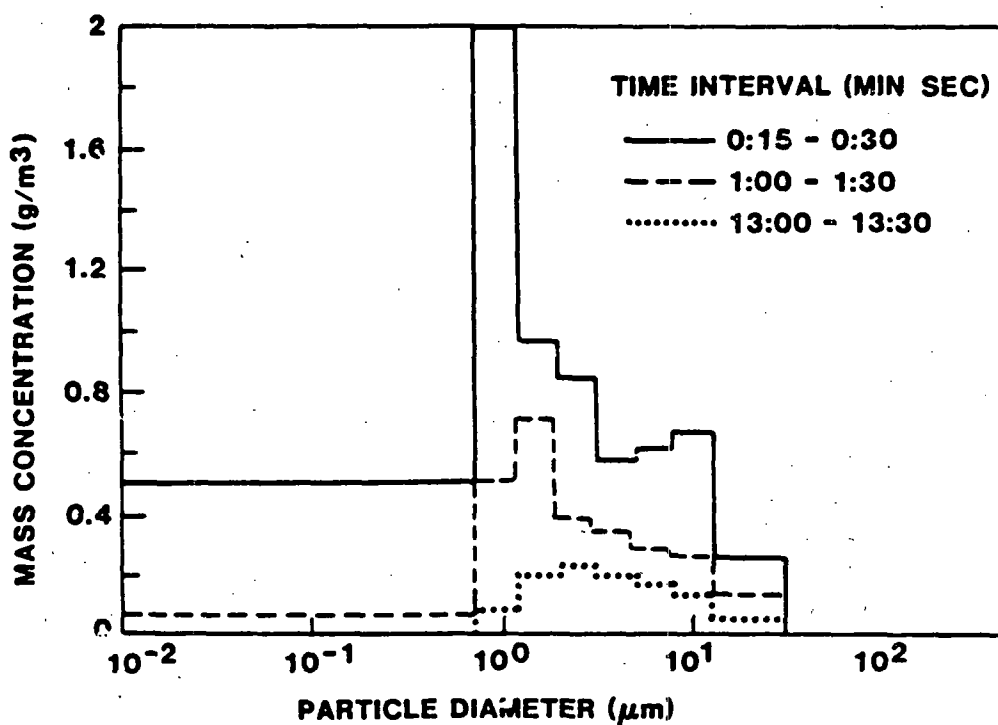


Figure 4.5.14. Plot of Measured Aerosol Mass Concentrations Obtained From Sequenced Cascade Impactors for Full-Scale Reference Test. The impactor measurements were taken at 15 to 30 seconds, 1 to 1.5 minutes, and 13 to 13.5 minutes postdetonation.

4.5.3.1 Diffusive Wall Deposition

For calculating aerosol diffusive deposition losses, the boundary layer thickness must be specified. Since this parameter is not easily measured, it may be calculated from the measured aerosol mass loss. This calculated thickness can then be compared to other experimentally determined values to determine if the calculated boundary layer thickness is reasonable. A physically realistic calculated boundary layer thickness would support diffusive deposition as a mechanism for aerosol mass loss.

Under quiescent conditions, Harrison (1979)¹² has experimentally determined that the boundary layer thickness σ , may be approximated by

$$\sigma = 12(D/2)^{-1.7} \quad (4.5.3.1)$$

where D , the particle diameter and σ are in microns. For comparison, the aerosol diffusive deposition loss may be modelled as

$$\frac{dQ}{dt} = -\frac{D}{\sigma} \left(\frac{A}{V} \right) Q \quad (4.5.3.2)$$

where t is time, Q is the aerosol mass concentration, D is the particle diffusivity and A/V is the surface area-to-volume ratio of the chamber. Integrating Eq (4.5.3.2), we obtain

$$\sigma = Dt(A/V)\ln(Q_0/Q) \quad (4.5.3.3)$$

where Q_0 is the initial mass concentration. The chamber volume is 42.6 m³ and for a particle diameter of 1.0 μm , $D = 2.77 \times 10^{-7}$ cm²/s (Friedlander (1977) p. 33).¹³ The surface area for deposition is given in Table 4.5.3.

TABLE 4.5.3
Surface Area for Aerosol Deposition

<u>Part</u>	<u>Area</u>
Chamber Walls	74.4 m ²
Cask Body	12.7 m ²
Cask Fins	<u>32.7 m²</u>
Total	120.0 m ²

By substituting $Q_0 = 6.442$ g/m³, $Q = 2.712$ g/m³ and $t = 52.5$ s into Eq. (4.5.3.3), we obtain a boundary layer thickness of 3.6×10^{-3} μm .

However, from Eq. (4.5.3.2), $\sigma = 39 \mu\text{m}$. Note that the two results differ by 4 orders of magnitude. Even if D and (A/V) are each inaccurate by an order of magnitude, this would still not explain the extremely small boundary layer thickness needed to explain the observed rapid aerosol mass loss. Furthermore, it is doubtful that the turbulence remaining 15-30 seconds after the blast would reduce the boundary layer thickness by 4 orders of magnitude to 36 Å. Thus the data do not support diffusive deposition as a significant mechanism for aerosol removal.

4.5.3.2 Gravitational Settling

Over the initial time measurement intervals, the largest aerosol mass loss was for particles in the diameter range 0.75-1.23 μm . For a particle, 1.0 μm in diameter, the settling velocity is 3.52×10^{-3} cm/s (Friedlander p. 33).¹³ Thus after 52.5 seconds, a spherical particle would have fallen only 0.185 cm. Clearly, since this distance is much smaller than the chamber dimensions, the data do not support gravitational settling alone as a significant mechanism for aerosol mass removal. Note that if the nonspherical shape of the particle is accounted for, the settling velocity would be even smaller than that given above.

4.5.3.3 Coupled Coagulation and Settling

A. Preliminary Assessment

Although coagulation alone does not remove aerosol mass and settling has been previously shown not to be a significant removal mechanism, the combined effects of particle growth by coagulation and gravitational settling may explain the data. One can quickly assess the feasibility of this process by satisfying two criteria. First, the time scale for coagulation must be less than 52 seconds to enable particles to grow over the time scale of interest. Second, the particle size needed to attain a settling velocity large enough to account for the data should be physically realistic. We can evaluate both criteria as follows.

The coagulation coefficient β , for particle sizes of interest is in the range 10^{-9} to 10^{-8} cm³/s (Friedlander p. 193).¹³ The characteristic time scale for coagulation is approximately $\tau = 1/\beta N$, where N is the aerosol number concentration. To estimate N , consider the particles in the diameter range 0.75-1.23 μm , to be spherical and 1.0 μm in diameter, with a density of 1.0 g/cm³. Thus since the initial mass concentration is 1.986 g/m³, the number concentration is approximately

$$N = \frac{60}{\pi \rho D^3} = 3.8 \times 10^6 \text{ cm}^{-3} \quad (4.5.3.4)$$

and

$$\tau = 1/\beta N = 2.6-26 \text{ sec.} \quad (4.5.3.5)$$

Since $\tau < 52$ seconds, coagulation is significant over the first sampling period and the first criterion is satisfied.

For gravitational settling loss, Q may be modelled by

$$\frac{dQ}{dt} = - \nu \left(\frac{A}{V} \right) Q \quad (4.5.3.6)$$

where ν is the settling velocity. Since the particles are much larger than the mean free path of air, Stokes law may be used to obtain

$$\nu = \frac{\rho R D^2}{18 \mu} \quad (4.5.3.7)$$

where ρ is the particle density, g is the gravitational constant and μ is the viscosity of air. The material density is approximately 8 g/cm^3 and based on the work of Gieseke and Reed (1977)¹⁴ one would expect an effective particle density of at least 1.6 g/cm^3 . Substituting Eq. (4.5.3.7) into Eq. (4.5.3.6) and integrating, results in

$$D^2 = \frac{18 \mu}{t \rho g} \left(\frac{V}{A} \right) \ln(Q_0/Q) \quad (4.5.3.8)$$

The projected horizontal surface area is approximately 18.9 m^2 and thus using a particle material density range of $1.6\text{-}8.0 \text{ g/cm}^3$, the particle geometric diameter needed to explain the rapid mass loss is $12\text{-}28 \text{ }\mu\text{m}$ which is equivalent to an aerodynamic diameter of $35 \text{ }\mu\text{m}$. However, since Q hardly varied over the sampling time of 52.5 to 105 sec, a factor of 2 in time would reduce the aerodynamic diameter from 35 to $25 \text{ }\mu\text{m}$. Since $25\text{-}35 \text{ }\mu\text{m}$ is a reasonable particle size range, the second criterion is satisfied.

B. Coagulation-Settling Model Description

The model used in this work solves the basic differential equation governing coagulation and settling as discussed by Gelbard and Seinfeld (1980).¹⁵ The basic assumptions are:

1. The particles are uniformly distributed in space, which is supported by the relatively constant mass density measured at several sampling ports in the full-scale test.
2. Coagulation is due to Brownian motion, turbulence and differential gravitational settling.
3. Particles are removed from the atmosphere by settling.
4. Particles can be uniquely characterized by their mass.

The fourth assumption is best suited for spherical liquid droplets. However, due to coagulation of solid particles in these experiments, we are usually dealing with irregular shaped agglomerates. Unfortunately the theory

for irregular shaped particles is not well developed and one generally resorts to introducing correction factors to the equations governing spherical particle dynamics (Gieseke et al, 1978).¹⁴

By using the above assumptions one can develop a set of mass balances for the aerosol mass within a set of particle size ranges. The net rate of aerosol mass accumulating in each size range is equal to the aerosol mass forming in that size range by coagulation minus that leaving the size range by coagulation and settling. The expressions for the rates of coagulation and settling are rigorously derived for spherical particles and corrected for nonspherical shapes.

C. Results

Figure 4.5.15 shows the total suspended aerosol mass concentration as a function of time. Note that the data, as shown by the solid line, indicates a very rapid initial mass loss. To account for the nonspherical nature of the particles, the agglomeration shape factor γ , was varied in the calculations. For ideal spherical particles $\gamma = 1$, and a larger value of γ enhances the coagulation process. Unfortunately, γ is not a readily determined parameter and is usually adjusted to fit the data. Due to the formation of void space in the fluffy agglomerates, the effective density should be less than the material density of 8.0 g/cm^3 . Since the work of Gieseke and Reed (1977)¹⁶ indicate a reduction by at most a factor of 5, the effective density was varied from 1.6 to 8.0 g/cm^3 .

In the absence of coagulation, it was shown that gravitational settling could not explain the rapid drop in aerosol mass concentration. From Figure 4.5.15 it is noted that by increasing γ , which enhances coagulation, thus more quickly forming large particles, rapid drop in aerosol mass concentration with time can be obtained. Furthermore, it is seen from Figure 4.5.15 that a value of $\gamma = 10$ can result in a rapid aerosol loss by coagulation and settling which could not be achieved by any of the previously discussed models. Although it appears that the initial processes may be modelled by coagulation and settling, Figure 4.5.16 shows that the calculated aerosol distribution does not agree with the measured distribution after 52.5 seconds of sampling. The calculations predict more aerosol in larger particle sizes than was actually measured. The calculated results are not surprising since as previously shown, an aerodynamic particle diameter of $25\text{--}35 \mu\text{m}$ is needed to justify settling as the removal mechanism. Furthermore, note from Figure 4.5.16, if the dynamic shape factor X is 2, thus halving the settling velocity, even more mass remains airborne for larger particle sizes. (A value of $X = 1$, which was used in Figure 4.5.15 neglects reduced settling velocities due to nonspherical particles.) Thus for coagulation and settling to explain the rapid aerosol mass loss larger particles should have been present than were measured from the cascade impactors. Even if one only considers settling alone, particle diameters in the chamber would have to be $25\text{--}35 \mu\text{m}$, which is much larger than reported by the cascade impactors. Thus one is lead to the hypothesis that the impactor data are artificially skewing the data toward smaller particle sizes. This type of error is well known and can often be

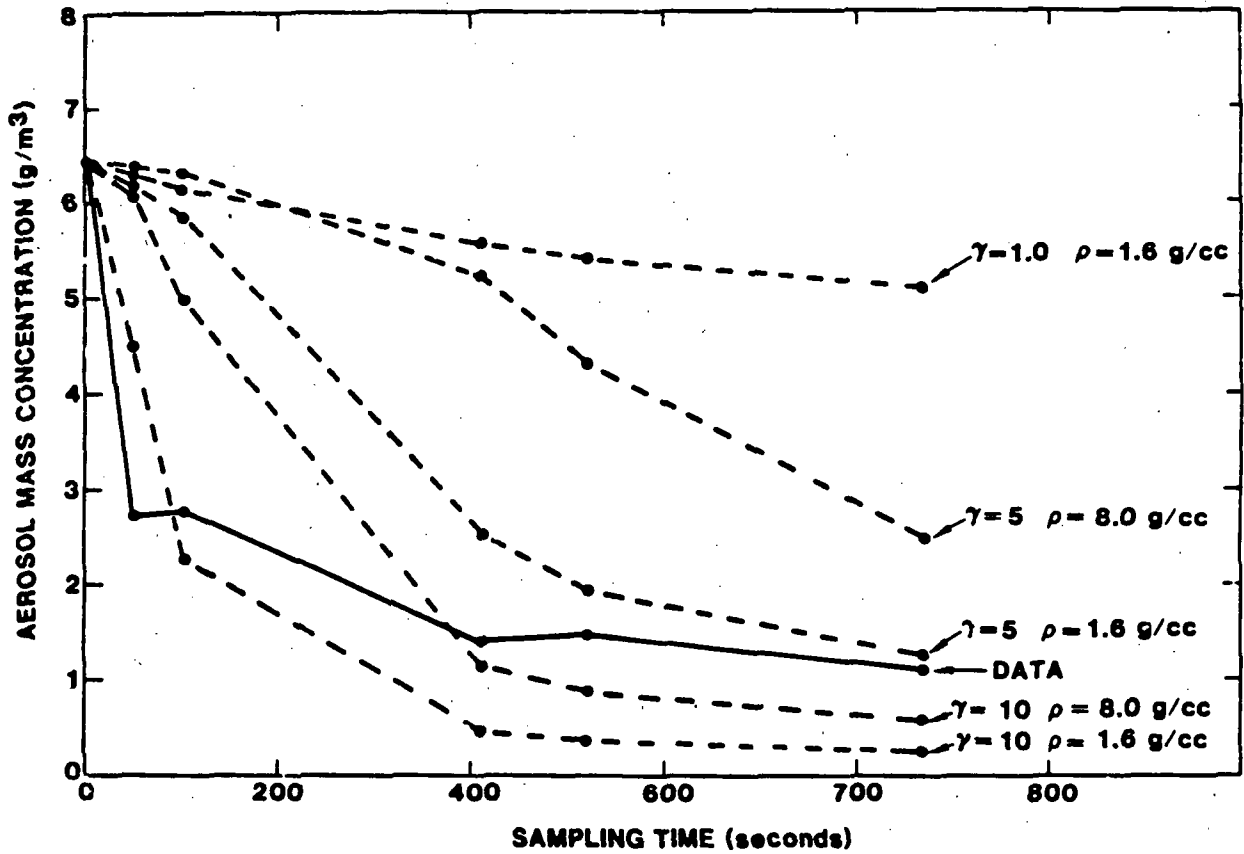


Figure 4.5.15. Plot of Total Suspended Aerosol Mass Concentration as a Function of Time. Solid line indicates measured total aerosol mass based upon sequential filters. Dotted lines are for different agglomeration shape factors, γ .

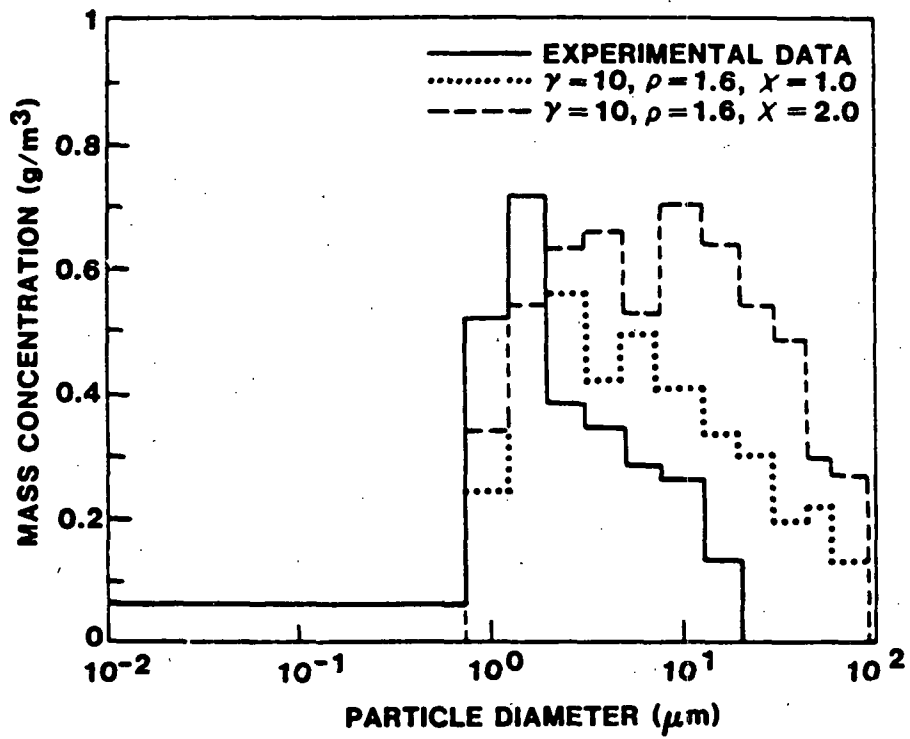


Figure 4.5.16. Plot Showing Comparison of Calculated Mass Concentration From Model With Measured Values After 52.5 Seconds Postdetonation

attributed to particle bounce (Cheng and Yeh, 1979)¹⁷ and to agglomerate breakage when passing through the impactor. Also, the extractive sampling line geometry (multiple bends in the sample lines) tends to provide an inherent maximum particle sampling diameter which precludes larger particles ($>10 \mu\text{m}$) from reaching the sampling instruments (G. J. Newton, private communication, 1983). Note that these errors should not affect the total mass concentration measurements which do agree with the filter measurements.

4.5.3.4 Conclusions

Three models were used to explain the observed rapid aerosol mass loss. First, diffusive deposition would require an unrealistically small diffusion boundary layer thickness to support this mechanism as an explanation. Second, gravitational settling alone of the measured particle sizes was too slow to explain the rapid mass loss. Finally, a combined coagulation-settling model, in which particles grew by coagulation and settled out could explain the rapid aerosol mass loss. This model, however, indicates larger particles should have formed than those reported from the cascade impactors. Since an aerodynamic particle diameter of $25\text{--}35 \mu\text{m}$ is needed to obtain a settling velocity which would explain the data, it is hypothesized that the impactor size distribution data is in error due to overloading of the impactor stages and that the actual aerodynamic diameters were larger than measured. This hypothesis is supported by the observed rapid loss in total aerosol mass concentration which is reported from both the cascade impactors and the total filters. Using the calculated results shown in Figure 4.5.16, the median aerodynamic diameter was larger than $2.0 \mu\text{m}$. Since neglecting coagulation would indicate that particles formed at 15-30 seconds postdetonation were $25\text{--}35 \mu\text{m}$ in diameter, $2.0 \mu\text{m}$ is considered to be a lower limit of the median aerodynamic diameter at about 1 minute postdetonation. Note that this airborne particle size underestimation does not affect the uranium mass concentration measurements upon which the health consequence estimates in this study are based. The fact that coagulation and gravitational settling plays a dominant role in the rapid loss in total aerosol mass concentration in these confined volume tests becomes a secondary mechanism in an atmospheric free-volume explosive event in which the important consideration is the early time ($t \approx 0$) primary particle concentration upon which this study's release fractions and health consequence estimates are based.

4.6 Analysis of Radiological Health Effects

The health consequences due to radioactive release from spent fuel casks subjected to sabotage were estimated using the consequence reactor safety model CRAC⁵ employed in the Urban Study.^{1,3} Although CRAC was not developed specifically for transportation accident environments, CRAC may be used to provide useful consequence estimates if interpreted with appropriate regard for the modeling assumptions. The Urban Study^{1,3} has reported that CRAC estimates are generally in good agreement with those of other calculational techniques. However, CRAC was selected for this study primarily because the NRC interim regulations regarding civilian reactor spent fuel transportation in the US are based upon the CRAC estimates as reported in the Urban Study.¹

The consequence model uses calculated airborne and ground radionuclide concentrations to estimate the public's exposure to (1) external radiation from airborne radionuclides in the cloud and radionuclides deposited from the cloud onto the ground and (2) internal radiation from radionuclides inhaled directly from the passing cloud, inhaled resuspended radionuclides and ingested contaminated food and milk. Radiation exposure from sources external to the body is calculated for time periods over which individuals are exposed to those sources and the exposure from sources internal to the body is calculated over the remaining life of the exposed individual.

Based on the calculated radiation exposure to individuals downwind, the consequence model estimates the number of public health effects that would result from a radioactive release. Early injuries, early fatalities, latent cancer fatalities, and thyroid and genetic effects are computed. Early fatalities are defined to be those fatalities that occur within 1 year of the initial exposure. They are estimated on the basis of exposure to the bone marrow, lung, and gastrointestinal tract. Bone marrow damage is the dominant contributor to early fatalities. Early fatalities are calculated assuming supportive medical treatment of the exposed individual. Early injuries (i.e., morbidities) are defined as nonfatal, noncarcinogenic illnesses that appear within one year of the exposure and require medical attention or hospital treatment. Latent cancer fatalities occur over any time subsequent to the exposure as a result of the initial exposure (early cancer fatalities) and of any long-term chronic exposure to low-levels of radioactive contamination (chronic cancer fatalities).

The expected health consequences were calculated using the measured release fractions shown in Table 4.6.1 as input to CRAC. The solid particulate release fractions of 3.4×10^{-5} and 2.4×10^{-5} of the solid radionuclide inventory for 1 and 3 PWR fuel assembly casks, respectively, are based on the full-scale test data. The noble gas release of 0.5 and 0.34 for 1 and 3 PWR fuel assembly casks are based upon the mass loss sustained by 50 percent of the 223 fuel rods used in the full scale test (Section 4.3) and are extrapolated to a 3 PWR fuel assembly sabotage scenario. Thirty-four percent (222 fuel rods) of the total fuel rod inventory of a 3 PWR fuel assembly truck cask are estimated to sustain some kind of cladding failure and that each failed rod would release all gases contained in the plenum. This assumes that only two out of three fuel assemblies could sustain maximum damage if the longest path of interaction for each assembly is assumed. Other input data required for CRAC include (1) site-related data such as meteorology and population distributions, (2) radionuclide inventories and release parameters, and cooling periods analyzed exterior to the CRAC code, and (3) emergency response scenarios.

The spent fuel radionuclide inventory used for this analysis has been generated using the fuel burning code ORIGEN¹⁸ assuming light water reactor fuel with 33,000 MWD/t of heavy metal burnup at 40 kw/kg power density and 150 days cooling. A 1 PWR fuel assembly shipment and a 3 PWR fuel assembly truck cask shipment were used for this analysis. The 1 and 3 PWR fuel assembly casks were assumed to contain 0.5 t and 1.4 t of heavy metal charged to the reactor, respectively. The 1 PWR fuel assembly radionuclide inventory used in this study is shown in Table 4.6.2. The 3 PWR fuel assembly inventory may be obtained by multiplying the Curie inventory of Table 4.6.2 by 3.

TABLE 4.6.1

Measured Release Fractions for a 1 PWR Fuel Assembly and
Calculated Release Fractions for a 3 PWR
Fuel Assembly Truck Cask.

<u>Inventory</u>	<u>One^a Assembly</u>	<u>Three^b Assemblies</u>
Noble Gases (Xe, Kr ^d)	0.5	0.34
Solid Radionuclides ^c	3.4×10^{-5}	2.4×10^{-5}

^a Based upon an inventory of 0.5 t of heavy metal

^b Based upon an inventory of 1.4 t of heavy metal

^c Solid radionuclides are airborne particles having smaller than a 10 μ aerodynamic diameter.

^d Gas release based upon cladding failure in 50 percent (111 fuel rods) of the total number of fuel rods (223) used in the full-scale reference test (see Section 4.3).

The detailed population distribution employed in this model is equivalent to the Manhattan borough of New York City. The detailed distribution is shown in Table 4.6.3. The detailed population distribution accounts for the fact that there is no population in the researched area by setting the population equal to zero in certain segments. The total population used in CRAC closely approximates the actual population within 800 km of the assumed release point.

One hundred sequences of New York City weather conditions representative of weather near the release point were used in these calculations. The estimated time of release was midafternoon and a street intersection was the assumed release point. A thermal source in CRAC was used to account for the effects of high explosives lofting the material and thus reducing the close-in ground level concentrations. All the consequence estimates have been made with the population in place. No attempt was made to model or account for evacuation to avoid early exposure because evacuation may not be possible in all instances.

Table 4.6.4 shows the results of the CRAC calculation for experimentally determined releases of a single and three assembly cask sabotage event. Because the source terms used never produced the threshold dosage for early fatalities and morbidities, the number of early fatalities and morbidities predicted are zero. The total latent cancer fatalities are a result of initial exposure, particle resuspension and long-term exposure to contaminated ground. For the reference base event of a sabotage attack on a one assembly truck mounted cask in downtown New York City, total latent cancer fatalities of 2/7 (mean/peak) are predicted. For a three assembly cask sabotage event in downtown New York City, total latent cancer fatalities of 4/14 (mean/peak) are predicted.

Peak thyroid and bone marrow dose in rems was also calculated as a function of distance from the release point. Table 4.6.5 lists peak thyroid and bone marrow dose for a one assembly and three assembly truck cask release. At a distance of 30 m from a three assembly cask release, the peak bone marrow dose was calculated to be 900 mrem and the peak thyroid dose was calculated to be 455 mrems. At 1.61 kilometers from the release point, the peak bone marrow dose was calculated to be 22.3 mrems and the peak thyroid dose was calculated to be 15.8 mrems for a three assembly cask. The Protective Action Guide¹⁹ (PAG) threshold for these distances is 1 rem. The peak bone marrow and thyroid dose for distances of 30 m or more from the release point for a single and three assembly cask are significantly less than PAG threshold. In summary, the early latent cancer fatalities calculated using the experimentally determined releases from a three assembly truck cask are smaller by a factor of 350,433 (mean/peak) than the original 1978 Urban Study¹ predictions upon which the NRC interim regulations for U.S. transport of spent fuel were based.

Table 4.6.2

Spent Fuel Cask Radionuclide Inventory Used in This Study

0.5 MTHM Charged to Reactor (1 Assembly)

33,000 MWd/MTHM Burnup at 40 kW/kg

150 Days Cooling

<u>Radionuclide*</u>	<u>Curies</u>
Co-58	1.09×10^3
Co-60	5.17×10^1
Kr-85	5.25×10^3
Sr-89	7.48×10^4
Sr-90	4.61×10^4
Y-90	4.01×10^4
Y-91	1.14×10^5
Zr-95	1.91×10^5
Nb-95	3.37×10^5
Rn-103	5.79×10^4
Ru-106	1.95×10^5
Te-127	2.94×10^3
Te-127m	3.00×10^3
Te-129	1.23×10^3
Te-129m	1.93×10^3
Cs-134	1.20×10^5
Cs-136	1.10×10^1
Cs-137	5.32×10^4
Ba-140	2.79×10^2

*Radionuclides with significant health effects based upon
Reactor Safety Study, NUREG 75-014 (WASH 1400)

TABLE 4.6.2 (cont'd)

<u>Radionuclide*</u>	<u>Curies</u>
La-140	3.21×10^2
Ce-141	3.71×10^4
Ce-144	4.57×10^5
Pr-143	4.23×10^2
Nd-147	2.99×10^1
Np-239	1.02×10^1
Pu-238	1.48×10^3
Pu-239	1.55×10^2
Pu-240	2.29×10^2
Pu-241	5.18×10^4
Am-241	6.78×10^1
Cm-242	8.73×10^3
Cm-244	1.46×10^3

*Radionuclides with significant health effects based upon Reactor Safety Study, NUREG75-014 (WASH 1400)

TABLE 4.6.3

Population Distribution Used for This Analysis

<u>Radius From Release</u> (km)	<u>Population Density</u> (people/km ²)
10	39,000
10-16	16,000
16-48	3,900
48-88	380
88	38

TABLE 4.6.4

CRAC Computed Health Consequences
for This Experimental Study

RELEASE FRACTION	EARLY FATALITIES ^c mean/peak	EARLY MORBIDITIES ^d mean/peak	EARLY LCF ^e mean/peak	TOTAL LCF ^f mean/peak
One Assembly Cask ^a	0/0	0/0	0.3/1.3	2/7
Three Assembly Cask ^b	0/0	0/0	1/3	4/14

- a. 50% of the noble gases and 3.4×10^{-3} % of the total solid inventory
- b. 34% of the noble gases and 2.4×10^{-3} % of the total solid inventory.
- c. Early fatalities occur within one year after exposure to the radioactive material.
- d. Early morbidities are illnesses appearing within one year after exposure.
- e. Early latent cancer fatalities are a result of the initial exposure only and can occur over any time subsequent to the initial exposure.
- f. Total latent cancer fatalities are the sum of early and long-term-exposure cancer fatalities and can occur at any time subsequent to exposure.

TABLE 4.6.5

Peak Thyroid and Bone Marrow Dose as a Function of Distance
from Release Point

Distance ^a (m)	Peak Bone Marrow Dose ^b (mrem)		Peak Thyroid Dose ^b (mrem)	
	One Assembly Cask	Three Assembly Cask	One Assembly Cask	Three Assembly Cask
30	424.0	900.0	215.0	455.0
1400	12.2	25.8	8.6	18.1
1600	10.5	22.3	7.4	15.8
2000	7.3	15.4	5.2	11.1

- a. Distance from release point.
- b. External ground exposure for 24 hours.

5. CONCLUSIONS

5.1 Measured Source Term Release for a Full-Scale 1 PWR Fuel Assembly Truck Cask Reference Event

Table 5.1 summarizes the measured source term release parameters for a single PWR fuel assembly truck cask (containing 0.5 metric tonnes of heavy metal charged to a light water reactor) subjected to a simulated sabotage event. A released quantity of 17 g of respirable radioactive particulates was determined based upon full-scale and subscale test data. A solid respirable particulate release fraction of 3.4×10^{-5} of the solid radionuclide inventory and a release fraction of 0.5 of the noble gas inventory was determined for the reference base event.

5.2 Calculated Source Term Release for a 3 PWR Fuel Assembly Truck Cask Sabotage Event

Table 5.2 summarizes the calculated source term release parameters for a three PWR fuel assembly truck cask (containing 1.4 metric tonnes of heavy metal charged to a light water reactor) subjected to a simulated sabotage event. A release of 34 g of respirable radioactive particulates was calculated based upon full-scale and subscale test data. A respirable particulate release fraction of 2.4×10^{-5} of the total solid radionuclide inventory and a release fraction of 0.34 of the noble gas inventory was calculated for a three element truck cask sabotage event.

5.3 Calculated Health Effects

5.3.1 1 PWR Fuel Assembly Truck Cask Referenced Event

Table 5.3.1 summarizes the health consequences due to a radioactive release from a single PWR assembly (0.5 t) spent fuel cask subjected to a simulated sabotage event. The reactor safety model CRAC employed in the Urban Study was used to calculate the health consequences. The experimentally determined release parameters summarized in Table 5.1 were used as input to the CRAC estimates. Because the source terms used never produced the threshold dosage for early fatalities and morbidities, the number of early fatalities and morbidities predicted are zero. The total latent cancer fatalities for a hypothetical attack on a one PWR assembly truck cask in downtown New York City are predicted to be 2/7 (mean/peak).

5.3.2 3 PWR Fuel Assembly Truck Cask Sabotage Event

Table 5.3.2 summarizes the health consequences due to a radioactive release from a three PWR assembly (1.4 t) spent fuel cask subjected to a simulated sabotage event. The calculated release parameters summarized in Table 5.2.1 were used as input to the reactor safety model CRAC to compute the health effects. The consequences were calculated for a simulated release in downtown New York City at midafternoon. The number of early fatalities and morbidities are predicted to be zero. Total latent cancer fatalities of 4/14 (mean/peak) are predicted.

TABLE 5.1

Summary of Release Parameters for a
1 PWR Assembly Cask Event

PARAMETER	VALUE
Total Fractured Fuel Mass (kg)	20.820
Total Spent Fuel Mass Removed From Assembly (kg)	5.460
Total Spent Fuel Released From Cask ^a (kg)	2.549
Total Spent Fuel Released as Respirable (g)	17
Fraction of Fuel Inventory Released ^a	5.1×10^{-3}
Fraction of Fuel Inventory Released as Respirable	3.4×10^{-5}
Fraction of Noble Gas Inventory Released	0.5

^aAll sizes

TABLE 5.2

Summary of Release Parameters for a
3 PWR Assembly Cask Event

PARAMETER	VALUE
Total Fractured Fuel Mass (kg)	41.612
Total Spent Fuel Mass Removed From Assembly (kg)	10.918
Total Spent Fuel Released From Cask ^a (kg)	5.098
Total Spent Fuel Released as Respirable (g)	34
Fraction of Fuel Inventory Released ^a	3.6×10^{-3}
Fraction of Fuel Inventory Released as Respirable	2.4×10^{-5}
Fraction of Noble Gas Inventory Released	0.34

^aAll sizes

TABLE 5.3.1

Health Consequences for a 1 PWR Assembly Truck Cask Sabotage Event

Release Fraction	Early ^a Fatalities	Early ^b Morbidities	Early ^c LCF	Total ^d LCF
	(mean/peak)	(mean/peak)	(mean/peak)	(mean/peak)
0.50 Noble Gases	0/0	0/0	0.3/1.3	2/7
3.4 x 10 ⁻⁵ Solid Inventory				

^aEarly fatalities occur within 1 year after exposure to the radioactive material.

^bEarly morbidities are illnesses appearing within 1 year after exposure.

^cEarly latent cancer fatalities are a result of the initial exposure only and can occur at any time subsequent to the initial exposure.

^dTotal latent cancer fatalities are the sum of early and long-term-exposure cancer fatalities and can occur at any time subsequent to exposure.

TABLE 5.3.2

Summary of Computed Health Consequences for a
Three FWR Assembly Truck Cask Sabotage Event

Release Fraction	Early ^a Fatalities	Early ^b Morbidities	Early ^c LCF	Total ^d LCF
	(mean/peak)	(mean/peak)	(mean/peak)	(mean/peak)
0.34 Noble Gases	0/0	0/0	1/3	4/14
2.4 x 10 ⁻⁵ Solid Inventory				

^aEarly fatalities occur within 1 year after exposure to the radioactive material.

^bEarly morbidities are illnesses appearing within 1 year after exposure.

^cEarly latent cancer fatalities are a result of the initial exposure only and can occur at any time subsequent to the initial exposure.

^dTotal latent cancer fatalities are the sum of early and long-term-exposure cancer fatalities and can occur at any time subsequent to exposure.

5.4 Degree of Precision And Accuracy of Measured Parameters and Calculated Results

The accuracy of the calculated health consequences is dependent upon at least three parameters: (1) the accuracy of the CRAC model to predict health effects, (2) the accuracy of the measured full-scale and subscale released UO_2 mass, and (3) the accuracy of the correlation ratio between spent fuel and surrogate fuel. The accuracy of the measured release mass is in turn a function of the uncertainty in the measurement of the uranium mass by uranium fluorometry, the flow rate of the samplers, the sampling period, the pressure chamber volume and the ability to fit the data and extrapolate to $t = 0$. The uncertainty of the measured parameters such as flow rate, uranium mass determination by fluorometry, pressure chamber volume, etc, has been estimated and using standard error propagation methods, the uncertainty of the derived UO_2 released respirable mass has been determined. The estimated most probable error of the released UO_2 respirable mass is ± 7 percent.

The accuracy of the measured correlation ratio between spent fuel and UO_2 fuel can be estimated using the results of two independent studies. The NRC sponsored study at BCL indicates a value of 1 ± 0.75 for the correlation spent fuel: D - UO_2 ratio. The EG&G/INEL experiments indicate an average value of 3.06 ± 2.54 with outlying values of 0.53 and 5.6. The most probable error for both the BCL and EG&G/INEL experiments is ± 83 percent, maximum. For conservatism in the health risk assessment, the maximum value of 5.6 was used for the correlation ratio.

The accuracy of the CRAC model's health consequence predictions was also considered in this study. Because of the large uncertainties in weathering and decontamination assumptions of CRAC and the assumptions used in the dispersion and deposition submodel of CRAC, it is difficult to quantify the uncertainty or accuracy of the health consequence predictions. However, because the assumptions and statistical approximations used in CRAC and its submodels are conservative and assume conservative values for most of the model's parameters, it is expected that the maximum total latent cancer fatality values of 7 and 14 for a one and three PWR assembly fuel cask, respectively, are conservative and represent the largest values possible for the type of simulated sabotage events considered in this study. This together with the fact that a maximum value of 5.6 was used for the correlation ratio provides the basis for a conservative upper bound estimate of the health consequences that could result from a sabotage event in downtown New York City.

5.5 Comparison of This Study's Results with Other Study's Results

Table 5.5.1 summarizes and compares the results of this experimental study with those of the 1980 Urban Study³ for a simulated sabotage event. This simulated sabotage event assumes an attack on a 150 day cooled three PWR assembly fuel cask containing 1.4 metric tonnes of heavy metal fuel charged to the reactor. The reference HED is the assumed attack device in both cases. The 1978 and 1980 Urban Studies were based upon engineering judgement and limited data available at the time of the study. No comparisons were made with the 1978 Urban Study release parameters because the release fractions reported in that study were based upon a range of attack devices and not exclusively on the reference device used in this experimental study and the 1980 Urban Study. The predicted respirable fuel mass released from a three PWR fuel assembly cask as a result of the simulated attack is 29 times larger for the 1980 Urban Study than for this study.

Table 5.5.2 compares the CRAC model computed health consequences based upon this study's experimental data with the 1978 Urban Study's predictions. Early latent cancer fatalities are 350/433 (mean/peak) times higher based upon the 1978 Urban Study¹ analyses than that of this study.

TABLE 5.5.1. COMPARISON OF EXTRAPOLATED TEST RESULTS WITH
1980 URBAN STUDY^a RESULTS

	THIS STUDY ^b	URBAN STUDY ^b
TOTAL FRACTURED FUEL MASS (g)	41,612	140,000
TOTAL REMOVED FUEL MASS (g)	10,918	--
TOTAL FUEL MASS RELEASED FROM CASK (ALL SIZES) (g)	5,098	14,000
TOTAL FUEL MASS RELEASED AS RESPIRABLE (g)	34	980
FRACTION OF FUEL INVENTORY RELEASED (ALL SIZES)	3.6×10^{-3}	1×10^{-2}
FRACTION OF SOLID FUEL INVENTORY RELEASED AS RESPIRABLE	2.4×10^{-5}	7×10^{-4}
FRACTION OF GAS FUEL INVENTORY RELEASED FROM CASK	0.34	0.1

^a NUREG/CR0743 ^b THREE PWR FUEL ASSEMBLY CASK

TABLE 5.5.2. COMPARISON OF CRAL COMPUTED HEALTH EFFECTS WITH THE 1978 URBAN STUDY^a RESULTS

	THIS STUDY	URBAN ^a STUDY
EARLY FATALITIES (MEAN/PEAK)	0/0	4/60
EARLY MORBIDITIES (MEAN/PEAK)	0/0	160/1600
EARLY LCF ^c (MEAN/PEAK)	1/3	350/1300
TOTAL LCF ^c (MEAN/PEAK)	4/14	b

a. 1978 URBAN STUDY SAND77-1927

b. NOT REPORTED IN 1978 URBAN STUDY

c. LATENT CANCER FATALITIES

7. REFERENCES

1. A. R. DuCharme, JR., et al, Transport of Radionuclides in Urban Environs: Working Draft Assessment, US Nuclear Regulatory Commission Interim Report SAND77-1927, Sandia National Laboratories, May 1978.
2. Code of Federal Regulations, Title 10, Part 73.37, "Requirements for Physical Protection of Irradiated Reactor Fuel in Transit," January 1, 1982.
3. N. C. Finley, et al, Transportation of Radionuclides in Urban Environs: Draft Environmental Assessment, NRC Research and Development Report, NUREG/CR-0743, Sandia National Laboratories, Albuquerque, NM, July 1980.
4. E. W. Schmidt, M. A. Walters, B. D. Trott, J. A. Gieseke, Final Report on Shipping Cask Sabotage Source Term Investigation, US Nuclear Regulatory Commission, NUREG/CR-2472, October 1982.
5. I. B. Wall, et al, Overview of the Reactor Safety Consequence Model, NUREG-0340, US Nuclear Regulatory Commission, Washington, DC, October 1977.
6. E. L. Wilmot, Transportation Accident Scenarios for Commercial Spent Fuel, SAND80-2124, Sandia National Laboratories, February 1981.
7. R. P. Sandoval, J. P. Weber and G. J. Newton, "Safety Assessment of Spent Fuel Transportation in Extreme Environments," Waste Management '81 ANS Topical Meeting, February, 1981.
8. Final Environmental Statement on the Transportation of Radioactive Material by Air and Other Modes, Vols I and II, NUREG-0170, Office of Standards Development, US Nuclear Regulatory Commission, Washington, DC, December 1977.
9. Federal Actions Are Needed to Improve Safety and Security of Nuclear Materials Transportation, Comptroller General of the United States, Report to Congress, EMD-79-18, May 7, 1979.
10. J. F. VanderVate, Investigations Into the Dynamics of Aerosols in Enclosures as Used for Air Pollution Studies, ECN-86, Netherlands Energy Research Foundation, Petten, Netherlands, 1980.
11. Personal Communication from Dr. J. L. Alvarez, EG&G/INEL, September 17, 1982.
12. A. W. Harrison, "Quiescent Boundary Layer Thickness in Aerosol Enclosures Under Convective Stirring Conditions," J. Colloid Interface Science 69, 563.

13. S. K. Friedlander, Smoke, Dust, and Haze, John Wiley (1977).
14. J. A. Gieseke, K. W. Lee, and L. D. Reed, "HAARM-3 User's Manual," BMI-NUREG-1991, 1978.
15. F. Gelbard and J. H. Seinfeld, "Simulation of Multicomponent Aerosol Dynamics," J. Colloid Interface Sci., 78, 485, 1980.
16. J. A. Gieseke and L. D. Reed, "Aerodynamic and Thermophoretic Behavior of Coagulated Sodium Oxide Aerosols," Airborne Radioactivity, ANS Winter Meeting, California (1977).
17. Y. S. Cheng and H. C. Yeh, "Particle Bounce In Cascade Impactors," Environmental Science and Technology 13 (1979).
18. D. E. Bennett, SANDIA-ORIGEN User's Manual, NUREG/CR-0987, SAND79-0299, Sandia National Laboratories, Albuquerque, NM, October 1979.
19. Manual of Protective Action Guides and Protective Actions for Nuclear Incidents, EPA-52011-75-001, September 1975, JS Environmental Protection Agency.

DISTRIBUTION:

DOE/TIC-4500-R70 UC-71 (277)

Battelle Columbus Laboratories
505 King Avenue
Columbus, OH 43201
Kenneth D. Kok
Richard J. Burian
B. Dale Trott
M. Audeen Walters

Inhalation Toxicology Research Institute
P. O. Box 5890
Kirtland Air Force Base
Albuquerque, NM 87115
R. McClellan
G. J. Newton (10)
S. C. Yeh
B. B. Boecker
B. A. Wong
Y. S. Cheng

Oak Ridge National Laboratories
P. O. Box X
Oak Ridge, TN 37830
A. P. Malenauskas (5)
G. W. Parker

EG&G Idaho National Engineering Labs.
P. O. Box 1625
Idaho Falls, ID 83415
R. W. Marshall, Jr. (10)
J. Sanders
J. L. Alvarez

Office of Nuclear Regulatory Com.
Washington, DC 20555
W. R. Lahs (10)
C. Sawyer (10)
T. Sherr
R. Nolsen
R. F. Burnett
T. Margulies

U. S. Department of Energy
Div. LWR Fuel Cycle Projects
NE 43
Washington, DC 20545
A. Katz
F. Falci (10)
G. Ortel
R. B. Chitwood (10)

U. S. Department of Energy
Albuquerque Operations Office
Albuquerque, NM 87115
K. A. Carlson
R. Y. Lowrey

U. S. Department of Transportation
NE-341
Mail Stop B-107
Washington, DC 20585
Thomas D. Anderson

Sandia National Laboratories
Albuquerque, NM 87185
1822 H. Levine
1832 A. Romig
7533 F. Matthews
7533 J. Weber
9268 D. Tomasko
9413 J. D. Johnson
9413 N. C. Finley
9414 D. M. Ericson
9415 D. J. Alpert

9761 J. Jackson
9780 R. M. Jefferson
9781 R. E. Luna
9781 R. P. Sandoval (30)
9782 R. B. Pope
9783 G. C. Allen
9783 E. L. Wilmot
9784 B. D. Zak
9784 H. Church

Fre Gelbard
861 South Glencliff
Apt 31
La Habra, CA 90631

E. I. duPont de Nemours and Co.
Savannah River Plant Atomic
Energy Division
Bldg. 773-28A
Aiken, SC 92808
R. Baxter

E. I. duPont de Nemours and Co
Savannah River Laboratory
Bldg. 773-11A
Aiken, SC 92808
R. Moyer

Dr. Klaus A. Schneider
Transnuclear GmbH
Postfach 110030
D-6450 Hanau 11

I. H. Fraser
810 Belfast Rd
Ottawa, Ontario K1A 0R2

James G. Tosces
Commonwealth Edison
P. O. Box 767
Chicago, IL 60690

Gerald Womack
Central Electricity Generating Board
Barnwood
Gloucester, England

Dr. Florentine Lange
Gesellschaft für Reaktor Sicherheit
Schwertnergasse
D 5000 Köln
FRG

G. I. W. Llewelyn
U. K. Atomic Energy Authority
11 Charles Street
London, SW14 42P

W. R. Merritt
810 Belfast Rd.
Ottawa, Ontario K1A 0R2

Nello Bonicelli
Chief, Test Reactors Branch
U. S. Department of Energy
550 Second St.
Idaho Falls, ID 83401

Marty Semonin
Illinois Department of Nuclear Safety
1035 Outer Drive
Springfield, IL 62704

H. F. Mac Donald
Central Electricity Generating Board
Gloucester, England
GL139PB

D. R. Poulter
UKAEA Safety And Reliability Directorate
Wigshae Lane, Culcheth
Cheshire, England

END

DATE FILMED

10 / 17 / 83

NTIS does not permit return of items for credit or refund. A replacement will be provided if an error is made in filling your order, if the item was received in damaged condition, or if the item is defective.

*Reproduced by NTIS
National Technical Information Service
U.S. Department of Commerce
Springfield, VA 22161*

This report was printed specifically for your order from our collection of more than 2 million technical reports.

For economy and efficiency, NTIS does not maintain stock of its vast collection of technical reports. Rather, most documents are printed for each order. Your copy is the best possible reproduction available from our master archive. If you have any questions concerning this document or any order you placed with NTIS, please call our Customer Services Department at (703)487-4660.

Always think of NTIS when you want:

- Access to the technical, scientific, and engineering results generated by the ongoing multibillion dollar R&D program of the U.S. Government.
- R&D results from Japan, West Germany, Great Britain, and some 20 other countries, most of it reported in English.

NTIS also operates two centers that can provide you with valuable information:

- The Federal Computer Products Center - offers software and datafiles produced by Federal agencies.
- The Center for the Utilization of Federal Technology - gives you access to the best of Federal technologies and laboratory resources.

For more information about NTIS, send for our *FREE NTIS Products and Services Catalog* which describes how you can access this U.S. and foreign Government technology. Call (703)487-4650 or send this sheet to NTIS, U.S. Department of Commerce, Springfield, VA 22161. Ask for catalog, PR-827.

Name _____

Address _____

Telephone _____

*- Your Source to U.S. and Foreign Government
Research and Technology.*